The Role of Oligodendrocytes in Demyelinating Pathologies of the CNS

Dissertation

zur

Erlangung der naturwissenschaftlichen Doctorwürde

(Dr. sc. nat.)

vorgelegt der

Mathematisch-naturwissenschaftlichen Fakultät

der

Universität Zürich

von

Giuseppe Locatelli

aus

Italien

Promotionskomitee

Prof. Dr. Burkhard Becher (Vorsitz und Leitung der Dissertation)

Prof. Dr. Thorsten Buch (Leitung der Dissertation)

Prof. Dr. Peter Sonderegger

Prof. Dr. Esther Stöckli

Zürich, 2012

DISCLAIMER

The thesis is based upon and partly adapted from the publication:

Primary oligodendrocyte death does not elicit anti-CNS immunity

Giuseppe Locatelli, Simone Wörtge, Thorsten Buch, Barbara Ingold, Friederike Frommer, Bettina Sobottka, Martin Krueger, Khalad Karram, Claudia Bühlmann, Ingo Bechmann, Frank L. Heppner, Ari Waisman, Burkhard Becher (*Nature Neuroscience*, *2012*).

CONTENTS

SUMMARY

Oligodendrocytes (ODCs) are glial cells of the central nervous system (CNS), best known for the production of myelin which insulates axons. Recent investigations have highlighted additional roles of ODCs as the maintenance of axonal integrity, and ODC impairment has been associated to several human pathologies stressing the importance of these cells in neurodegeneration and in the neuroimmunological interplay. Primary ODC death is debated for initiating multiple sclerosis (MS), a pathological condition in which inflammation and neurodegeneration sustain the typical progressive clinical impairment. To specifically test ODC death as a trigger for anti-CNS immunity in MS, we inducibly killed ODCs through diphtheria toxin administration in a transgenic mouse model. However, even conditions favoring autoimmunity – bystander activation, removal of regulatory T cells, presence of myelin-reactive T cells, and application of demyelinating antibodies – did not result in the development of CNS inflammation after ODC death. We could thus show that diffuse ODC death alone or in conjunction with immune activation is an unlikely trigger of sustained anti-CNS immunity.

Next, we investigated the relevance of ODC damage in animal models of neurodegeneration focusing on the insulin-like growth factor 1 receptor (IGF1R) pathway. In MS, surviving ODCs surrounding sclerotic lesions upregulate IGF1R and Insulin-like growth factor 1 (IGF-1), indicating a role of this pathway in response to inflammatory demyelination**.** IGF-1 is an anti-apoptotic, myelinogenic stimulus in the ODC lineage. In our oIGF1R mouse model, a deletion of this receptor specifically in mature ODCs resulted in ameliorated clinical disabilities in the inflammatory model for MS, experimental autoimmune encephalomyelitis (EAE), despite increased ODC mortality and decreased remyelination capabilities following cuprizone intoxication. Hence, we confirmed the anti-apoptotic role of IGF1R in the ODC lineage while highlighting a surprising benefit of IGF1R absence from mature ODCs during prolonged neuroinflammation.

Finally, we were interested in creating a mouse model that would allow us to image these dynamics of demyelination and remyelination in vivo. Thus, we created the oLucR transgenic mouse strain, in which the luciferase reporter gene is specifically expressed in mature ODCs under the control of a β-actin promoter. Using oLucR mice we were able to observe defined and reproducible increases in the in vivo bioluminescence signal at beginning of induced demyelination and CNS inflammation,

pointing out the possibility that under demyelinating conditions ODCs might adopt an “active phenotype” characterized by renewed cytoskeleton motility.

ZUSAMMENFASSUNG

Oligodendrozyten (ODZ) sind Gliazellen. des Zentralen Nervensystems (ZNS), welche vor allem zuständig sind für die Produktion des Myelins, welches Axone isoliert. Neue Untersuchungen heben allerdings zusätzliche Funktionen der ODZ neben der Erhaltung axonaler Integrität hervor. So wurde die Schädigung von ODZ mit einigen neuroimmunologischen und -degenerativen Pathologien des ZNS assoziert. Zum Beispiel wurde der primäre Tod von ODZ als Trigger der Multiplen Sklerose (MS) postuliert, einer ZNS Erkrankung, in der Neuroinflammation und –degeneration progrediente klinischen-neurologischen Defizite verursachen. Um die Hypothese zu prüfen, dass sterbende ODZ in MS eine gegen das ZNS gerichtete Immunantwort auslösen können, haben wir mittels eines transgenen Mausmodells selektiv ODZ durch Gabe von Diphtherietoxin geschädigt. Sogar Bedingungen, die eine Autoimmunantwort favorisieren – wie z.B. die Bystander-Aktivierung, die Anwesenheit myelin-reaktiver T-Zellen, die Depletion regulatorischen T-Zellen oder Applikation demyelinisierender Antikörper – führen in Kombination mit induziertem ODZ-Untergang nicht zur Entwicklung einer gegen das ZNS gerichtetet Autoimmunität. Wir konnten folglich zeigen, dass diffuser ODZ Tod alleine oder in Verbindung mit einer Aktivierung des Immunsystems sehr wahrscheinlich kein Auslöser einer persistierenden ZNS-Autoimmunität ist.

Zum Zweiten haben wir die Bedeutung Insulin-ähnlicher Wachstumsfaktoren (IGF1R) in autoimmunen und toxischen Demyelinations modellen der Maus untersucht. Überlebende ODZ, die MS Läsionen im ZNS umgeben, regulieren IGF1R und Insulin-ähnliche Wachstumsfaktoren 1 (IGF-1) hoch, was auf einen Einfluss dieser Zytokine auf die Formation entzündlicher Demyelinisierungsherde hinweist. Frühere Studien konnten ausserdem zeigen, dass IGF-1 ein anti-apoptotischer, myelinogener Stimulus für ODZ sein kann. Mit Hilfe eines zweiten Mausmodells (oIGF1R) konnten wir IGF1R selektiv in reifen ODZ ausschalten. Dies führte zu verbesserten klinischen Symptomen nach Induktion einer gegen das Myelin-gerichteten Immunreaktion und entzündlichen ODZ Schädigung (ExperimentelleAutoimmune Enzephalomyelitis, EAE). Im Gegensatz hierzu führte der toxische ODZ Tode nach Gabe von Cuprizone zu erhöhter ODZ Sterblichkeit und verringerter Remyelinisierung in Abwesenheit des IGF1R. Diese Ergebnisse weisen auf eine unterschiedliche Rolle des IGFR1 in Abhängigkeit von der Art des OLZ Schadens (inflammatorisch versus toxisch) hin

Zum Dritten haben wir ein Mausmodell generiert (oLucR), um die Dynamik der Demyelinisierung und Remyelinisierung in vivo und Echtzeit bildlich darzustellen Hierzu haben wir das Reportergen Luciferase nach Cre-vermittelter Rekombination in reifen ODZ unter der Kontrolle des β-Actin Promoters exprimiert. Im oLucR Modell konnten wir reproduzierbar eine Zunahme der in vivo Biolumineszenz messen, die mit dem Beginnder Neuroinflammation und Demyelinisierung im ZNS zeitlich korrelierte. Dieses deutet darauf hin, dass ODZs unter demyelinisierenden Bedingungen einen “aktiven Phänotyp“ annehmen können, welcher sich durch eine gesteigerte Zytoskelettmotilität auszeichnet.

INTRODUCTION

Glia

In virtually every animal species, the nervous system comprises neurons and glial cells. The latter have continuously grown in number along the course of evolution of complex nervous systems, and in the primate order glia strongly outnumber neurons constituting 90% of the cells of the central nervous system (CNS) [1]. Glial cells were first discovered by the groundbreaking work of Virchow, who was able to discern these new cells from neurons defining them “nerve glue”. Subsequently, especially thanks to the contributions of Ramon y Cajal and Rio Hortega, three cell types were distinguished dividing neuroglia into astrocytes, microglia, and oligodendrocytes (ODCs) (**Fig. 1**). Since then, a reductive vision of these cells as mere “holding glue” of the CNS has stigmatized their biological importance compared to the “effectory” components of the CNS, the neuronal cells. However, this misleading simplification has been outdated in recent times thanks to a growing number of evidences pointing at glial cells for countless vital functions in supporting neurons and, most importantly, finally stressing their role in human diseases.

Astrocytes and microglia

Astrocytes are highly heterogeneous glial cell type. They are usually divided into two groups: protoplasmic, found in the CNS gray matter and directly controlling blood vessels and synapses, and fibrillary, mainly found in the CNS white matter and contacting nodes of Ranvier besides blood vessels. Astrocytes extend a fine network of thousands of membranous processes that contact directly vessels and synapses (**Fig. 2**, left). Also, they are highly reactive upon stimulation and astrocyte activation is a result of virtually any perturbation of the CNS, implying both morphological changes and increased release of signaling mediators. Altogether, this reactive condition is defined as gliosis. Beyond this role in response to injuries, astroglia exert many other fundamental steady-state functions as the metabolic coupling of synaptic activities, the reuptake of neurotransmitters and ions (mainly K^+) from synapses and nodes of Ranvier, and participation in the formation of the blood brain barrier (BBB). The BBB (or neurovascular unit) is a functional feature of the CNS vasculature in which reduced

rates of endocytosis, diffuse tight junctions among endothelial cells, high membrane levels of active transporters and astrocytic end-feet create a biological separation between the CNS and the periphery (see *Immune-privilege in the CNS* section). It has been proven that astrocytes directly affect the formation and the number of neuronal synapses *in vitro* and *in vivo* controlling pre- and post-synaptic functions through the release of mediators such as thrombospondin and D-serine. These functions are influenced by neuronal ATP and neurotransmitter levels which produce intracellular Ca^{2+} waves in astrocytes and thus couple local neuronal activity to astrocytic support of synaptic formation. Also, similar mechanisms seem to govern synaptic plasticity following different pathological conditions [2, 3]. This functional coupling between astrocytes and neurons is also evident in the BBB, in which neurons can directly affect astrocytes controlling neurovascular permeability through effects on vasodilatation and vasoconstriction. Astrocytes are connected to the non-compacted myelin of ODCs through gap junctions, and thus possibly provide ODCs and internodes (see next section) with indirect access to blood metabolites. Along this line, it has been proven that impairment in astrocytic function directly affects ODC survival, as shown in glial fibrillary astrocytic protein (GFAP)-null mice and in human patients suffering from Alexander disease [4, 5]. Finally, astrocytes are also known as important providers of growth factors for neurons (alike ODCs, which produce factors as NGF, BDNF, NT-3 and Insulin Growth Factor 1, IGF-1 – reviewed in [6]).

The other major glial cell type in the CNS is microglia, which constitute about the 15% of the cells of the adult CNS and the only member of the immune system in the CNS parenchyma. Microglia originate from uncommitted myeloid progenitors derived from the Yolk sac and invading the CNS before embryonic day 9 [7]. As astrocytes, microglia are highly sensitive and display numerous membranous symmetrical extensions which are highly motile and sample the extracellular space with high turnover in a seemingly random fashion (**Fig. 2**, right). As cells of the immune system, microglia possess phagocytic capabilities and can act as antigen presenting cells (APCs) through antigen internalization and presentation in the context of Major histocompatibility complex-I (MHC-I) and MHC-II molecules (see *The immune system* section). Hence, one of the main functions of microglia appears to be the communication of parenchymal distress towards the peripheral immune system through the aforementioned antigen presentation and through release of inflammatory cytokines as TNFα. Also, it seems that microglia play a developmental role in the formation of

neural circuits through the engulfment of inappropriate synaptic connections targeted by the complement factor C1q [8].

Importantly, microglia are homogenously distributed in the adult CNS and thus able to constantly screen the entire brain parenchyma [9]. However, this constant surveillance of their microenvironment is generally not reflected by classic activation markers of the monocyte lineage. In fact, microglia display few phagocytic markers and very low levels of membrane ligands and opsonic receptors which are usually associated to activated macrophages as FcγRs, CD11b/CD18 (also known as complement receptor type 3), mannose receptor and CD14, the receptor mediating the effects of LPS [10]. Different kinds of stimuli and danger signals result in strong upregulation of these markers along with morphological changes which render microglia more similar to effector cells of the macrophage lineage. In their constant surveillance, microglia appear to be strongly influenced by the local neurochemical environment, in a complex interplay between pro-activation factors as ATP and suppressing mediators as neuron/glial-produced neurotrophins (also show to contrast activatory effects of IFNγ and LPS). In this delicate balance, microglia response is continuously shaped and downregulated by direct cell-to-cell neuronal signaling including members of the so-called “neuroimmune regulatory proteins” as OX2A, CD47, CD200, and fractalkine (CX3CL1). Signaling through these membrane-bound molecules represent thus a tonic signal which limits microglial activation in the healthy CNS, protecting parenchymal cells from the possibly detrimental effects of sustained immune activation. Nonetheless, activated microglia seem to play a major role in CNS inflammation both as producers of pro-inflammatory cytokines and immune regulatory molecules (IL6, IL1, TNFα, IL12, IL18), and as producers of anti-inflammatory components (Il10, IL1Ra, TGFβ). The control mechanisms behind these opposite function are still unclear, with mediators as IFNγ, IL4 and prostaglandins shown to play a major role [10]. Altogether, and similarly to astrocytes, the exact range of microglial functions is still unknown and both their hypothetical harmful and protective role in different CNS pathologies remain hotly debated.

Oligodendrocytes and myelin

ODCs are the myelinating cells of the CNS. These cells exist in different loosely-characterized subtypes which vary according to different studies [11-13] and have their

peripheral counterpart in Schwann cells, which evolved in parallel to CNS ODCs and myelinate peripheral nerve fibers. Myelin is a multi-layered, lipid-enriched biological membrane which is wrapped around neuronal axons thus allowing faster signal conduction (**Fig. 3**). Little is known about the effective resistance of this insulating membrane, but its average properties seem to vary between CNS regions and possibly between ODC subtypes [14]. While simpler nervous systems generally display mere glial engulfment of axons with clustering of ion channels, myelin is a specialized accomplishment of late animal evolution [15]. Myelin is produced by ODCs in their last developmental stage (see next section) and insulates up to 50 neuronal axons, thus creating an extensive and complex network between ODCs and surrounding neuronal cells. Myelination is a tightly regulated process in that ODCs envelops contemporaneously all their target axons in a sharp time frame of 10-18 hours [16]. It was calculated that during this active phase of myelination every ODC produces almost 5000 μm^2 of myelin surface per day, and a final total myelin surface of 1-20 x 10^5 μm^2. Naturally, this is reflected by high metabolic demands and high plasticity of the ODC cytoarchitecture (actin filaments and microtubules). In the main white matter regions of the CNS, ODCs myelinate only axons with a diameter larger than 0.2 µm [17], while in other regions as cortex and optic nerve also smaller axons can be enwrapped. Larger axons are the first to recruit glial progenitors and receive more layers of myelin when compared to small diameter axons. Nonetheless, the ratio between inner axonal and fiber diameter, called g-ratio, remain constant among all CNS axons. Also, several studies have shown that the presence of a myelin sheath increases the axonal diameter promoting local accumulation and phosphorylation of neurofilament (NF) subunits [18]. On the same axons, adjacent myelin sheaths always belong to different ODCs and mark the borders of small unsheathed regions known as nodes of Ranvier, in which clustered voltage-gated Na^+ channels allow saltatory impulse conductance along the axon. The flanking paranodal axo-glial junction creates an almost impermeable diffusion barrier and is organized by a complex set of adhesion and scaffolding proteins. The myelinated region lying between nodes of Ranvier -hence called internode- is divided into structurally different and functionally specialized domains. During myelination, overlaying contiguous myelin membranes extrude their cytoplasm and become strongly interconnected to form “compact myelin”, mostly responsible for fast neuronal signaling. At the same time, the surrounding myelin is organized in looser loops representing a direct continuation of the ODC cytosol, with a complex system of

microtubules sustaining this metabolically active part of the membrane hosting numerous ion transport channels and enzymatic activities. The underlying cytoarchitecture is incredibly complex, with actin filaments mostly associated to 2'-3'-cyclic nucleotide 3'-phosphohydrolase (CNP-1), a typical ODC marker. Compared to microtubules, which are distributed throughout the cells body and in large myelin processes, actin filaments play a main role during OPC migration, axon targeting and subsequently in thinner membrane domains of the myelin sheath [19].

As reported above, the dry weight of myelin (which has only 40% of water content) is mainly composed of lipids which comprise 32% glycolipids, 26% cholesterol and 42% phospholipids; together, these components account for the physical insulation properties of the membrane. Compared to other biological membranes, myelin is relatively poor in proteins (30% of dry weight), which however comprises countless protein types, the most abundant being proteolipid protein (PLP) and its alternative spliced isoform DM20 (50% of total protein content), myelin basic protein (MBP), myelin associated glycoprotein (MAG), myelin oligodendrocyte glycoprotein (MOG), and CNP. Every myelin protein is specific in function and in the localization between compact or non-compact myelin, with some appearing to be strictly necessary for correct myelination and ODC survival. Among these, mutations in PLP, a cholesterol-binding protein responsible for compaction and stabilization of the membranes, and in MBP, also implied in stabilization of compact myelin, have been shown to result in severe CNS hypomyelination and ODC cell death (see *Oligodendrocyte support of axonal integrity* section).

Oligodendrocyte origin and differentiation

The origin and differentiation of ODCs have been thoroughly investigated (**Fig. 4**). These cells originate as multipotent neuroectodermal $Nestin^{+}$ precursors of the subventricular zone, which mature into postmitotic myelinating cells while migrating to their final destination. ODCs populating the spinal cord originate in two waves: the first from the ventral ventricular zone, which give rise to ODC precursors cells (OPCs) migrating dorsally through the entire spinal cord; the second wave originates from the dorsal spinal cord, and makes up for at least 10% of the ODCs in the spinal cord. In the brain, OPCs initially originate in the medial ganglionic eminence and in the anterior entopeduncular area of the ventral forebrain. Then, a subsequent wave from the caudal

and lateral ganglionic eminences and a final wave within the postnatal cortex complete the OPC population. These developmental waves of cells appear to be functionally redundant, as depletion of one population is compensated *in vivo* by subsequent waves of OPCs. Nevertheless, different waves compete with each other in populating CNS regions in a process regulated by limited amounts of growth factors (as platelet-derived growth factor, PDGF) [20]. For instance, cells from the first wave of forebrain OPCs, possibly an evolutionary relic, are eventually lost from the adult pool.

Newly-produced OPCs must travel long distances to get to their final destination, and this complex migration is aided by direct contact with extracellular matrix components, axons and astrocytes, and soluble factors such as growth factors (among these, PDGF, fibroblast growth factor; FGF, hepatocyte growth factor; HGF), chemotropic proteins (netrins and semaphorins) and chemokines (i.e. CXCL1) [21]. OPC differentiation comprises different stages defined by sequential expression of developmental markers and changes in proliferative capacity, migratory ability, and morphology. The earliest marker specific for the ODC lineage during the neuroectodermal progenitor stage is Olig2, as shown by Olig2-deficient mice which lack completely ODCs. OPCs are kept in an undifferentiated proliferating stage by the steady-state expression of inhibitory factors as Id2, Id4, Hes5, and Sox6. It was shown that the decrease of extracellular inhibitory signals allows the downregulation of these factors and in turns the derepression of the pro-differentiation transcription factors Nkx2.2, Sox10, YY1, Olig1, and TCf4. These players form a complex with the newly-expressed myelin gene regulatory factor (MRF) and lead to a postmitotic myelinating stage. At the same time, intrinsic differentiation control is exerted by chromatin remodeling mechanisms (such as histone deacetylases-driven inhibition of the Wnt/β-catenin pathway) and by microRNAs, with molecules such as miR-219 and miR-338 shown to play pivotal role in the downregulation of the anti-differentiation factors PDGFR, Sox6, and Hes5.

Together with Olig2, Olig1, and PDGFR, the progenitor stage is also characterized by expression of the sulfate proteoglycan NG2 and precedes a stage defined by expression of glycolipids identified by the O4 antibody. In the latter, ODC behaviour changes drastically as loss of cell motility and decrease of the PDGFR-related mitogenic response are observed [22]. Eventually, OPCs maturate into pre-oligodendrocyte and start expressing RIP and the first myelin proteins in CNP-1, GalC, MBP, MAG and PLP. It has been shown that within single ODC processes, the switch from the expression of the early isoform DM-20 to PLP indicates the actual beginning of

myelination [23], with MOG being the last major myelin protein to be expressed [24]. Altogether, the exact timing of myelination is controlled by an intrinsic molecular clock and by external factors such as secreted molecules, axonal surface ligands, and axonal activity. ODC myelination seems to be fairly independent *in vivo* from the activating NRG1/ErbB signaling, which is instead necessary for the myelination process in peripheral Schwann cells [25]. Most of the axonal ligands discovered so far are actually inhibitory, acting to suppress myelination or to actively maintain an undifferentiated state in OPCs. These axonal factors include Jagged, PSA-NCAM, and LINGO-1. An important role in this context is also played by the aforementioned Wnt/β-catenin pathway, which is transiently active in between differentiation from OPCs to mature ODCs. However, while axonal signaling accounts for every step in the differentiation and maturation of Schwann cells in the PNS [26], neurons and neuronal activity seem to be surprisingly dispensable for correct *in vitro* OPC differentiation and myelination, again highlighting the existence of an intrinsic cellular clock. Even so, it was observed that most OPCs express the ionotrophic glutamate receptor as well as voltage gated-ion channels and respond to glutamate input with miniature post-synaptic excitatory potentials. An elegant hypothesis has thus been put forward postulating that firing naked axons could directly influence nearby OPCs and stimulate their differentiation in myelinating ODCs. Also, adenosine released by neural activity seems to have a direct effect in inhibiting OPC proliferation and enhancing differentiation [27], while axonal electric activity has a primary role in the localization of PLP proteins to the myelin membrane by exocytosis [28]. At the same time, astrocytes were proven to be indirectly involved in connecting neural activity to OPC differentiation through their release of leukemia inhibitory factor, an enhancer of ODC myelination, in response to ATP released from nearby firing neurons [29].

Oligodendrocyte susceptibility to damage

ODCs are highly susceptible to oxidative damage. Indeed, the main reason for this sensitivity is the metabolically-demanding maintenance of the myelin membrane, which constitutes approximately 100 times the cell body weight [30]; accordingly, actively myelinating ODCs are even more sensitive. Myelination requires an enormous amount of both oxygen and ATP which can lead to toxic byproducts such as reactive oxygen species, and an intense protein production which increases the risks of protein

misfolding within the endoplasmic reticulum [31] [32]. Furthermore, ODCs show an intrinsic high production of hydrogen peroxide in peroxisomes and constitute the largest sink for iron in the CNS [33], as many myelin-related enzymes require iron as a co-factor. Thus, these aspects and the low concentrations of intracellular anti-oxidative agents (i.e. glutathione) strongly increase the risk of intracellular free radicals, especially under harmful conditions [34].

Oxidative damage in ODCs is known to activate the sphingomyelinase/ceramide pathway, which can be also triggered during injury, infections or inflammation [35]. In these conditions, activated sphingomyelinase enzymatically releases ceramide from sphingolipids within ODCs, thus leading to apoptosis.

Also, cells of the ODC lineage are susceptible to excitotoxic death in that they express NMDA, AMPA, kainate and ATP (P2X7) receptors, and can thus be damaged by high levels of extracellular glutamate or ATP [36] [37] [38]. Furthermore, ODC-specific NMDA and AMPA receptors show structural differences and lack many control features compared to their counterparts in other cells, and can thus be dangerously activated at low potentials [39]. However, with the important exception of the NMDA receptor -possibly playing a role in the neuron/ODC unit-, these receptors are solely express in OPCs and are heavily downregulated after maturation [32].

ODCs can also be damaged by activated astrocytes, reactive macrophages and inflammatory cells (see *Oligodendrocytes and immunity in the sclerotic CNS* section). For instance, ODC degeneration can be caused by inflammatory mediators produced by reactive microglia/astroglia such as oxygen and nitric oxide-radicals (affecting mitochondrial respiration), glutamate, TNFα, and IFNγ [40] [41]. These molecules play important roles in bystander ODC death and demyelination during virtually any CNS disease as ischemic stroke, traumatic injury, radiation necrosis, leukodystrophies and MS, although in the latter case additional adaptive immune destructive mechanisms do take place.

Oligodendrocyte support of axonal integrity

More than mere myelinating cells, ODCs have been proven fundamental also for functional integrity and long term survival of axons. This aspect has been investigated in different transgenic animal strains and is important in the understanding of human diseases such as MS (see *Multiple sclerosis* section) and inherited leukodystrophies of the CNS. In these pathologies, prolonged demyelination is associated with neuronal

death and thus contributes to the accumulation of clinical disabilities [42]. Leukodystrophies arise in patients carrying a mutated ODC-related gene and include different pathologies such as Pelizaes-Merzbacher disease (PMD, *PLP-1* mutations, myelin gene), PMD-like disease (*GJC2* mutations, gap junction protein), Canavan disease (*ASPA* mutations, aspartoacylase enzyme), X-linked adrenoleukodystrophy (*ABCD1* mutations, peroxisome gene), and metachromatic leukodystrophy (*Arylsulfatase A* mutations, myelin enzyme).

The characteristic ODC dysfunctions in these pathologies lead to myelin degeneration which deprives axons both of electrical insulation and of a physical barrier isolating them from the CNS environment. Therefore, naked axons become extremely vulnerable to matrix metalloproteinases (MMPs) produced by inflammatory infiltrates and to the diffusion of nitric oxide (NO) produced by activated microglia, which leads to a perturbation in mitochondrial ATP generation [43]. Mere demyelination can lead to neuronal distress even in the absence of inflammatory components: the absence of insulation itself leads to a drastic redistribution of axonal voltage-gated Na^+ channels, thus resulting into higher energy consumption. In this scenario, an energetic threshold can be reached in which Na^+/Ca^{2+} exchangers would reverse direction of ionic flow, thus filling the axon with Ca^{2+} ions and leading to mitochondrial impairment followed by Wallerian-like axonal degeneration. This may trigger a vicious circle in which sudden glutamate release from degenerating axons leads to glutamate excitotoxicity in ODCs and additional neurons.

However, some transgenic mice show that myelin absence *per se* does not necessarily lead to neuronal death. In the *shiverer* mouse strain, resulting from a major deletion in the *MBP* gene, axons are generally enwrapped by few non-compacted myelin layers and many large-caliber axons remain virtually unmyelinated. However, in this mouse model normal ODC survival and no neuronal loss were described, even in the presence of higher mitochondrial numbers in the unsheathed axons [44]. Evidently, axonal survival can be maintained by surviving ODCs without the support of properly formed myelin. Interestingly, it has been observed that some minor myelin abnormalities which do not lead to demyelination can actually cause neuronal impairment and death. In the *PLP-1* null mouse, electrical conductance is normal and minor myelin alterations are solely detectable by ultrastructural analysis. However, after few months these mice show reduced axonal transport and subsequent neuronal degeneration in the presence of a physically stable myelin. Mice carrying a mutation in the *CNP-1* gene show a similar

albeit faster clinical pathology: after exhibiting an apparently normal developmental myelination, a degeneration in the paranodal junctions leads to axonal defects and neuronal death. Evidently, axonal impairment does not solely rely on the missing insulation properties of myelin but most likely on unclear fine changes in cell-to-cell signaling.

In this respect, the complete scenario of interactions and mutual communications between ODCs and neurons is far from being understood. 99% of the axonal surface are covered by internodes which deprive the neuronal surface of free exchange of metabolites; consequently, ODCs must be the main players in defining the extracellular milieu suitable to the axon. It has also been postulated that active diffusion of metabolites and specific transporters would play a role in this cellular interplay. From this perspective, ODC dysfunctions could account for neuronal impairment also in classic neurodegenerative disease (i.e. Alzheimer), and as such should be investigated in human patients and animal models [42].

The immune system

The immune system is composed by many interdependent cell types that protect the body from external pathogens and from the growth of tumor cells. Every cell in the system shows different highly-specialized functions such as bacteria engulfment, killing of parasites, depletion of infected and degenerated cells, and fine functional regulation of other cell types. The immune system can be broadly divided into two effector arms: an innate arm, which include cells able to immediately respond to harmful elements through the recognition of common pathogenic molecules, and an adaptive arm, including cells (such as lymphocytes) which are highly specific towards a particular antigen and able to confer long-lasting protection to the host through the development of an immunological memory. Regardless of their functions, all cells of the immune system derive from bone marrow stem cells in a process called hematopoiesis (**Fig. 5**). In this, while most cells (for instance B cells) mature directly within this organ, others (i.e. T cells) migrate elsewhere to maturate further. In the thymus, T cell precursors undergo a complex multistep maturation while being tested for correct expression (positive selection) and specificity (negative selection) of their T cell receptor (TCR) (**Fig. 6**). Antigen specificity, and activation of T cells, relies on specific TCR recognition of a target antigen presented in the context of MHC-I (for $CD8^+$ cytotoxic T cells) and MHC-II (for helper $CD4^+$ T cells) molecules (**Fig. 7**). In this fine selection

process, dangerous T cells which are able to recognize self antigens with high affinity and hence to trigger autoimmune inflammation are forced to undergo apoptosis and thus removed from the effector pool. While in primary immune organs such as thymus and bone marrow this selection process is mediated by local specialized parenchymal APCs, naïve and mature circulating lymphocytes are able to recognize their cognate antigens only when presented by professional APCs as B cells, macrophages, and dendritic cells.

Immune-privilege in the CNS

The importance of the immune system is evident in immunodeficiency disorders, pathologies characterized by the absence of certain cellular components or by defective functioning of immune cells and inflammatory cascades. Nonetheless, along animal evolution certain organs have developed a striking resistance to the development of inflammation, a quality called “immune privilege”. The concept of an immune privilege of the CNS dates back almost one century to the first experiments of tumor grafting from the rat to the mouse brain: while the transfer of foreign tissues would result into immediate local inflammation and graft rejection in most organs, the mouse brain showed a surprising lack of inflammation. The absence of an immune-mediated rejection showed that the CNS was somehow disconnected from the peripheral immune system, a finding confirmed through several additional experiments of tissue grafting and viruses, vectors, and bacteria administration. In parallel, the concept of a BBB protecting the CNS grew strong and the two findings reinforced each other resulting into a scientific paradigm that has been only recently revised and redefined [45]. From an evolutionary perspective, the immune privilege represents an adaptive advantage in protecting delicate and essential organs from the detrimental consequences of acute and chronic inflammation. As such, it is extended to testicles, eyes, and placenta. The immune privilege of the CNS is actually limited to the sole parenchyma: intraventricular or meningeal administration of pathogens or tumors trigger a normal and sustained adaptive immune response. In fact, these extra-parenchymal CNS areas are constantly surveyed by APCs: macrophages and dendritic cells are present both in choroid plexus and meninges, and perivascular macrophages surround small and medium-size blood vessels displaying phagocytic and immune regulatory functions [10]. On the contrary, the uninflamed parenchyma seems to be devoid of APCs (in particular dendritic cells) able to bear antigens from an immune-challenged CNS to peripheral immune organs such as lymph nodes (LNs) and spleen; even during CNS

inflammation, no evidence of APCs migrating to peripheral organs could be found. Antigen-specific lymphocyte activation might thus happen *in situ*, as shown by the formation of follicle-like structure in the less-immune-privileged meninges. Nonetheless, even though devoid of cellular routes of antigen drainage, the CNS constantly allows the passage of soluble antigens to the periphery. Interstitial parenchymal antigens can reach the cerebrospinal fluid (CSF) along the artery walls, and from there the spleen through the arachnoid villi and the venous sinuses; furthermore, a continuous albeit limited lymphatic flow reaches the deep cervical (dp) lymph nodes from the brain area and the lumbar lymph nodes from the spinal cord [46].

Several other mechanisms exist to avoid sustained inflammatory damage to the CNS. The main barrier towards the establishment of immune reactions within the CNS is the expression level of MHC-I and MHC-II molecules: at steady state, all cells express very low levels of MHC-I and virtually no CNS cell express MHC-II molecules. Astrocytes actively suppress the effector functions of activated T cells through cytokine signaling and are able to induce direct apoptosis through FasL-Fas interaction (as neurons do), while microglia express co-stimulatory molecules as B7-H1 which negatively impact T cell activation. Also, an elegant study by Liu et al. [47] has recently shown that neurons possess the faculty to skew activated T cells into suppressive regulatory T cells (Tregs) in a TGFβ-dependent manner. Lastly, the already described BBB limits the entry of solutes and ions and allows a tight control over cell migration. Altogether, the CNS possess a strongly anti-inflammatory environment which limits the detrimental effects of immune reactions while decreasing drastically the potential benefits of neuroinflammation in pathogen clearance and repair (**Fig. 8**). The reasons for this compromise are clear: once immune cells are effectively primed towards CNS antigens, the immune privilege is lost and inflammation sets in along with sustained tissue destruction. This scenario is best reflected in the CNS of MS patients.

Multiple Sclerosis

MS is a chronic inflammatory and demyelinating disease of the CNS with largely unknown etiology and no effective cure. The symptoms of the disease are diverse, but include tremor, fatigue, and paralysis [48]. The first description of MS dates back to 1868 with clinical observations by Jean-Martin Charcot. Nowadays, MS represents the most common neurological disorder in young adults in particular in northern Europe,

North America and southern Australia, affecting more than two million people worldwide with a prevalence ranging between 2 and 150 : 100.000 [49]. Disease initiation is commonly associated with early adulthood and is more common in females, with a 2 to 1 female/male ratio among patients [48]. Under the definition of MS lie a series of clinically heterogeneous pathologies which can broadly be divided into a more common relapsing-remitting (RR) form (80% of patients), characterized by episodic disease progression, and a primary progressive form, with disabilities slowly accumulating over time. Often, the RR form develops into a secondary-progressive stage characterized by absence of remitting phases.

Histopathologically, MS presents with large, multifocal demyelinated lesions scattered throughout the CNS. These lesions are known as sclerotic plaques [50]. They are usually detected by gadolinium-enhanced T1-weighted or T2-weighted MRI analysis, which are the most common non-invasive diagnostic tools for MS (**Fig. 9**). In affected areas ODC death and axonal degradation, gliosis, and activation of microglia are observed [51, 52] and perivascular and parenchymal accumulation of T cells, B cells and macrophages [53] are found (**Fig. 9**). Such inflammatory infiltrates are thought to reflect an immune response against the CNS, especially myelin antigens, resulting in the disruption of the myelin sheath. Oligoclonal bands in chromatograms of cerebrospinal fluid from patients indicate antibody production within the CNS, possibly targeted towards myelin antigens [54]. Genetic linkage analysis identified several genetic regions belonging to the immune system with HLA-DR loci as major and IL2RA and IL7R loci as minor risk factors for MS [55-57]. At the same time, increased susceptibility was also associated to CNS-specific genes as GalC and a neuronal kinesin [58]. In summary, these observations suggest that MS is an autoimmune disease targeting an hypothetically inflammation-prone CNS. The targets of this detrimental adaptive response seem to be CNS antigens which are normally segregated from the peripheral immune system within the immune-privileged parenchyma. Myelin-reactive T cells are found in blood, CSF and brain tissue of patients. It is believed that these autoreactive lymphocytes evade the thymic negative selection process thanks to weakly-binding self-reactive TCRs. As possible activating mechanisms, molecular mimicry and bystander activation upon infection have been suggested [59]. In the latter scenario, pathogen-triggered chronic activation of lymphocytes and APCs would result into upregulation of co-stimulatory molecules, release of inflammatory mediators, and in turn to random bystander activation of self-reactive T cells. The concept of molecular

mimicry is based on the promiscuity of TCR specificity. Pathogenic components of virus and bacteria "mimicking" self peptides could thus activate autoreactive T cells as has been shown *in vitro* for several MBP-reactive T cell clones. The list of common pathogens candidates for disease initiation includes Epstein Barr virus, herpes simplex virus, and *Chlamydia pneumonia* [60], although up to now none of these could be causally linked with the pathoetiology of MS. Despite the activation trigger is still unclear, the mechanism of T cell invasion in the CNS parenchyma has been intensively studied. Different lymphocyte adhesion molecules have been implicated in MS and among these very late antigen 4 (VLA4) and lymphocyte-function associated antigen (LFA-1) with their binding partners VCAM1 and ICAM1 on the vascular system. These molecules are highly upregulated on the blood vessels of MS patients and are held responsible for the perivascular accumulation of lymphocytes. Accordingly, one of the most effective drugs in MS therapy, natalizumab, binds to VLA-4 thus inhibiting T cells invasion and resulting in a good amelioration of clinical conditions [61]. After perivascular accumulation, extravasation of inflammatory cells to the CNS through a disrupted BBB is aided by release of MMPs and by unbalances in the regulatory elements called "tissue inhibitors of MMPs" (TIMPs). MMPs are produced by a variety of cell types including monocytes, macrophages, endothelial cells and are used in the healthy CNS by parenchymal glial cells for plasticity and repair [61].
Following accumulation and CNS invasion, activated T cells and blood-derived macrophages can cause ODC damage through different mechanisms.

Oligodendrocytes and immunity in the sclerotic CNS

Evidence that ODCs are heavily depleted within sclerotic lesions dates back to the first comprehensive literature regarding MS; since then, ODC absence and demyelination are considered hallmark features of the disease [62]. Whether demyelination can be uncoupled from cell death is however still unclear. Several reports indicate ODC survival within heavily-demyelinated sclerotic lesions, often in close proximity to myelin-containing macrophages [62]. A dutch study of post-mortem CNS tissues went further in showing that demyelinated adult MOG^+ cells could survive *in situ* after immune attack [63]. Other reports indicate the existence of phenotypically "hyperplastic" ODCs which are engulfed by reactive astroglia in a process called "emperipolesis", possibly representing a peculiar protective mechanism [62]. Nevertheless, the majority of ODCs within sclerotic plaques die. In this, different

mechanisms and cellular mediators could account for the destructive process and include macrophages and microglia, astrocytes, and different lymphocyte subsets among which γδ T cells, $CD4^+$ T cells, $CD8^+$ T cells, and B cells (**Fig. 10**).

The first demonstration of a humoral component in the pathology of MS dates back to 1964 [64], when it was shown that MS sera were capable of triggering demyelination in organotypic CNS slice cultures through the induction of ODC lysis in a IgG dependent-manner [62]. Also recent histopathological investigations seem to indicate antibody-mediated demyelination as a common pathogenic mechanism in chronic MS, as shown by the high and consistent presence of $Fc\gamma^+$ phagocytic macrophages within demyelinating plaques. At the same time, diffuse presence of complement and antibody suggests that antibody- and complement-mediated demyelination play an important role [65]. Thus, B cell activation seems to be a destructive hallmark of the disease. As for T cells, many different subtypes seem to play a role in a complicated interplay which is still somewhat elusive. For instance, γδ T cells have been implicated in perforin-dependent lysis of ODCs *in vitro* and *in vivo* within MS lesions. Clonal expansion of cytotoxic $CD8^+$ T cells was demonstrated in lesions, blood and CSF, and ODCs are shown to express MHC-I in animal model of CNS inflammation and in MS. On the contrary, MHC-II expression by ODCs, -controversially reported in some *in vitro* ODC cultures [66]- has never been proven *in vivo* [67]. Nonetheless, $CD4^+$ T helper 1 cells can activate surrounding APCs to release pro-inflammatory mediators and thus indirectly harm ODCs. A possible reason for the sustained activation of pro-inflammatory T cells can be found in impairment in Tregs, which displayed a lower *in vitro* ability to suppress activated T cells when isolated from MS patients [61]. In this delicate balance among lymphocyte subsets, $CD4^+$ T helper 2 cells can have beneficial effects through the release of anti-inflammatory mediators as IL4, IL10, and IL13 (**Fig. 8**). Accordingly, different drugs used in MS clinical testing (as glatimer acetate) have proven that clinical amelioration and reduction of relapses in patients is associated with skewing of the immune balance towards T helper 2 cells instead of T helper 1 cells.

As already mentioned, also microglia can participate in tissue destruction and demyelination. For instance, ODCs in MS lesions overexpress the death receptors for TNFα, TNFβ (Lymphotoxin, LT), and Fas, while reactive microglia in proximity express high levels of FasL, LTs, and TNFα. Although this overexpression of death mediators is considered a mechanism to deplete Fas-expressing lymphocytes in the

inflamed CNS (apoptotic lymphocytes have in fact been reported several time in MS), this could also clearly result in ODC death [44]. Furthermore, activated by lymphocytes *in situ*, microglia (and astrocytes) can trigger demyelination also through the release of reactive oxygen and nitrate species within MS lesions. Lastly, astrocytes can indirectly harm ODCs through an unbalanced glutamate reuptake from synapses which can result into ODC excitotoxic death. Altogether, countless demyelinating mechanisms exist within the inflamed CNS.

However, ODCs are not only passive targets of tissue destruction. In the presence of inflammatory mediators and within ischemic/hypoxic environments, ODCs have been shown to upregulate factors of hypoxic preconditioning as HIF1α, HSP70 and HSP32, thus showing the activation of intrinsic protective mechanisms in response to inflammation. Also, ODCs can express several growth factors as IGF-1, NGF and TGFβ, all shown to be protective in different models of MS. Interestingly, ODCs in the context of the normal-appearing white matter (NAWM) of MS patients upregulate components of the STAT6 pathway as STAT6, JAK1, IL4R, and IL13R, better known for their necessary function in the anti-inflammatory T helper 2 subset, and chemokines as CXCL10, CCL2, and CCL5 after stimulation with IFNγ [67]. Altogether, it seems that ODCs are able to condition the surrounding environment and can possibly act as immunomodulators. Thus, these cells can play a role in limiting inflammatory responses and damage.

Is MS a primary neurodegenerative disease?

In the last decade, histopathological analyses have suggested that neurodegenerative mechanisms independent of inflammation are responsible for some aspects of MS pathology. Although ODC degeneration is a hallmark of the disease, reports of apoptotic ODCs are highly controversial along the history of MS research and different laboratories have challenged the idea of widespread ODC apoptosis in MS, considering these events as a minor aspect of the disease [44]. However, a study from Barnett and Prineas has recently proposed ODC apoptotic death as the first pathological event in the formation of MS plaques [68, 69]. This assumption was based on several autoptic histological analyses from MS patients who died shortly after the onset of their last relapse. These “early stage” plaques revealed extensive death of ODCs in the presence

of reactive microglia, with basically no infiltration of blood-derived inflammatory cells (**Fig. 11**). Consequently, a hypothesis has been put forward proposing MS to be a primary neurodegenerative disease in which secondary adaptive immune involvement develops. In support of such a scenario it was observed in MRI studies that subtle focal changes in the white matter can be observed weeks before a classical new lesion is formed [68, 70, 71]. Although these studies put an autochthonous degenerative process at the beginning of the disease, it remains unclear how primary loss of ODCs induces inflammation. Normally, apoptotic material is considered to have immunosuppressive properties and is rapidly removed [72]. Despite this, it has been suggested that extensive apoptotic death can overwhelm the clearance of dead cells, allowing immune recognition of exposed autoantigens [73] and thus causing the development of autoimmunity [74-76]. In this etiological scenario, MS may start with autochthonous ODC death resulting in microglia/macrophage activation and antigen leakage into CNS-draining LNs. Myelin-derived antigens presented in the periphery by APCs, that might have received additional inflammatory/danger signals, would lead to clonal expansion of CNS-reactive T cells. These could finally invade the CNS and drastically amplify myelin damage (**Fig. 12**), leading to full immunity-driven MS. In order to model this hypothesis, we have developed the oDTR mouse model of inducible ODC death (see *Results*). However, other animal systems exist in which ODC death and demyelination play a primary role, and are briefly summarized in the following section.

Animal models of demyelination and neuroinflammation

To understand the processes of neuroinflammation and demyelination, several animal models of chemically-induced or immune-triggered ODC depletion have been developed over the years (**Fig. 13**). Among the chemically-induced ones, administration of the toxin bis-cyclohexanone oxaldihydrazone (cuprizone) in C57/BL6 mice at 6–8 weeks of age results in localized dysfunctions affecting primarily the corpus callosum and cerebellar areas (superior peduncle). In these areas, extensive demyelination along with ODC death, microglia activation with engulfment of myelin, and gliosis are observed, with virtually all local neurons showing naked axons and 90% of mature ODCs depleted from the areas within 3 weeks of toxin feeding. Cuprizone is a copper chelator and has been shown to impair the activity of mitochondrial enzymes such as cytochrome oxidase and monoamine oxidase, thus resulting into mitochondrial

dysfunctions and subsequent disturbances in energy metabolism. It is still unclear why cuprizone uptake results in specific death of ODCs, but the already discussed metabolically-demanding maintenance of the myelin membrane might be responsible for the selective depletion. Cuprizone intoxication does not activate the peripheral immune system. This was clearly shown by the absence of an adaptive anti-CNS immune response and by a comparable demyelination pattern in immune-deficient animals [77] [78].

Other chemically-induced demyelination models include ethidium bromide (EtBr) injection and lysolecithin administration. Following surgical preparation, a 0.01–0.1% solution of EtBr can be stereotactically injected into the thoraco-lumbar dorsal funiculus of the spinal cord or in the caudal cerebellar peduncle causing local acute demyelination within 48 hours. EtBr can also be injected in the subarachnoid space of Sprague–Dawley or Wistar rats thereby causing demyelination of the optic nerves and the chiasm. The size of the lesion and the timing of demyelination depend both on drug concentration and injection volume. As EtBr is an intercalating DNA agent, the lesion extends to other local cell types such as astrocytes, which are strongly depleted within the lesion.

Lysolecithin is a detergent-like membrane solubilizing agent that can be stereotactically injected into the CNS as a 1% solution. Lysolecithin administration results into demyelinating lesions in adult mice or rats, with local myelin completely removed 7 days after lesion trigger [79, 80]. No death of astrocytes or axons is observed in this demyelinating model, and most OPCs are spared during lesion production [81].

While all these models do not result into a strong activation of the immune system, proper investigation of anti-CNS immunity has been aided by the animal model experimental autoimmune encephalomyelitis (EAE). EAE is induced through subcutaneous injection of myelin self-peptides belonging to the proteins MOG [82], MBP [83], or PLP [84] mixed with bacterial adjuvant (Complete Freund Adjuvant, CFA) in susceptible animal strains [85]. In addition, the concomitant administration of pertussis toxin (PT) is often used to enhance disease incidence and severity.

EAE originates from Pasteur's experiments with rabies vaccination in the late 19th century. The first injections of the vaccine, constituted by spinal cord extracts from rabies-infected rabbits, resulted in protection from rabies while affecting a small proportion of patients with a progressive ascending paralysis [86]. Years later, the association between this severe side-effect and a immune response was found and the

administration of CNS lysates together with CFA started to be a classical approach for studying demyelinating diseases such as MS. The latter and EAE have in common the presence of multiple white matter lesions and their perivascular localization, the presence of immunoglobulins, the timing of demyelination, and the destruction of myelin sheaths with relative preservation of neuronal structures. The pathogenesis and pathology of EAE vary considerably depending on the animal model and on the immunogenic peptide used. After EAE induction through sub-cutaneous myelin peptide and adjuvant applications, auto-aggressive T cells are first activated in the periphery where they become encephalitogenic. Subsequently, these pre-activated cells migrate to the CNS where they must be re-stimulated through binding of their cognate antigen on local competent APCs, finally initiating inflammatory cascades leading to tissue destruction. During EAE, death of ODCs is widely observed and seems to be partially responsible for demyelination and axonal death [87]. However, the mechanisms behind this degeneration are still not well defined, and both necrotic and apoptotic processes seem to be implicated [88, 89].

EAE has been fundamental in the understanding of different aspects of immune activation, tissue destruction, and in the development of some anti-inflammatory MS therapies (such as natalizumab or glatimer acetate). However, most promising drugs elaborated from EAE studies have failed clinical application. The conundrum of EAE efficacy in designing drugs to treat MS is exemplified by IFNγ treatment, which showed a protective role in EAE but strongly aggravated disease when administrated in MS patients [90]. Also, EAE studies mainly lead to the development of anti-inflammatory therapies, which are not efficient in the treatment of progressive forms of the disease characterized by low inflammation. Thus, albeit the most used MS model up to date, EAE is far from recapitulate the human disease and, being an inducible model, it also cannot be used to investigate the triggering phase of the pathology. In my opinion, these severe limitations should encourage the development of better models in the future of MS research.

Remyelination

Myelin destruction in the CNS naturally leads to remyelination, a process in which *de novo*-produced myelin enwraps demyelinated axons restoring saltatory conduction and

resolving functional deficits. The first evidence for this process was given in 1961 by the Bunge group, which showed that remyelination was ultrastructurally similar to developmental myelination [13]. More precisely, remyelination enwraps naked axons with a thinner and shorter myelin layer that the one built-up during primary myelination. Since this event results in an increased axonal g-ratio, the latter constitutes an important tool allowing investigators to distinguish normally myelinated versus *de novo* remyelinated axons in the context of demyelinating disorders. However, the mechanisms behind this structural difference are still unclear [43].

Remyelination has been thoroughly studied in different animal models of demyelination. Synthetically, these studies showed that the process is quite efficient and that is able to restore complete functionality in an age-dependent manner [43]. In the cuprizone model, spontaneous remyelination is evident starting 6 weeks p.a., and removal of the toxin from the diet results into complete lesion remyelination within 3 to 4 weeks. Spontaneous remyelination also occurs in the EtBr and lysolecithin demyelination models, with tissue repair becoming extensive 3 months following lesion production in the EtBr model, and being slightly faster following lysolecithin administration [81].

Importantly, remyelination seems to be less effective in the inflamed CNS of the EAE model and in human MS. In the latter disease, complete remyelination is observed in many early acute lesions but tissue repair becomes utterly insufficient as lesions become chronic, thus resulting in the accumulation of clinical disabilities (see *Oligodendrocyte support of axonal integrity* section).

Remyelination is performed by newly-matured ODCs derived from the OPC pool, which is constituted by highly frequent cells (9% of parenchymal cells) homogenously distributed between white and gray CNS matter, and characterized by the expression of NG2 and PDGFRα markers [91-94]. OPCs can also derive directly from the stem cell pool of the SVZ, as it was shown for cells from different precursors stages which could migrate to the injured corpus callosum and start a remyelination program *in situ* [21, 95]. Also, the latter process seems to have relevance for human pathologies as it was observed that cells in the SVZ display higher rates of proliferation and increased number in MS patients compared to controls [43]. OPC activation, migration and proliferation strongly rely on astroglia- and microglia-derived factors as IGF-1, FGF and PDGF. These lead to a phenotype switch in which several genes related to developmental myelination become upregulated. Nonetheless, the developmental

production of myelin was proven to differ consistently from the remyelination process, with Notch and Olig1 proven dispensable for the latter. Also, inflammation plays a primary role. The presence of activated phagocytic cells as microglia and macrophages seems to be essential as it results into local production of inflammatory mediators like IL1β, TNFα, LT, and MHC-II, all proven to be important for remyelination efficiency [43]. Moreover, chemically-induced demyelinating models clearly show that macrophage- and microglia-mediated removal of myelin debris is essential before repair [96], as presence of myelin seems to strongly inhibit the repair process both *in vitro* and *in vivo*.

However, despite extensive inflammation, remyelination fails in chronic MS. This phenomenon cannot be explained by mere lesion area, insult chronicity *per se*, and failure in OPC activation and recruitment, as several studies have consistently proven a diffuse presence of OPCs within areas of demyelination. Rather, remyelination failure could be attributed to the properties of the chronic lesions, with the hypothetical presence of myelination-inhibitor factors and absence of pro-remyelination factors. Accordingly, chronic lesions show a much lower inflammatory activity than acute ones and produce less pro-remyelination inflammatory mediators [43].

As for mature ODCs, their remyelination capability is still unclear. Earlier observations in MS lesions seemed to show some degree of mature ODC proliferation within remyelinating areas [97], and *in vitro* ODCs were shown to regenerate damaged myelin processes and to display some degree of migratory capability after maturation [97]. Mature ODCs have also been shown to extend their processes and to produce some myelin membranes, albeit in a limited fashion and never directly enwrapping axons [93, 98]. Altogether, these observations support an interesting hypothesis in which *in vivo* mature ODCs would maintain a certain degree of structural plasticity possibly enhanced within CNS pathologies. Nonetheless, several studies failed to prove this point and transplanted mature ODCs were shown to lack the ability for tissue repair in different experimental approaches [91, 99, 100] [101]. Thus, although still a matter of debate, several evidences show that remyelination in the CNS is performed by the sole OPC pool.

IGF-1 functions in ODCs and demyelinating diseases

The IGF-1/IGF1R signalling pathway is one of the main players in controlling cells of the ODC lineage. Its involvement in myelination and neuroprotection has been under investigation for several years. IGF1R has three natural ligands in IGF-1, IGF-2, and insulin, although the last two molecules bind with extremely low affinity to the receptor [102]. The latter is expressed by virtually all resident cells of the CNS and by invading inflammatory cells as macrophages and lymphocytes. In the periphery, IGF-1 is under the control of growth hormone and is mainly produced by the liver. In the CNS, IGF-1 is mostly produced by ODCs, microglia, and astrocytes in a paracrine manner. IGF1R is a member of the transmembrane tyrosine kinase family and it comprises two αβ subunits linked together by disulfide bonds. In this structure, the α subunit provides an extracellular binding site for the ligand while the β subunit comprises an intracellular site for tyrosine autophosphorylation upon ligand binding [103]. Activation of the receptor results in recruitment of the Irs-2 binding protein and in intracellular signalling cascades which can involve Ras/MAPK, PI3K/Akt, and mTOR pathways. Interestingly, IGF-1 signalling is tightly regulated by a complex homeostatic system of IGF-binding proteins (IGFBPs) and IGFBP-proteases, which regulate factor stability and localization [102].

During development, IGF-1 and IGF1R are widely expressed throughout the CNS [104, 105]. It was shown that transgenic IGF-1 overexpression promotes myelination in development [100, 106-108], while absence of the receptor on ODC progenitors led to hypomyelination and reduced brain size [101]. It is, however, currently unclear whether IGF1R signalling in ODCs is also a requirement for successful remyelination after myelin damage. Recently, several groups showed that IGF-1 acts as a post-traumatic neuroprotective and myelogenic agent [106, 109-113], although in other studies [101, 114] such an effect was not observed. IGF-1 signalling has been implicated in enhanced survival in virtually all cell types. In the CNS, IGF-1 is strongly neuroprotective in animal models of ischemia, axotomy, age-induced hippocampal neuronal death, dopamine-induced granule cell death, cortical neuron apoptosis by serum deprivation, and glutamate-induced motor neuron apoptosis [115]. Also, IGF1R was shown to directly protect immature ODCs from apoptosis *in vitro* [116] and *in vivo* in different experimental conditions as TNFα-induced injury and cuprizone-mediated intoxication [106]. In the latter model, cuprizone-induced ODC death triggers *per se* IGF-1

upregulation in the surrounding parenchyma [117-119]. IGF1R signalling may also play an important function in MS, as surviving ODCs surrounding sclerotic lesions upregulate IGF1R and IGF-1, indicating a role of this pathway in response to inflammatory demyelination [120]. However, in the EAE model, the role of IGF1R on ODCs is hotly debated because of the contrasting results published in literature. While some works show that expression of IGF-1 in the CNS failed to protect mice from EAE [121], or even worsened the disease [114], other reports [122] [113] [123] showed transient clinical amelioration and slightly improved remyelination during acute EAE. Yet another study [124] showed reduction of number and area of demyelinating EAE lesions. Nonetheless, none of these studies displayed cell-specific deletion of IGF1R or specific delivery of the growth factor to certain cell types, thus preventing the reader from drawing any specific conclusion. In fact, since IGF1R plays a role in most cell types in EAE, and it was shown to exert important effects on encephalitogenic T cells and activated glia [125], data interpretation in the absence of specific genetic manipulations becomes virtually impossible. Thus, new animal models bearing deletions of IGF1R on distinct cell types would allow better understanding of this signaling pathway in ODCs, both in steady state and under demyelinating stress.

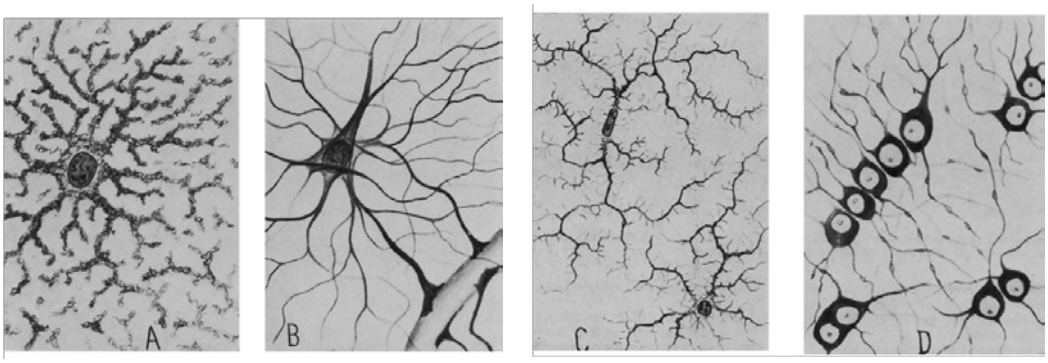

Fig.1 – Del Rio-Hortega's four types of glia.

A: Gray matter protoplasmic neuroglia. B: White matter fibrous neuroglia. C: Microglia. D: White matter interfascicular glia (ODCs)

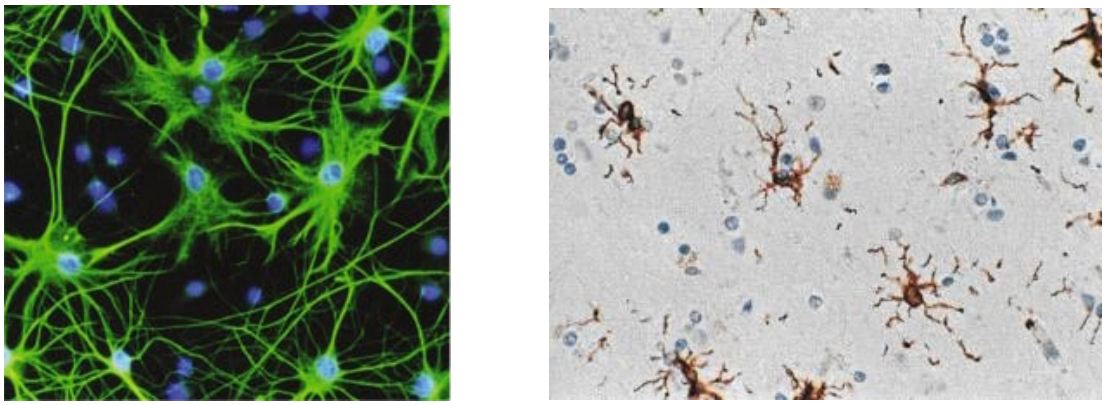

Fig.2 – Astrocyte and microglia morphology.

On the left, GFAP-specific immunostaining (green) and DAPI nuclear staining (blue) show the typical appearance of parenchimal astrocytes. On the right, Iba1-specific staining (brown) depict the ramified morphology of resting microglia.

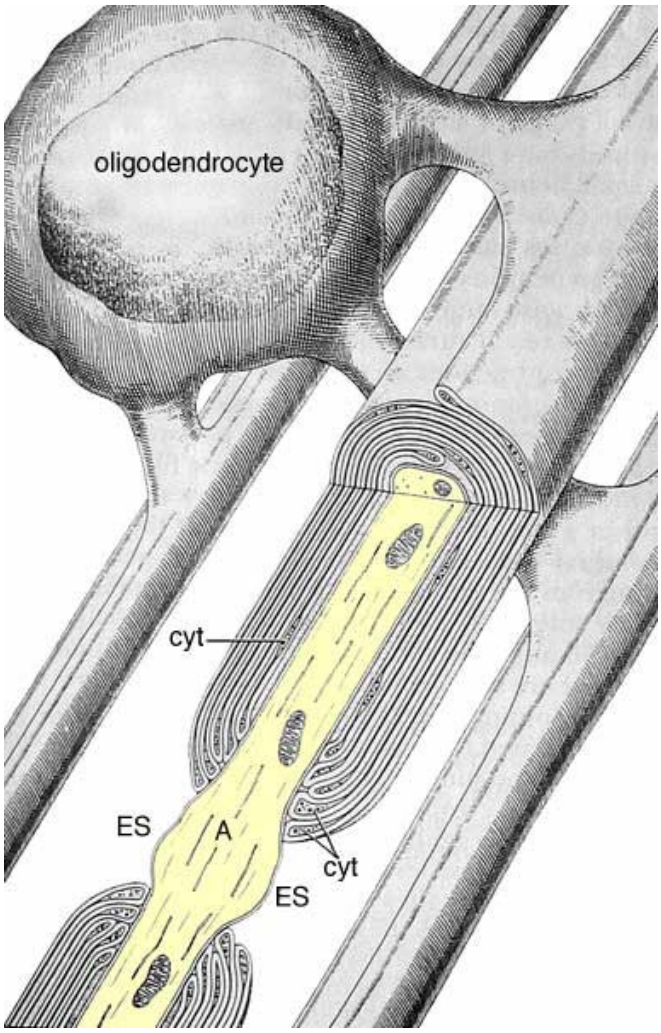

Fig.3 - Visual representation of an oligodendrocyte.

The cell is wrapping different axons (A) in between nodes of Ranvier, the only axonal regions in which the extracellular space (ES) is accesible to neurons. Note the multi-layered disposition of the myelin sheath and the small cytosolic content (cyt) within the wrapping membranes.

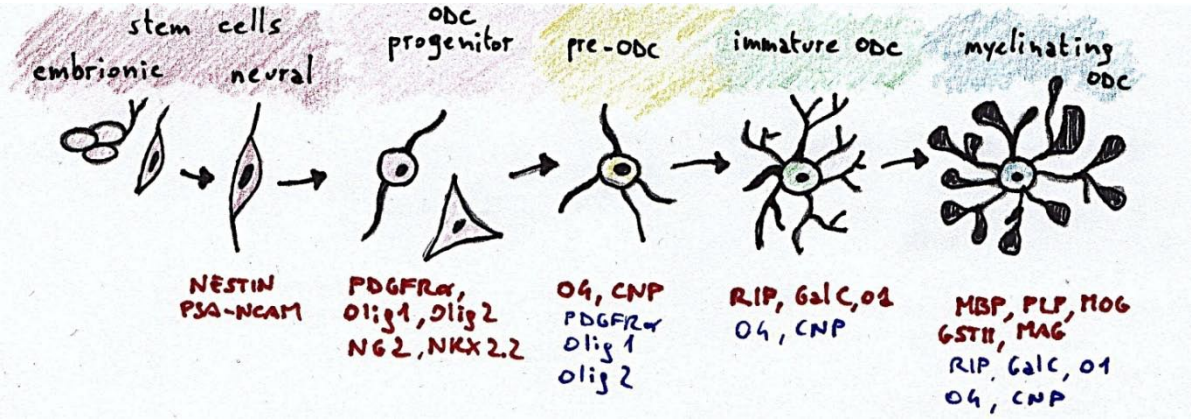

Fig.4 – Cell differentiation in the ODC lineage

Different stages in ODC differentiation are here depicted with the main markers expressed per cellular stage.

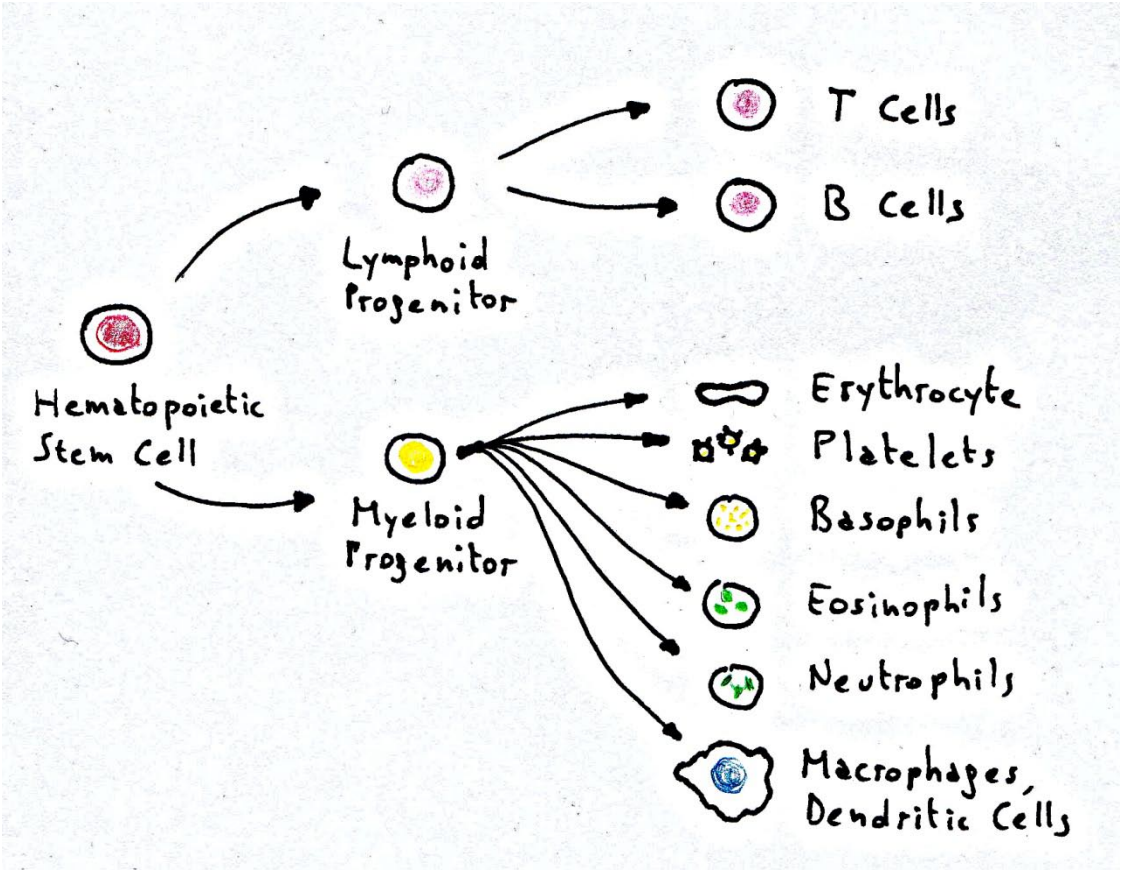

Fig 5 – Hematopoiesis.

Here represented the process of hematopoiesis, which illustrates the development of the immune system from a common bone-marrow precursor named hematopoietic stem cell (HSC). HSCs develop further into a lymphoid and a myeloid progenitors, which give respectively rise to the premature cells of the adaptive and the innate arms of the immune system.

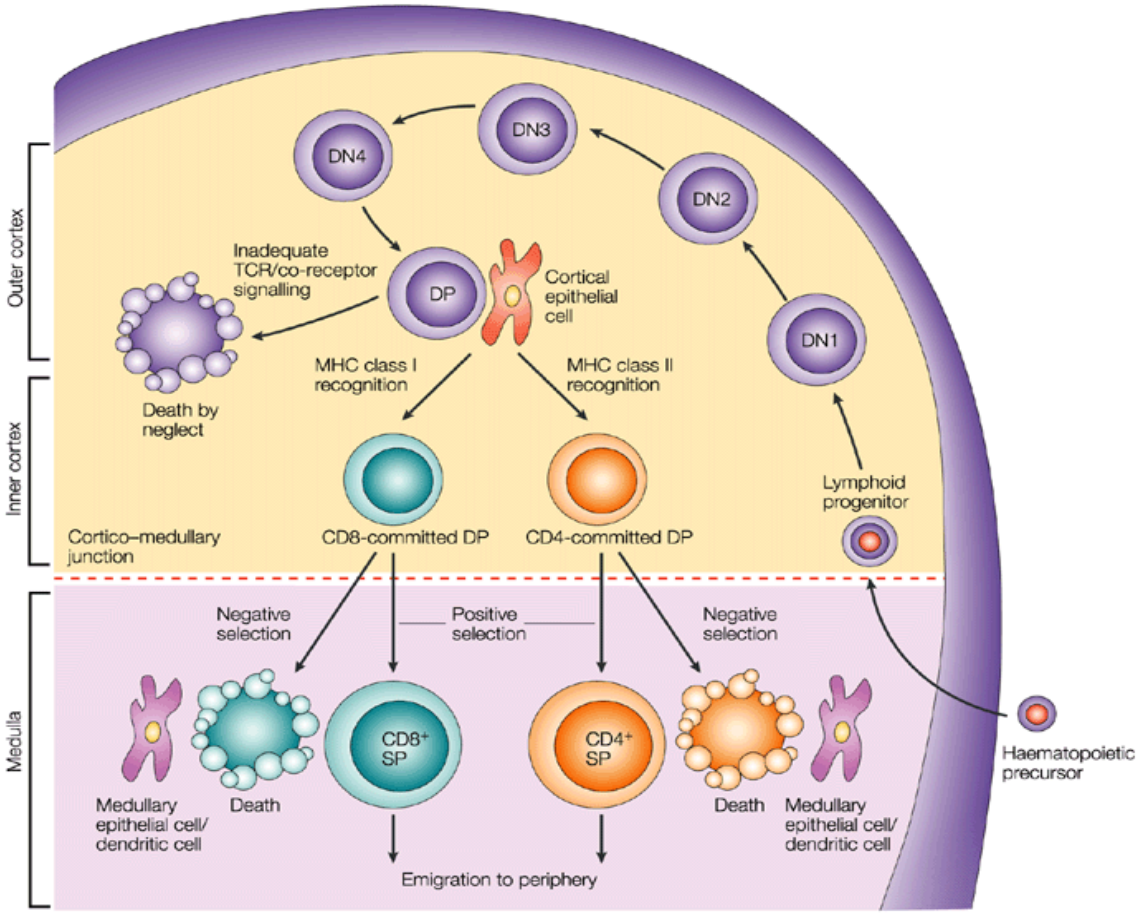

Fig.6 – Positive and negative T cell selection in the thymus.

Pre-T cells continue their development from lymphoid precursors migrating from the bone marrow to the thymus. Within the latter, different developmental "double negative (DN)" stages precede the expression of a TCR in the "double positive (DP)" CD4+ CD8+ stage and the following positive selection by cortical epithelial cells in the thymic cortex. Surviving cells procede to a single positive (SP, either CD4+ or CD8+) stage in which they are tested for autoreactivity in a negative selection exerted by medullary dendritic cells. Only surviving thymocytes can migrate to the periphery as naïve T cells.

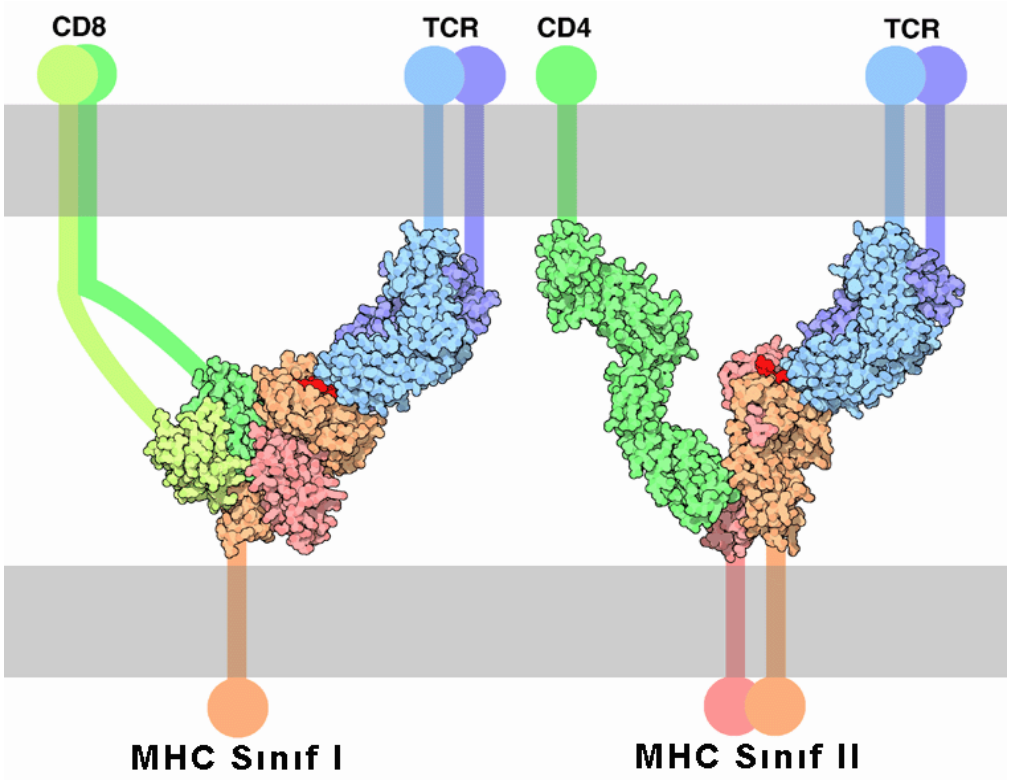

Fig.7 –The immunological synapse.

The image represents the so-called immunological synapse, a cell-to-cell signaling in which T cells can recognize through their specific TCRs their cognate antigen presented in the context of MHC-I (left) and MHC-II (right) molecoles by APCs. As depicted in the image, CD4 and CD8 on helper and cytotoxic T cells respectively act as co-receptors in the specific interactions with MHC-I or MHC-II molecules.

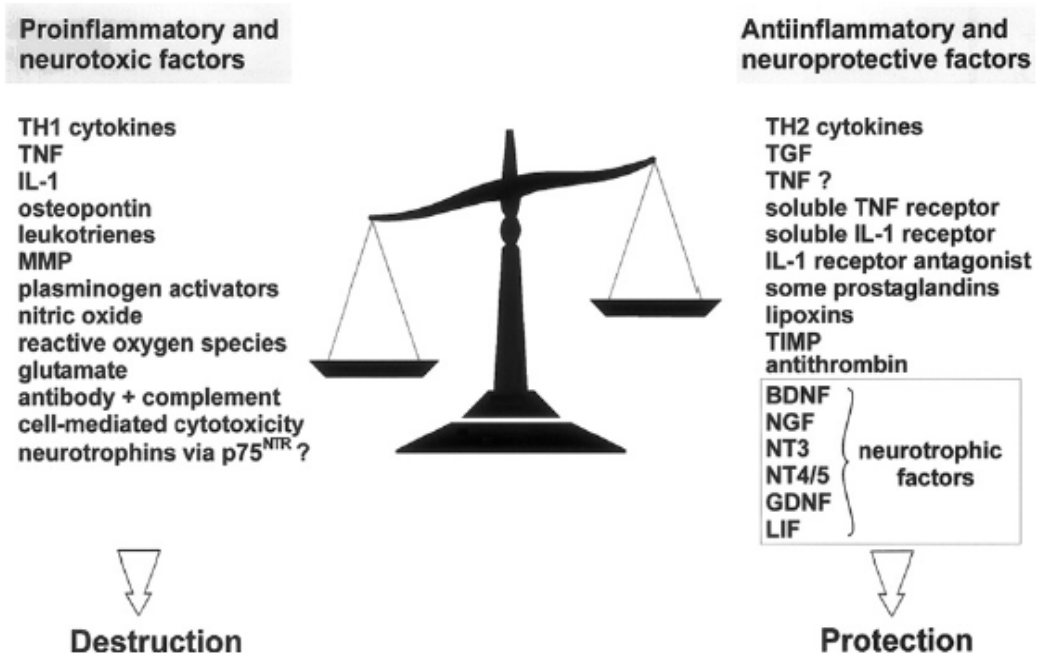

Fig.8 – The neuroimmune balance.

Immune cells during inflammation are potentially capable to mediate both neurodestruction and neuroprotection. The final outcome of this balance depends on the particular interplay of in situ signaling.

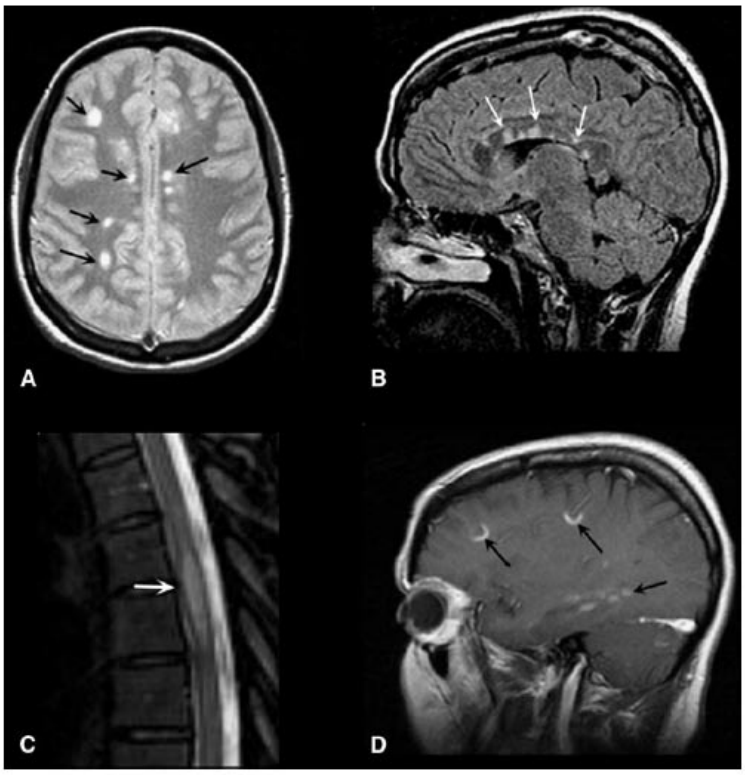

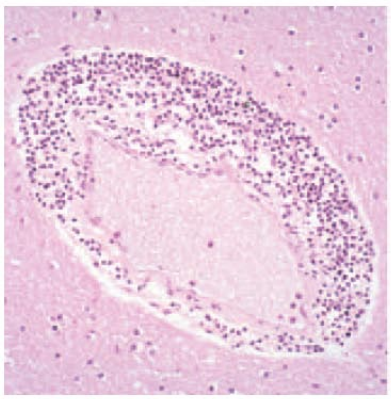

Fig 9 –MS lesions and perivascular cuffs.

On the left, a) Axial image from T2-weighted sequence shows multiple lesions in white matter tissue. b) Sagittal T2-weighted FLAIR image. Areas of corpus callosum displaying brain edema and demyelination appear high in signal. c) Sagittal T2-weighted image showing lesion in the mid-thoracic spinal cord. d) Gadolinium-enhanced sagittal T1-weighted image revealing focal areas of BBB disruption, here high in signal. On the right, a perivascular cuff of mononuclear cells in NAWM of a RR-MS patient as detected by H/E staining.

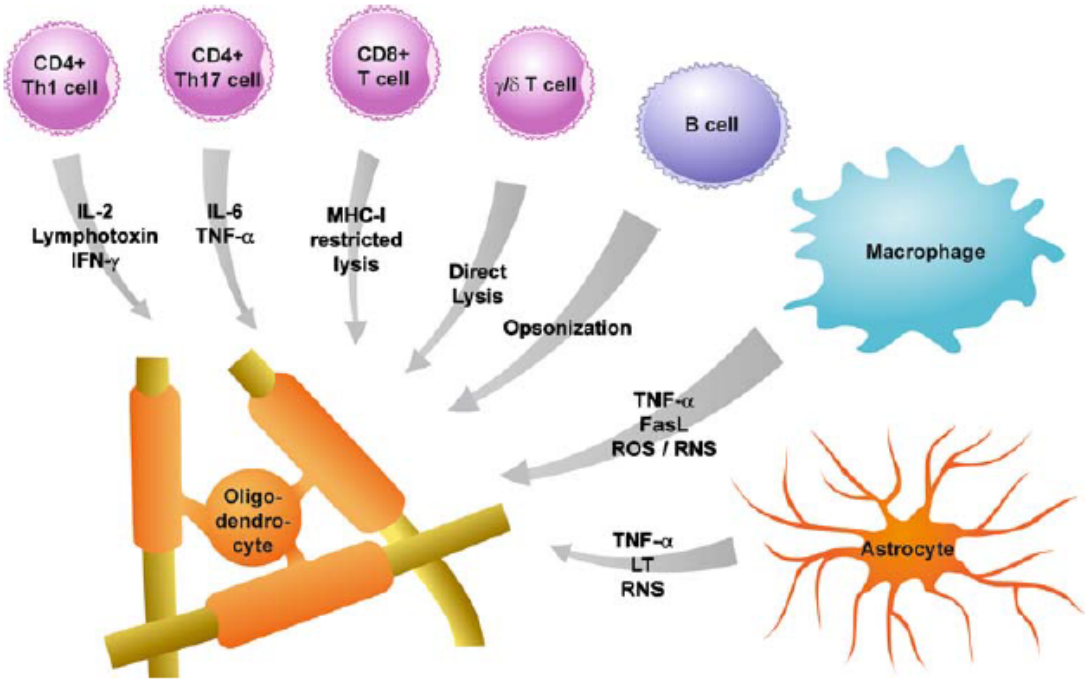

Fig 10 – Cells mediating ODC injury within MS lesions.

Different cells can damage ODCs through the release of inflammatory soluble mediators affecting the target cell directly or through astrocytes/microglia/macrophages. Other cells, as γδ T cells and cytotoxic T cells, can lyse directly ODCs through the release of perforin and granzymes.

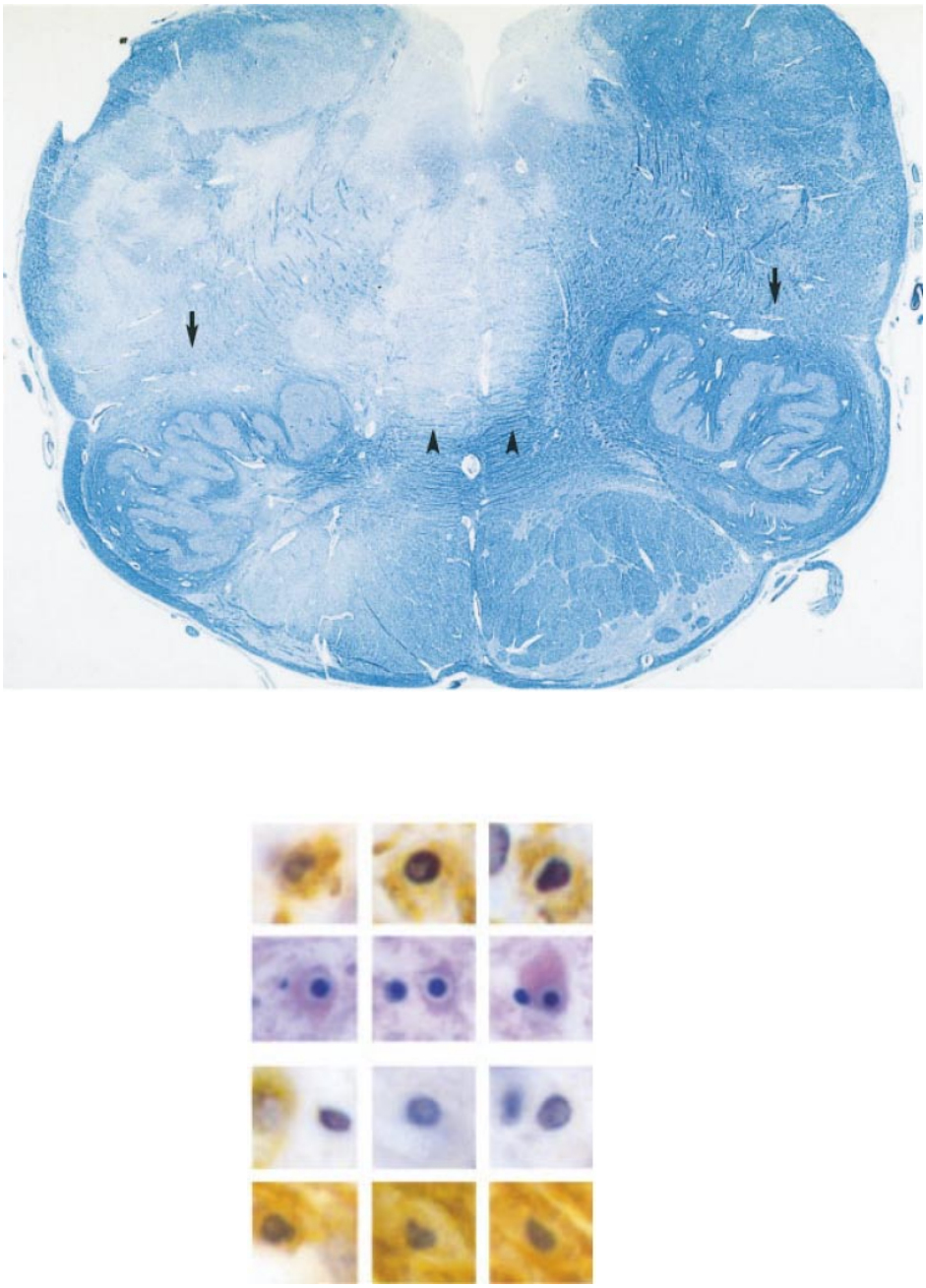

Fig.11 – ODC apoptosis as an hallmark of early sclerotic lesions.

On the left, medullary demyelinated lesion of a patient who died 17 hours after the symptomatic onset of the lesion. In no area myelin loss is complete. On the right, morphology of apoptotic ODC nuclei in prephagocytic areas. All show a reduction in nuclear volume together with condensed chromatin.

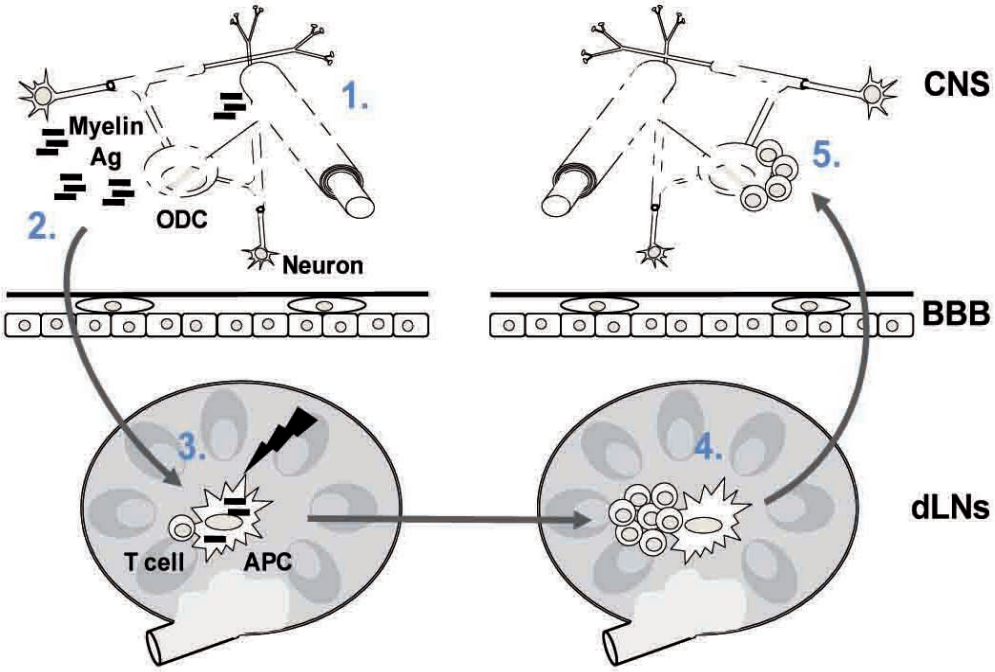

Fig.12 – A neurodegenerative hypothesis for MS pathogenesis.

ODC death (step 1) leads to release of myelin antigens (step 2) to CNS-draining lymph nodes, where autoreactive T cells are primed by APCs activated by a danger signal (step 3). Myelin-specific T cells expand clonally (step 4) and migrate to the CNS (step 5) triggering further tissue destruction.

Model	Species	Demyelinating agent	Time to demyelination	Lesion location	Axonal loss	Spontaneous remyelination time
Lysolecithin	Rat, mouse	1% lysophospha-	48 hrs	CCP	Minimal	1 week start
		tidylcholine		dorsal funiculus SC		4-6 weeks complete
Ethidium	Wistar or SD rat	0,01-0,1%EtBr	48 hrs start	CCP	Minimal	6-8 weeks start
bromide (EtBr)			2 weeks complete			3-4 months complete
Cuprizone	Wistar rat	0,6%cuprizone	2 weeks start	Global white	Minimal	2 weeks significant
				matter		
	C57Bl/6 mouse	0,2% cuprizone	3 weeks start	Global white	Minimal	4 weeks significant
			5 weeks complete	matter		
EAE	DA rat	rSCH, MOG	3 weeks start	Cervical SC	Significant	Unknown
	SJL/J mouse	PLP_{1-139}	3 weeks start	Lumbar SC	Significant	Unknown
	C57Bl/6 mouse	$MOG_{r35-55,\ h1-125}$	10–14 days	Lumbar SC	Significant	Unknown

Fig.13 – Animal models of demyelination.

The table summarizes the main chemically-induced and neuroinflammatory animal models for demyelination. The typical species used in research, the timing and quality of the demyelination insult are also depicted in the table. The last column to the right recapitulates the known remyelination scenarios in the different models.

SPECIFIC AIMS

Oligodendrocytes (ODCs) are important players in most degenerative and inflammatory pathologies of the CNS. However, little is known about the direct influences of ODC damage and death on immune activation. Also, utterly unclear are the intrinsic ODC responses within inflammatory environments, and the degree of neuronal impairment without ODC support. With the work presented in this thesis, I intend to investigate these essential issues:

a) Studying the impact of ODC death on adaptive immunity and neuronal survival

We wanted to test the neurodegenerative hypothesis for MS pathogenesis in a mouse model of inducible ODC death, the oDTR strain. ODCs marked with a transgenic diphtheria toxin receptor were specifically killed through DT application. This allowed to analyze the activation status of innate and adaptive immune cells in a time-controlled manner following ODC death. In addition, different immune activation paradigms could be applied following ODC death and their impact on the immune response could be followed.

b) Understanding the role of IGF1R signaling in adult ODCs under demyelinating conditions

IGF1R signaling affects survival, metabolism and myelination in the ODC lineage. Through our animal model (oIGF1R) we wanted to define the importance of this pathway in post-mitotic ODCs and to understand the unclear role of ODCs in the pathogenesis and damage progression of autoimmune-inflammatory diseases such as EAE and MS.

c) Developing a mouse model to quantify *in vivo* demyelination and remyelination

In demyelinating disease models, quantification of ODC death and myelin loss is possible only through analyses of autoptic material. We generated and evaluated a new animal model (oLucR) in which the expression of luciferase within mature ODC was expected to allow *in vivo* quantification of myelin and thus permit the study of demyelination insults and tissue repair.

MATERIAL AND METHODS

Animal Maintenance and Genotyping

The animals were kept under SPF conditions according to Swiss animal law and institutional guidelines. Presence of respective transgenes was confirmed by PCR analysis on DNA from tail biopsies by use of the following primer pairs: *MOGi-cre* (WT 350 bp) GAC AAT TCA GAG TGA TAG GAC CAG GGT ATC CC and GCT GCC TAT TAT TGG TAA GAG TGG; *MOGi-cre* (knock-in, 700 bp) TCCAATTTACTGACCGTACAC and CATCAGCTACACCAGAGACGGAAATC; *iDTR* (WT 600 bp, KI 845 bp) AAA GTC GCT CTG AGT TGT TAT, GGA GCG GGA GAA ATG GAT AAA GTC GCT CTG AGT TGT TAT, GGA GCG GGA GAA ATG GAT ATG, and AAT AGG AAC TTC GTC GAG AAT AGG AAC TTC GTC GAG C; IiMOG GGC TAC TGC TGA CTC TCA ACA TT, ATT TCG GTA GAG GTG AAC CAC GGC TAC TGC TGA CTC TCA ACA TT , ATT TCG GTA GAG GTG AAC CAC TC, and CAG GGT TTC CTT GAT GAT GGT TTC CTT GAT GAT GTC (WT 456 bp, KI 982 bp); *deleter-cre* GAA AGT CGA GTA GGC GTG TAC G and CGC ATA ACCAGT GAA ACA GCA T (600 bp).

Disease models

For EAE experiments 6 to 10 week old mice were immunized subcutaneously with 200 µg (each flank 100 µg) of myelin oligodendrocyte glycoprotein MOG_{35-55} peptide (MEVGWYRSPFSRVVHLYRNGK, Invitrogen) emulsified in Complete Freund's Adjuvant (CFA, H37 Ra, Difco laboratories), followed immediately and at day 2 by i.p. injection of 200 ng pertussis toxin (Sigma). To induce ODC apoptosis through DT administration, where not differently reported, oDTR and control animals were injected i.p. with 200 ng DT (Merck) daily over 7 days. Gender-specific differences regarding disease onset or progression were never observed. For activation of APCs and depletion of Treg cells anti-CD40 (FGK4.5, Bioexpress) and anti-CD25 (PC-61, Bioexpress) antibodies were used.

In the RotaRod experiments, the mice were placed on the rod in three consecutive trials with an acceleration from 5 to 50 rpm in 3 min and time to fall was recorded. In the

walking grid assay we counted the number of footfalls in each crossing over a 50 cm-long runway with irregularly arranged bars (0.5-2.5 cm) on a distance of 10 cm, fixing the maximum amount of errors as 10. The EAE score was calculated as follows: 0, no detectable signs of EAE, 0.5, distal limp tail; 1, complete limp tail; 1.5, limp tail and hind limb weakness; 2, unilateral partial hind limb paralysis; 2.5, bilateral partial hind limb paralysis; 3 complete bilateral hind limb paralysis; 3.5, complete hind limb paralysis and unilater forelimb paralysis; 4, total paralysis of fore and hind limbs; 5, death. Tremor was measured on a scale from 0-3, with 0, representing total absence of tremor; 1, slight tremor observed during motor tests; 2, strong tremor observed during motor tests, slight tremor during normal behavior; 3, strong tremor observed during motor tests and during normal behavior. To assemble the different data in the combinatorial score, each measurement was first re-calculated into percentages, assuming the weight and RotaRod score measured before DT administration, a grid walking test without error, and absence of tremor as 100%.

Cell Culture and Flow Cytometry

For *in vivo* proliferation experiments cells were prepared from LNs and spleens of 2D2 mice, underwent erythrocyte lysis (BD Biosciences) and were purified by MACS using CD4 microbeads (Miltenyi Biotech). Subsequently, they were incubated with 1 ml CFSE solution (5(6)-CFDA,SE, Invitrogen, 5 µM in DMEM) per 10^7 cells for 10 min at 37°C. The reaction was stopped with 10 ml ice-cold FCS and after washing with phosphate buffered saline (PBS), 10^7 of the cells were injected i.v. in 200 µl PBS.

For flow cytomentric analysis of CNS-invading cells, mice were killed with CO_2 and perfused intracardially with PBS. Spinal cord and brain were removed, mechanically homogenized, and strained through a nylon filter (70 µm, SPL lifesciences). After centrifugation, cells were resuspended in 30% Percoll (Pharmacia) and centrifuged at 18,500 g for 30 min, 4°C. The interphase was collected, the cells were washed and treated with Fc-block (1 µg per 10^6 cells, 2.4G2) before staining. Fluorescence staining was performed as previously described [126]. The following antibodies were purchased from BD: 53-6.7 for CD8, N418 for CD11c, H57 for TCRβ, 7AD/PC61 for CD25, IM7 for CD44, 30-F11 for CD45, MEL-14 for CD62L M1/70 for CD11b, M5/114 for MHCII; from Biolegend: RM4-5 for CD4; from eBiosciences: BM8 for F4/80 and FJK-

16s for Foxp3. Dead cells were excluded by LIVE/DEAD® Fixable Dead Cell staining (Invitrogen), Topro-3 (10 nM, Invitrogen), or Propidium Iodide (0.2 mg/ml, Sigma-Aldrich). Analysis was performed on a FACSCantoII (BD Biosciences) and analyzed by FlowJo software. For radioactive proliferation assays we placed 2×10^5 LN cells per well in complete IMDM in a 96-well. Cells were plated as quadruplicates and pulsed with 60 µg/ml MOG_{35-55} (Genscript), 20 µg/ml PLP protein (AbD serotec), 20 µg/ml MBP protein (Chemicon international), 10 µg/ml concanavalin A (Sigma-Aldrich), 5 µg/ml anti-CD3e (2C11, BioXcell) or 5 µg/ml anti-CD28 (37N, Bioexpress). After 48 h, cells were pulsed with ^{3}[H]-thymidine (GE healthcare; final concentration 5 µCi/ml) and incubated for an additional 24 h before they were harvested and thymidine incorporation was assessed using a cell harvester (Perkin-Elmer) and Wallac 1450 Microbeta scintillation counter (Perkin-Elmer).

Histology

Mice were euthanized with CO_2 and perfused with PBS. For cryosections, brain and spinal cord were isolated, embedded (Mdite), frozen on dry ice and stored at -80°C. Tissues were cut sagittally at 10 µm and thaw-mounted onto glass slides (Menzel GmbH). Sections were air dried over night, fixed with 4% paraformaldehyde (PFA; AppliChem) for 10 min and washed 3x with PBS. The TUNEL staining was performed after antibody stainings using the In Situ Cell Death Detection Kit (Roche) according the manufactures guidelines. For vibratome sections the tissue was fixed overnight with 4% PFA, cut sagittally in 40 µm thick sections and stained as described before (Spergel et al., 1999) with antibodies or antisera against following antigens: GFAP (DAKO), aspartoacylase (ASPA; rabbit polyclonal serum, Dr. Matthias Klugmann, Mainz, Germany), proteolipid protein (PLP; rat, homemade), F4/80 (rat, homemade) nerve glia antigen 2 (NG2; rat monoclonal, Dr. Jacqueline Trotter, Mainz, Germany) and ionized calcium binding adaptor molecule 1 (Iba1; rabbit, Wako Pure Chemical Industries). Detection was accomplished using either horseradish peroxidase-conjungated secondary antibodies or biotinylated secondary antibodies, streptavidin-horseradish peroxidase (Vector Laboratories) and 3,3`diaminobenzidine (DAB; Sigma-Aldrich Fluka). A MHC-class-II-specific antibody (rat, BD Biosciences) and tomato lectin (FITC conjugated, Sigma-Aldrich) were used for immunofluorescence. Secondary antibodies were labeled with Cy3 or FITC (Dianova). Sections were covered with Vectashield

(Vector Laboratories) and analyzed by confocal (Leica SP5) or fluorescence (Olympus BX50) microscope. For paraffin sections, animals were additionally perfused with 4% PFA in PBS. Brain and spinal cord were fixed in 4% PFA for additional 3 to 12 hours. Tissues were embedded in paraffin and 5µm thick paraffin sections were cut. Deparaffinized sections were stained with hematoxylin-eosin (H/E), Nissl as well as Luxol Fast Blue and Periodic Acid Schiff (LFB/PAS) according to standard protocols. Briefly, for H/E and myelin staining, paraffin slices were dewaxed with xylol, rehydrated and stained with hematoxilin 7211 and eosin Y (Microm International). For myelin staining, a LFB-solution (0.1% LFB in 95% isopropanol containing 0.05% acetic acid, stained overnight at 60°C) and hematoxylin (stained for 1 minute at room temperature; Microm international) were used. Lithium carbonate solution (0.05%) was used for color differentiation of the LFB. Myelin-degradation products were detected with 0.3% (w/v) oil-red O (ORO) (Gurr) in 60% 2-propanol and counterstained with hematoxylin. Immunohistological staining to ionized calcium binding adaptor molecule 1 (Iba1; rabbit, Wako) and CD3 (Neomarkers Thermo Scientific) was performed by a Ventana Benchmark XT automated staining according to manufacturers guidelines. For NF staining, paraffin sections were first dewaxed and rehydrated followed by antigen retrieval in citrate buffer pH 6,0 for 10 minutes. Sections were then incubated in 0,3% of hydrogen peroxide and blocked with 3% NGS and 0,3% Triton X100 in PBS. NF-specific antibody (Millipore) was incubated for 12 hours at room temperature. A biotinylated secondary antibody (goat anti-ms, Vector) was used for detection. The staining with DAB was developed using Vectastain ABC kit (Vector) according to the manufacturer's protocols. Sections were counterstained for two minutes with hemalaun (Dr. Hollborn and Sons).

Transmission electron microscopy

Anaesthetized mice were perfused with PBS followed by freshly prepared 1% (v/v) glutaral aldehyde (GA), 2% (w/v) paraformaldehyde and 0.2% (v/v) picric acid in 0.1 M phosphate buffer, pH 7.4. Brain regions as indicated were taken and post-fixated in 2.5% GA in PBS for 1h followed by fixation with 2% osmium tetroxide in PBS for 2h. Samples were then dehydrated using the automated tissue processor Leica EM TP (Leica) and were embedded in Epon at 60°C for 48h. 70 nm ultra-thin sections were stained with 4% uranylacetate and lead citrate as described previously [127]. Samples

were visualized using a Phillips CM 100 transmission electron microscope (FEI) equipped with a digital Gatan 4k x 3k camera (Gatan Inc.).

Iodine labeling of MOG-specific antibody and radioactivity detection

$Na^{125}I$ (629 GBq/mg, Perkin Elmer) was activated in a Pierce pre-coated iodination tube (Thermo Scientific) and then mixed with MOG-specific antibody (818C5, homemade). The reaction was stopped with a saturated solution of tyrosine (10 mg/ml) and the antibody purified through a 10 ml polyacrylamide desalting column (Thermo Scientific). Fractions containing the purified antibody were identified on a nitrocellulose membrane and pooled. 12 hours after the injection of the ^{125}I-antibody, mice were sacrificed, perfused and CNS was analyzed for antibody incorporation in a Kontron Gamma-matic (Sertec electronics).

Immunoblotting

Mouse tissue was digested in lysis buffer (Tris-Cl 35mM, NaCl 150mM, NP-40 1%, Sodium deoxycholate 0.5%, Triton 1%, Na_3VO_4 1mM, leuptinin 1ug/ml, NaF 5mM, PMSF 5mM) for 30', sonicated and centrifuged at 13000 rpm at 4°C for 20 min. Protein concentration was quantified with a BCA assay (Thermo Scientific). Proteins were detected with anti-Vinculin (Cell Signaling), anti-MOG (818C5, homemade), anti-MBP (Santa Cruz), anti-NG2 (Millipore). Samples for anti-NG2 immunoblotting were previously digested with Chondroitinase ABC (Seikagaku) for 1 hour at 37°C.

Organotypic cerebellar slice cultures

After sacrifice of P9 pups the cerebellum was extracted and cut 350 µm thick. The tissue was immediately collected in dissecting medium (1mM kynurenic acid in HBSS containing 100U/ml penicillin and 100 mg/ml streptomycin) where the slices were separated from each other under a microscope. Slices were transferred into washing medium (HBSS:MEM = 1:1 both with P/S and 25nM HEPES) on ice. The slices were finally transferred on cell culture inserts (Millipore) with 1ml slice culture medium (for 400 ml: 100ml heat inactivated-horse serum, 100ml HBSS containing 100U/ml penicillin and 100mg/ml streptomycin, 200 ml MEM containing 100U/ml penicillin and

100mg/ml streptomycin, 4ml 50% glucose, 2mM L-glutamine) and then incubated at 37°C and 5% CO_2. The medium was changed every 2 days.

RNA isolation

Samples were homogenized in 1ml TRIZOL and incubated for 5min at room temperature (RT). 200µl chloroform per sample was added, incubated for 3min at RT, and centrifuged at 8000 rpm for 15min at 4°C. The aqueous phase containing RNA was transferred into a fresh tube and precipitated adding 500µl isopropyl alcohol after 10min incubation at RT and centrifugation at 800 rpm for 10min at 4°C. The supernatant was removed and the RNA pellet washed with 1ml 75% ethanol. Samples were centrifuged at 5000 rpm for 5 min at 4°C and the RNA pellet then was let drying out for 15min at RT. The RNA was finally dissolved in 45µl RNase free water with 5µl of 10x incubation buffer and 1µl DNAseI. The samples were incubated at 37°C for 20min, then 1µl 0.5 M EDTA was added and incubated at 75°C for 10min and finally chilled on ice.

cDNA synthesis

1µl random primers (100ng/µl), 1µl dNTP (10 mM), 4µl First-strand buffer (5x), 2µl DTT (0.1 M), and 1µl RNase OUT were incubated for 2min at 37°C and then 1µl M-MLV RT (200U/µl) was added.
5 µg RNA was diluted in 10µl RNase free H_2O, heated to 65°C for 5min and quenched on ice. Afterwards, 10µl Master Mix were added to the RNA, incubated 10 min at 21°C, 50 min at 37°C and finally 15 min at 70°C. The cDNA was finally diluted 1:10.

RT-PCR

5µl of cDNA per real time reaction were mixed with 12.5 µl SYBR Green, 6.5 µl H_2O, 0.5 µl F-Primer, 0.5 µl R-Primer for a total volume of 25 µl. The RT-PCR was performed in BIORAD machine with the following primers:
β-actin, F: AGAGGGAAATCGTGCGTGAC; R: CAATAGTGATGACCTGGCCGT
Nestin, F: CAAGAACCACTGGGGTC; R: CCCTCCTGGTGATTCCACA
NG2, F: GTTGGGATGCTTGCTGG; R: TGAAAGCTGCAGAAGCA
MPB, F: ATCCAAGTACCTGGCCAC; R: CCTGTCACCGCTAAAGAA
MOG, F: AAATGGCAAGGACCAAG; R: AGCAGGTGTAGCCTCCTT

OLIG1,F: ACCAACGTTTGAGCTTGCTT; R: GGTTAAGGACCAGCCTGTGA
OLIG2, F:AGCAATGGGAGCATTTGAAG; R: CAGGAATTCCAGGGATGAA

Bioluminescence imaging

Bioluminescence was detected *in vivo* with an ultrasensitive IVIS machine (Xenogen) which consists of a cooled charged coupled device (CCD) camera bound to a dark box. The mice were anesthetized with isoflurane, shaved and measured 3 times a week after intraperitoneal luciferin injection (150mg/Kg). Luminescence signal was quantified as photons/s/cm^2/steridian (sr) using the LIVING IMAGE software version 2.50 (Xenogen) and integrated over a period of 2 min. The animals were measured for a whole experiment length of 22 minutes and data represent the average of the values obtained over the 4-22 minutes periods. To quantify the signal, photon emission was obtained from a region of interest (brain, spinal cord, whole body) that was kept in a constant area and position during all the experiments. To have a baseline imaging for reliable bioluminescence comparison, luminescence recording begun at least 11 days before the beginning of the experiment.

Preparation of luciferin for *in vivo* bioluminescence assay

D-Luciferin Firefly, Potassium salt, 1g (Xenogen Catalog XC-1001) was used for a stock solution with a concentration of 30mg/ml diluted in PBS. The solution was filtered through a 0.2 μm filter, aliquoted and frozen at -20°C.

Bioluminescence in brain slices

The animals were sacrificed, perfused with PBS and brains were collected and cut in half. From one half of the brain 1mm thick slice was made, bathed in 150 μg/ml luciferin and recorded for 2 minutes with the IVIS camera.

RESULTS

DT-induced ODC death leads to progressive motor dysfunction

To investigate whether ODC death could result in an inflammatory disease of the CNS we generated the oDTR model in which specificity of the DTR-mediated cell ablation is achieved by an ODC-specific Cre strain (MOGi-Cre) crossed to a mouse strain carrying a Cre-inducible DT receptor (iDTR) [89, 128] (**Fig. 14a**). The toxin induces cell death through a well-known mechanism by termination of protein synthesis (**Fig. 14b**). DT-induced clinical disease is dose-dependent with progressive pathology clinically characterized by exacerbating ataxia, tremor, kyphosis, and cachexia [129]. Disease severity was quantified by measuring weight loss, tremor, and motor coordination (see *Material and Methods* and **Fig. 15a**). After symptomatic onset at around 5 to 6 weeks p.a., clinical manifestations of the disease became rapidly stronger (**Fig. 15a**). The mice lost up to 15% of the starting weight and exhibited increasing ataxia followed by tremor and rapid decrease in motor coordination eventually resulting in lethal paralysis. We combined these data in one unique composite score (**Fig. 15a**). DT-treated control animals never showed any signs of disease, confirming the specificity of ODC ablation in the oDTR system.

ODC death and demyelination follow DT administration in susceptible animals

Clinical disease progression was much slower in our model than in EAE in the same genetic background, although it was histologically more severe [129]. Starting one week p.a., Nissl-stained sections showed the majority of ODCs featuring shrunk nuclei and condensed cytoplasm (**Fig. 15b)**. Similar to the ODCs in lymphocyte-free early MS plaques described by Barnett and Prineas [68], these cells died through a caspase-independent mechanism, as we could detect neither $TUNEL^+$ nor activated $Caspase\ 3^+$ ODCs (data not shown). To better characterize the fate of the dying ODCs we therefore performed transmission electron microscopy (TEM) analysis of the murine CNS after application of DT. ODCs in the white matter of control mice displayed typical clumped chromatin and a large, dark grey cytoplasm full of mitochondria and ribosomes (**Fig. 16**). In contrast, electron micrographs of DT-treated oDTR animals showed shrunk ODCs with condensed cytoplasm (data not shown) and cells with intense vacuolisation

(**Fig. 16**). To directly quantify the loss of live ODCs, we stained CNS sections for the ODC-specific protein Aspartoacylase (ASPA)[130]. We observed that ODCs in all myelin-rich areas of the CNS started to disappear 2 weeks p.a. reaching up to 60% cell loss around 5 weeks p.a. (**Fig. 17a,b,c**). In histological samples of DT-treated oDTR mice, significant changes in myelin structure became evident starting 3 weeks p.a., with obvious vacuolic alterations in myelin-rich structures as cerebellum, pons, brain stem, and spinal cord (**Fig. 15b, Fig. 17d**) coinciding with pronounced demyelination as detected by LFB-PAS and myelin-specific stainings (i.e. PLP, **Fig 17d,e**). MAG and PLP mRNA levels in CNS tissue of DT-treated oDTR mice were dramatically reduced already 1 week p.a. (**Fig. 18a**), while at the protein level myelin oligodendrocyte protein (MOG), and myelin basic protein (MBP) amounts reduced more progressively (**Fig. 18b**). Fully demyelinated axons were found by TEM starting 5 weeks p.a. (**Fig. 18c**). To find obvious leukocyte infiltrations, we performed H/E staining but failed to detect any leukocytes within lesioned areas (**Fig. 17d**). Evans Blue analysis revealed no change in permeability between the blood brain barrier (BBB) of DT-treated oDTR and control animals (**Fig. 18d**). In conclusion, DT-treated oDTR animals show efficient and widespread ODC death, which leads to a chronic progressive demyelination.

ODC progenitor recruitment and remyelination following induced ODC death

While certain myelin abnormalities lead to axonal degeneration and neuronal death [131-133], it is still unclear to which extent the death of ODCs is a direct cause for neuronal impairment. Surprisingly, Traka et al showed that widespread ODC death did not significantly affect axonal number [134], while a similar study [135] in a comparable model clearly showed strong neuronal degeneration following ODC depletion. To evaluate the axonal integrity in our model we analyzed NF-stained CNS sections 2, 4, and 5 weeks p.a. and found axonal loss in DT-treated oDTR mice starting 4 weeks p.a. (**Fig 19a**). A detailed analysis through Fluoro Jade C stainings revealed widespread damage to neurons following ODC death (**Fig. 19b**) with the granular layer of the cerebellum showing an earlier involvement (asymptomatic, as shown in **Fig. 15a**). Along this line, one week p.a. we found evidence for neuronal death through TUNEL+ NeuN+ cells in the granular layer of the cerebellum of DT-treated oDTR mice (**Fig. 19c**). As mentioned above, TUNEL+ ODCs could not be observed.

Progressive accumulation of OPCs was observed throughout the CNS starting 3 weeks p.a. (**Fig. 20a**), and NG2 protein levels were significantly higher in oDTR than in control brain 5 weeks p.a. (**Fig. 20b**). Even though the mice ultimately succumb to the DT-induced ODC loss, some degree of remyelination took place as shown by g-ratio analysis of axons in the corpus callosum of DT-treated oDTR mice (**Fig. 20c**).

Antigen leakage into CNS-draining lymph nodes

The primary goal of this study was to assess the impact of ODC death on immunity. Even though immune responses are generally initiated within secondary lymphoid tissues, the sites for initial antigen presentation in MS remain unknown. In EAE, dc and lumbar LNs, the draining LNs of the CNS, were implicated in relapses and epitope spreading [46]. Myelin-containing dendritic-like cells were also found in these LNs in MS, *post mortem* [136] and *ex vivo* [137]. Thus, a spontaneous anti-CNS immune response might be initiated by antigen release in the CNS-draining LNs as in our working hypothesis (**Fig. 12**). To test the presence of CNS-derived antigens in such sites in the oDTR model, we analyzed dcLNs and inguinal LNs three weeks p.a.. In OilRedO (ORO) stained sections we detected a significant increase in lipids in the dcLNs (from 1.8 ± 0.35 to 12.4 ± 0.63 ORO^+ cells per field, $p < 0.001$) but not inguinal LNs of DT-treated oDTR animals (**Fig. 21a,b**), indicating the transfer of myelin material to CNS-draining LNs. To determine whether ORO reactivity represented actual myelin antigens, we analyzed protein extracts of lumbar LNs from DT-treated animals 1 and 2 weeks p.a. and detected increased MBP and MOG protein level specifically in DT-treated oDTR mice (**Fig. 21c).**

Antigen drainage from dying ODCs does not prime myelin-specific T cells

Myelin components in CNS-draining LNs should make myelin epitopes visible to auto-reactive peripheral T cells. To investigate this, we injected 10^7 CFSE-labeled T cells from the MOG_{35-55} specific TCR-transgenic mouse strain 2D2 [138] after inducing ODC death at different time points. Surprisingly, we observed in none of the DT-treated oDTR animals proliferation of these myelin-specific T cells (**Fig. 21d**).

Since T cells from 2D2 mice were modified to recognize a single epitope of a rather scarce myelin protein we decided to increase the amount of cognate antigen by

crossing the oDTR strain to the IiMOG strain, leading to increased expression of the antigenic MOG_{35-55} peptide [139] within ODCs. Again, induction of ODC death was followed by injection of CFSE-labeled 2D2 T cells. We also applied PT, commonly used as enhancer of anti-CNS inflammation, and an agonistic monoclonal antibody (mAb) against CD40 (30 µg/mouse at day 5) shown to increase priming of T cells [140]. Even under these extremely biased experimental conditions, only 40% of the mice showed a minor population of proliferating MOG-specific T cells five days later (**Fig. 22a**, bottom left), while the majority of animals did not show any kind of 2D2 proliferation (**Fig. 22a**, bottom right). A fully proliferating T cell population was found in all animals expressing MOG_{35-55} ubiquitously (del-cre/IiMOG) [139] (**Fig. 22a,** upper left).

Being aware that the 2D2 system narrowed antigen recognition [141], we also investigated immune responses toward additional myelin antigens. At d7, d14 and d30 p.a. cells from inguinal, axillary, and CNS-draining LNs were stimulated *in vitro* with PLP, MBP, MOG_{35-55} and the irrelevant protein ovalbumin (OVA). No proliferation to these antigens was detected after induced ODC death. Only cells of MOG_{35-55}/CFA immunized controls showed a response towards MOG_{35-55} (**Fig. 22b**). To exclude that DT treatments leads to a general impairment of T cell priming, we treated oDTR and control animals with DT followed by immunization with either keyhole limpet hemagglutinin (KLH, a neo-antigen) or with MOG_{35-55} in CFA. At 9 days p.i., cells were isolated from LNs and stimulated *in vitro* with KLH or $MOG_{35-55,,}$ respectively. Upon restimulation of LN cells from these animals 9 days p.i. we observed unaltered proliferative responses towards the immunizing antigens (**Fig. 22c**) excluding that DT would suppress priming. Thus, although we found myelin antigens in CNS-draining LNs after induced ODC death, these failed to initiate an anti-CNS response even under most biased experimental conditions.

Microglia/macrophage activation and gliosis but no T-cell recruitment after induced ODC death

Innate immune cells serve as a first line of defence by immediate clearance of pathogens and induce subsequent adaptive immune reactions upon reception of a danger signal [142]. The CNS-resident innate immune cell, microglia, make up the main cellular fraction within MS plaques (reviewed in [143, 144]). Such reactive

microglia/macrophages have the potential to serve as APCs through expression of MHC class I, II and co-stimulatory molecules [144].

We found that induction of ODC death resulted in progressive accumulation of $CD45^{int}$, $CD11b^{hi}$, $F4/80^{+}$ (**Fig. 23a**) and $Iba1^{+}$ (**Fig. 23b, Fig. 17b**) activated microglia/macrophage. The activation process started as soon as one week p.a. and persisted until the final stage of the disease (**Fig. 23a,b**). Also morphologically microglia/macrophages in white matter areas appeared reactive (**Fig. 23c**) and showed high expression of MHC-II and CD44 (**Fig. 23d, 24a**). Similarly, an overall progressive gliosis was shown by staining for GFAP (**Fig. 24b, Fig. 17b**). Yet, histological analysis showed the CNS of DT-treated oDTR to be devoid of B and T lymphocytes (**Fig. 24c**). Quantification of CNS infiltrating leukocytes by flow cytometry revealed no invasion of $CD4^{+}$ and $CD8^{+}$ T cells in CNS after induction of ODC death (**Fig. 24d**). Taken together, we observed profound activation of microglia and astrocytes in the affected areas, whereas adaptive immune cells were not found to invade the demyelinating CNS.

Chronically induced ODC death does not result in CNS inflammation

MS is a progressively developing disease with sparse focal demyelination. To better mimic this aspect of the disease we also tested a strategy leading to a chronic albeit more limited death of ODCs. Following a five months-long treatment with a weekly low dose of DT (50 ng i.p), we could detect mild demyelination and sparse ODC death specifically in oDTR mice (**Fig. 25a,b**) along with a clear increase in $Iba1^{+}$ microglia/macrophages (**Fig. 25c**). Clinical presentation in these mice was mild to absent (data not shown). Analysis of leucocytes along the course of the treatment (7 and 15 weeks p.a., data not shown) and at endpoint (19 weeks p.a., **Fig. 25d**) revealed no differences between DT-treated oDTR and control mice. Cells from LNs of both DT-treated oDTR and genetic control mice failed to show a proliferative response to MOG, PLP, MBP, MOG_{35-55}, and total brain homogenate (data not shown). Thus, even chronic ODC death and demyelination did not result into an anti-CNS adaptive immunity response.

Anti-myelin antibody does not modify the disease induced by ODC death

One of the most important diagnostic hallmarks in MS is the presence of oligoclonal

bands (immunoglobulins) and plasma cells in the CSF [145, 146]. As already mentioned, CNS-infiltrating B cell clones were suggested to produce autoantibodies [147] damaging and opsonizing myelin membranes and thus aiding myelin-specific T cell responses. We and others have previously shown in the EAE model that anti-MOG antibodies drastically increase clinical disease in a complement-dependent fashion [148, 149] and thus wanted to ask whether a similar effect could be achieved in the oDTR model. Since we had not detected any increased permeability of the BBB (**Fig. 18d**), we first confirmed that radio-labeled anti-MOG antibody accumulated in the CNS of DT-treated oDTR animals (**Fig. 26a**). We then injected oDTR and control animals with 200 µg of anti-MOG or anti-NP control antibody intravenously at days 14, 21, and 28 after DT application. Even though we did not detect any clinical difference between the two groups (**Fig. 26b**), anti-MOG application resulted in slightly higher ODC loss and glial activation compared to the anti-NP control group (**Fig. 27a,b,c**). Yet, again H/E- and anti-CD3-stained histological sections (data not shown) failed to reveal any accumulation of lymphocytes in CNS from both groups. Thus, in contrast to EAE, the application of anti-myelin antibodies does not exacerbate ODC death-induced disease or aid the development of anti-CNS immunity.

Bystander activation of APCs does not support development of CNS-autoimmunity after ODC death

In order to become activated, auto-reactive T cells must first encounter APCs already primed by a microbial trigger and/or a co-stimulatory signal [142]. EAE induction with the help of CFA results in a profound anti-CNS immune response, thus emphasizing the necessity for a strong danger signal over-riding tolerance [150]. To combine induced demyelination with adjuvant-driven immune activation, we treated oDTR and control mice with PT and CFA after DT application. Nonetheless, also in this experiment we could not observe any signs of EAE-like disease in experimental animals apart from the expected clinical degeneration (data not shown). To further enhance sensitivity and specificity of the system we crossed the oDTR mice to the 2D2 strain, reported to display only 5% incidence of spontaneous EAE [138]. We treated such oDTR/2D2 animals with DT and CFA/PT to increase spontaneous EAE incidence. In both, oDTR/2D2 and MOGi-Cre/2D2 mice a similar fraction developed symptoms of EAE (**Fig. 28a**) with comparable onset and severity (**Fig. 28b**). Taken together, massive

demyelination does not result in anti-CNS immunity even under conditions in which the majority of T cells are specific to myelin antigens and lymphocyte activation is indirectly aided by adjuvant use.

Another very strong stimulus to innate APCs is the artificial activation of CD40 signaling (reviewed in [151, 152]). Since in our model T cells apparently ignored the peripheral presence of CNS antigens, we activated APCs specifically by injection of an agonistic CD40-specific antibody during the course of DT-induced demyelination. CNS from oDTR animals treated with DT and CD40-specific antibody showed strong hyper-activation of microglia/macrophages (**Fig. 27c, Fig. 28c**) and astroglia (**Fig. 27b**), either due to antibody entry or through a peripherally induced cytokine storm. Also, double-treated animals displayed a slight reduction in ODC density compared to DT-only treated oDTR animals (**Fig. 27a**). Nevertheless, no clinical difference between the groups became apparent (**Fig. 28d**) and no parenchymal or perivascular accumulation of lymphocytes were detected in the demyelinated CNS (data not shown). Again, no specific lymphocyte response follows ODC death and strong activation of the immune system.

Absence of CNS inflammation is not due to T cell tolerance

As briefly discussed, self-reactive T cells are eliminated from the circulating pool through the thymic process of negative selection. Yet, as some clones usually evade this deletion process, different other mechanisms exist to limit the activation of autoreactive T cells. For instance, antigen recognition within a non-inflamed environment can lead T cells to deletion or to a state of immunological unresponsiveness named tolerance [153]. We therefore performed experiments to exclude that such tolerance prohibited the generation of an anti-myelin specific immune response in the oDTR model. First we tested whether induction of ODC death interfered with EAE induced by active immunization. oDTR mice and controls were treated with DT or BSA and then immunized with MOG_{35-55} in CFA (d0), with or without co-injection of PT (d0 and d2). The clinical disease course was not ameliorated but slightly more severe in MOG_{35-55} immunized oDTR animals in comparison to control animals (**Fig. 29a**), although disease incidence was equal in both groups (**Fig. 29b**). Moreover, a similar number of inflammatory infiltrates with equal activation states were found at disease onset by flow cytometry (data not shown). Taken together, no indication of tolerance was found in

these experiments. We performed an additional experiment in which CD90.2$^+$ oDTR/IiMOG and MOGi-Cre/IiMOG control mice received 10^7 CD90.1$^+$ CFSE-labeled 2D2 T cells after induction of ODC death. One day after the cell transfer, half of the mice from both groups were tolerized by injection of MOG_{35-55} in PBS. At day 6 after the initial cell transfer, all animals were immunized by subcutaneous administration of MOG_{35-55} in CFA. Ten days later, tolerized animals showed a reduced number of CD90.1$^+$ proliferating cells in LNs and spleen (**Fig. 29c**); however, this reduction was not affected by DT application in oDTR mice. Thus, MOG protein released from dying ODCs does not induce tolerance against the peptide MOG_{35-55}.

Lastly, to release unbridled T cell immunity, we deleted Tregs [154] . Although MS patients do not show a reduction in Tregs, defective suppressive activity of this population was observed in a number of studies [155, 156]. We removed Tregs after induction of ODC death using anti-CD25 mAbs (PC61)[154] with a control group receiving isotype control (IgG_1) antibody. A significant reduction in CD4$^+$CD25$^+$Foxp3$^+$ cells in blood from anti-CD25 treated mice was observed (**Fig. 30a**) at day 8 p.a.. No significant difference in clinical disease was found between the two groups (**Fig. 30b**). Some stronger activation of microglia and astroglia was found, however, in PC61/DT double-treated animals compared to DT-treated oDTR mice (**Fig. 27b,c**), probably indirectly caused by peripheral Treg cell depletion. However, neither H/E nor anti-CD3-stained sections revealed any lymphocyte infiltration or perivascular cuffs in both anti-CD25 and control-treated diseased CNS (data not shown). To test whether ablation of Treg cells led to sub-clinical activation of myelin-specific T cells lymphocytes LN cells from the two groups were stimulated *in vitro* with the major myelin proteins. Yet, also in this assay we did not detect any response towards myelin antigen (data not shown). Taken together, we could not find evidence for tolerance induction through antigen released by dying ODCs. Also, removing Tregs transiently during the course of induced demyelination did not lead to development of neither anti-CNS autoimmunity nor priming of myelin-specific T cells.

Absence of IGF-1 signaling on ODCs does not results in major myelin abnormalities

To study the role of the IGF-1 pathway in mature ODCs we developed a novel mouse model (oIGF1R, **Fig. 31a**) by crossing a mouse strain carrying a loxP-flanked 3rd exon of the IGF1R (IGF1Rfl/fl, generated by our collaborator Jens Brüning) to the MOGi-

Cre strain [89, 157]. The third exon of the IGF1R gene contains the region most important for ligand binding and its absence has been shown to incapacitate the receptor [102]. Since the deletion of the receptor in oIGF1R mice is restricted by the late expression of MOG, this model is intended to circumvent the developmental myelination deficits that have been described for conditional Cre-driven IGF1R ablation restricted by the earlier Olig1 or PLP promoters [101]. Accordingly, histological analysis of the CNS of oIGF1R-/- mice with LFB-PAS staining and with Iba1- and GFAP-specific antibodies did not reveal any major CNS anomalies compared to controls (**Fig. 31b**). Also, oIGF1R-/- mice compared to C57/Bl6 mice or littermate controls did not show any motor or behavioural abnormalities by composite motor test performed over the course of 1 month (**Fig. 31c**). To further investigate possible myelin abnormalities in our animal model, we analyzed CNS lysates of oIGF1R-/- and control mice at 3, 5, and 9 months of age by immunoblotting. However, we could not find any difference in the protein levels of MOG, MBP and PLP (**Fig. 32a,b,c,d**). Also, oIGF1R-/- animals did not show differences in ODC density in any CNS area analyzed (**Fig. 32e**). Accordingly, NG2 protein levels, indicative of number and activation state of OPCs, did not differ at 3, 5, and 9 months of age when compared to hemyzigous oIGF1R-/+ (IGF1Rfl/+, MOGi-Cre+) and wild type IGF1R+/+ control mice (**Fig. 32f**). However, at 9 months of age the brain/body weight ratio resulted significantly higher in male oIGF1R-/- mice compared to control oIGF1R+/+ mice (**Fig. 33a**). Nonetheless, female oIGF1R-/- mice did not display any brain/body weight ratio difference (**Fig. 33b**).

Impaired remyelination in oIGF1R-/- CNS following cuprizone intoxication

As already mentioned, cuprizone intoxication results in increased IGF-1 production in affected CNS areas, and IGF-1 over-expression *in situ* seems to protect ODCs from death and to increase remyelination [106]. To test demyelination and ODC survival in our model we thus fed oIGF1R-/-, oIGF1R-/+ and oIGF1R+/+ *ad libitum* for 6 weeks with cuprizone and followed weight loss over the whole period. Interestingly**,** oIGF1R-/- mice displayed less weight loss in the first weeks followed by a slightly impaired weight gain in the second half of the feeding period (**Fig. 34a)**. Microglia numbers were increased in oIGF1R-/- and oIGF1R-/+ animals 3 weeks p.a. as shown by FACS and histological analysis (**Fig. 34b,c**). LFB-PAS stainings in the corpus callosum did not

reveal huge differences in myelin status among experimental groups (**Fig. 35**). To further investigate myelin phenotype in cuprizone-fed animals, we sacrificed oIGF1R-/-, hemizygous and wt animals after 3 and 5 weeks of intoxication and analyzed CNS lysates by immunoblotting using PLP- and MOG-specific antibodies. A general decrease in PLP expression compared to normally fed mice was evident at both time points, but no significant differences could be detected between cuprizone-fed oIGF1R-/- and control mice (**Fig. 36a,b**). However, demyelination seems to be slightly enhanced in the CNS of oIGF1R-/- mice (**Fig. 36a,b**). Analysis of NG2 protein levels revealed increased accumulation of this OPC marker specifically in oIGF1R-/- after 3 weeks of cuprizone feeding (**Fig. 36c**). On the opposite, at the end of the intoxication period NG2 levels appeared significantly lower in oIGF1R-/- compared to controls (**Fig. 36d**). Finally, to assess the number of ODCs along the intoxication period, sagittal CNS sections were stained with ASPA-specific antibodies and $ASPA^+$ cells were counted in cerebellum (data not shown) and corpus callosum regions (**Fig. 36e**). While no difference could be detected among the different groups 3 weeks p.a., ODC density was much lower in oIGF1R-/- and oIGF1R-/+ animals after 5 weeks of toxin feeding (**Fig. 36e**). Thus, even though cuprizone administration did not result into grossly different myelin abnormalities in oIGF1R-/- compared to wt control mice, absence of IGF1R in oIGF1R-/- mice or reduction of receptor expression in oIGF1R-/+ animals lead to a decreased ODC density under demyelinating conditions.

MOG-immunized oIGF1R-/- mice show lower disease incidence and disabilities compared to controls

As already mentioned, the role of IGF-1 in the context of EAE is largely controversial [107, 109, 112, 121, 123]. To better investigate the role of this signaling pathway in ODCs under inflammatory autoimmune conditions, we immunized oIGF1R-/- and littermate controls with MOG_{35-55} in CFA (PT at d 0 and +2). Surprisingly, oIGF1R-/- mice showed in all experiments a significantly lower disease score and a lower incidence (**Fig. 37a,b**). Also, clinical amelioration at beginning and during the chronic phase of EAE was intrinsic for mice developing the disease (**Fig. 37c**). However, no difference in disease onset and average disease severity could be observed (**Fig. 37b**). Histological analysis of brain samples from experimental and control animals did not

reveal gross differences between oIGF1R-/- and control mice, both in chronic (1 month p.i., **Fig. 38a**) and acute phase of EAE (disease onset, data not shown). Nonetheless, in some sample we found evidence of increased microglia activation (Iba1-specific stainings, **Fig. 38a**). Also, western blot analysis of CNS lysates 1 month p.i. revealed decreased gliosis in the CNS of IGF1R-/- mice (**Fig. 38b**). Flow cytometry analyses of CNS inflammatory infiltrates did not reveal consistent differences between oIGF1R-/- and controls (data not shown). However, analysis of microglia/macrophages revealed a relative decrease in MHC-II expression in, regardless of disease severity (**Fig. 38c**), and a significant reduction in CD44 and CD95 expression in oIGF1R-/- compared to control animals (**Fig. 38d**). To further investigate myelin and ODC status during autoimmune inflammation, we immunoblotted CNS lysates using MBP- and MOG-specific antibodies and found these protein levels slightly reduced in the CNS of oIGF1R-/- mice compared to controls (**Fig. 39a**). Surprisingly, we found significant reduction in ODC density in the corpus callosum of MOG-immunized oIGF1R-/- animals, both at peak disease and in the chronic phase, but in no other affected brain region (**Fig. 39b,c**). Hemizygous animals displayed a similar reduction in ODC density in the corpus callosum (**Fig. 39c**). Also, analysis of NG2 protein levels revealed increased OPC accumulation and activation in the CNS of oIGF1R-/- animals (**Fig. 39d**). Altogether, deletion of IGF1R on mature ODCs resulted in significantly increased protection and amelioration of EAE clinical signs; however, only minor histopathological changes in myelin and microglia/macrophages activation could be observed. On the other hand, local variations in ODC density and overall increase in progenitor markers seem to indicate an higher susceptibility of ODCs to inflammation in MOG-immunized oIGF1R-/- animals.

A novel mouse model to quantify *in vivo* variations in myelin content

In order to follow the *in vivo* dynamics of demyelination and remyelination, we have generated a mouse model (oLucR) in which luciferase expression is restricted by Cre expression to mature ODCs. Once the genetic locus of luciferase is recombined, oLucR mice express the reporter gene under the control of an ubiquitous β-actin promoter [158] (**Fig. 40a**). Since ODCs selectively express luciferase, induced ODC death and demyelination should result into decreased bioluminescence; also, demyelination-

triggered differentiation of OPCs should provide a readout of remyelination as new MOG-expressing ODCs repopulate the lesion and express luciferase for the first time.

The mice were shaved, anesthetized and quantitatively measured in an ultrasensitive IVIS machine (Xenogen) after i.p. injection of 150 ng/Kg of luciferin (**Fig. 40b**). The average photon-*per*-second recording over the full kinetics of luciferin/luciferase reaction was used as readout *per* mouse, *per* measurement. Besides CNS-specific luminescence, unspecific photon emission was also detected from non-CNS areas (especially liver, tail, and paws as in [158]). Thus, in every experiment bioluminescence signals were recorded from the whole animal as well as from specific areas of interest as brain and spinal cord (**Fig. 40b**). Continuous measurements of oLucR mice over 1 month showed no significant changes in basal bioluminescence over time, indicating that luciferase expression remains stable in adult animals (data not shown).

Cuprizone- and DT-mediated ODC death results into increased bioluminescence in oLucR mice

To initially test the reporter system, oLucR mice were normally- or cuprizone-fed for 6 weeks and bioluminescence changes recorded 3 times a week over the whole period. Since cuprizone intoxication results into specific ODC death in the corpus callosum, we expected a progressive decrease in bioluminescence along the feeding period. Surprisingly, IVIS measurements revealed a progressive increase in luciferase expression during the intoxication period specifically in toxin-fed oLucR mice. This increase reached its peak around 5 weeks p.a., and decreased progressively after removal of cuprizone from the diet (**Fig. 40c**). 60 days after starting the feeding we analyzed luciferase expression in CNS lysates through a luminometer assay and *ex vivo* by luciferin-bathed brain slices, but could not find any significant difference between cuprizone- and normally-fed mice, in concordance to the *in vivo* measurement (data not shown).

Next, we wanted to test the effects of massive and diffuse ODC death on the bioluminescence readout in our model. Thus, we crossed oLucR mice to the oDTR strain, and injected the resulting oLucR/DTR animals and oLucR control with 200 ng of DT daily for a week. As expected, oLucR/DTR mice developed progressive motor

impairment starting 5 weeks p.a. (**Fig. 41a**). Surprisingly, bioluminescence recordings 3 times a week did not reveal any decrease in luciferase signal. Rather, we could observe two different periods of increased bioluminescence in DT-treated oLucR/DTR mice: the first, during and shortly following the administration period of DT; the second, 6 to 7 weeks p.a. (**Fig. 41b**). *In vitro* analysis of CNS lysates 7 weeks p.a. revealed increased expression of luciferase in cerebellum and brain stem (**Fig. 42a**). Accordingly, luciferin-bathed *ex vivo* brain slices showed predominant luciferase expression into these myelin-rich areas (**Fig. 42b**). RNA analysis of CNS samples during the first peak of bioluminescence showed decrease in MOG expression, and increase in the OPC marker NG2 in oLucR/DTR compared to oLucR control mice (**Fig. 42c,d**). To further investigate this unexpected increase in photon signal we then analyzed the expression level of β-actin, which is regulated by the same promoter controlling luciferase expression. Our data shows that β-actin level were increased in DT-treated oLucR/DTR compared to oLucR control mice (**Fig. 42e**).

MOG-immunized oLucR animals show increased bioluminescence around disease onset

Surprisingly, induced ODC death in the oLucR model did not result in decreased bioluminescence (**Fig. 40c, 41b**). Rather, IVIS analyses of oLucR mice revealed sudden increases in photon signal from the damaged CNS concomitant to demyelination and OPC recruitment, and most specifically in heavily affected areas as cerebellum and brain stem (**Fig. 42a,b,c,d**). Hence, we wanted to test the dynamics of bioluminescence over the course of EAE, in which ODCs die sparsely and demyelination is more prominent in the spinal cord and brain stem areas [21]. oLucR animals were immunized with MOG in CFA and analyzed in the IVIS machine every other day to follow bioluminescence changes. As control served not-immunized oLucR animals. After a transient and brain-specific increase in bioluminescence at day 2, luciferase signal unexpectedly peaked around disease onset by 12-fold (**Fig. 43a,b**). Following this sudden increase, bioluminescence returned to lower levels, although brain signal remained higher than in the pre-induction phase. CNS *ex vivo* analysis by luciferin-bathed slices and *in vitro* analysis by luminometer assay revealed accumulation of luciferase in spinal cord and brain stem 1 month p.a. in EAE-induced animals (**Fig. 43c,d**). Nonetheless, it is known that during the course of EAE the permeability of the BBB is increased (**Fig. 18d**). To exclude that the observed *in vivo* bioluminescence

changes would result from increased permeability of the BBB and higher luciferin influx in the CNS, we immunized oLucR animals with MOG in CFA and sacrificed mice every other day starting from day 5. *Ex vivo* brain slices bathed in luciferin showed increased expression in mice showing clinical disease (**Fig. 44a**) and the bioluminescence pattern recapitulated the one observed *in vivo* (**Fig. 43a**). We then tested the possible effects of PT on bioluminescence, as the toxin is supposed to transiently open the BBB aiding the development of a self-immune response [159, 160]. Hence, we injected oLucR animals with PT and recorded bioluminescence changes over time compared to BSA-injected animals. PT resulted in a low and transient increase in luciferase signal (**Fig. 44b**), which was comparable to the first bioluminescence increase as detected in the EAE experiment (**Fig. 42a**). Thus, the strong luciferase signal recorded around disease onset is an intrinsic *in vivo* characteristic of ODCs under immune attack. To further investigate ODC status at EAE onset, we immunized and sacrificed oLucR animals at day 11 p.i.. RNA analysis revealed decreased ODC markers such as MOG and Olig1, and a strong increase in stem cell and OPC markers as NG2 and Nestin (**Fig. 45a,b,c,d**). β-actin level was strongly increased specifically in the spinal cord of oLucR animals induced with EAE (**Fig. 45e**).

Antibody-mediated demyelination in organotypic slice cultures derived from oLucR mice

Induced ODC death and demyelination in the oLucR model resulted in a surprising *in vivo* increase in ODC-specific luciferase signal under different conditions (**Fig. 40c, 41b, 43a**). To investigate the oLucR system without confounding *in vivo* factors, we thus worked with cerebellar organotypic slice cultures derived from neonatal mice (see *Material and Methods*). Slices were kept in culture with the addition of luciferin and imaged in the IVIS machine every other day (**Fig. 46a**). As demyelinating method, antiMOG and complement were added to the culture for 48 hours and then washed out with fresh medium. Preliminary analysis of bioluminescence in these cultures showed a relative increase in bioluminescence in demyelinated slices from oLucR slice compared to oLucR untreated slices (**Fig. 46b**).

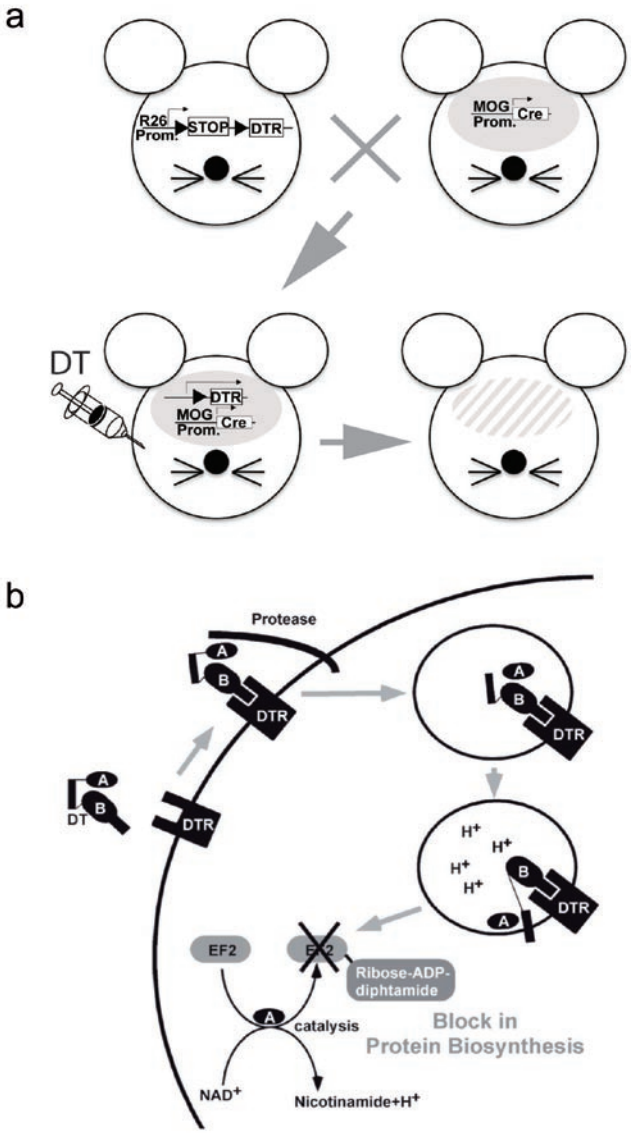

Figure 14

(a) The oDTR model: a mouse strain carrying a Cre-inducible diphtheria toxin receptor (iDTR) is crossed to a mouse strain expressing the Cre recombinase specifically in ODCs (MOGi-Cre). The double transgenic animals (oDTR) express the DTR on the surface of ODCs, which are thus rendered susceptible to DT. Upon injection of DT into such mice, OODCs die and demyelination iinitiated. (b) Scheme of the DT-induced death mechanism. The toxin binds to its receptor and is cleaved by a protease into its active components. After internalization and pH decrease, the A subunit is transferred by the B subunit in the cytosol where it enzymatically inactivates the elongation factor 2 (EF2).

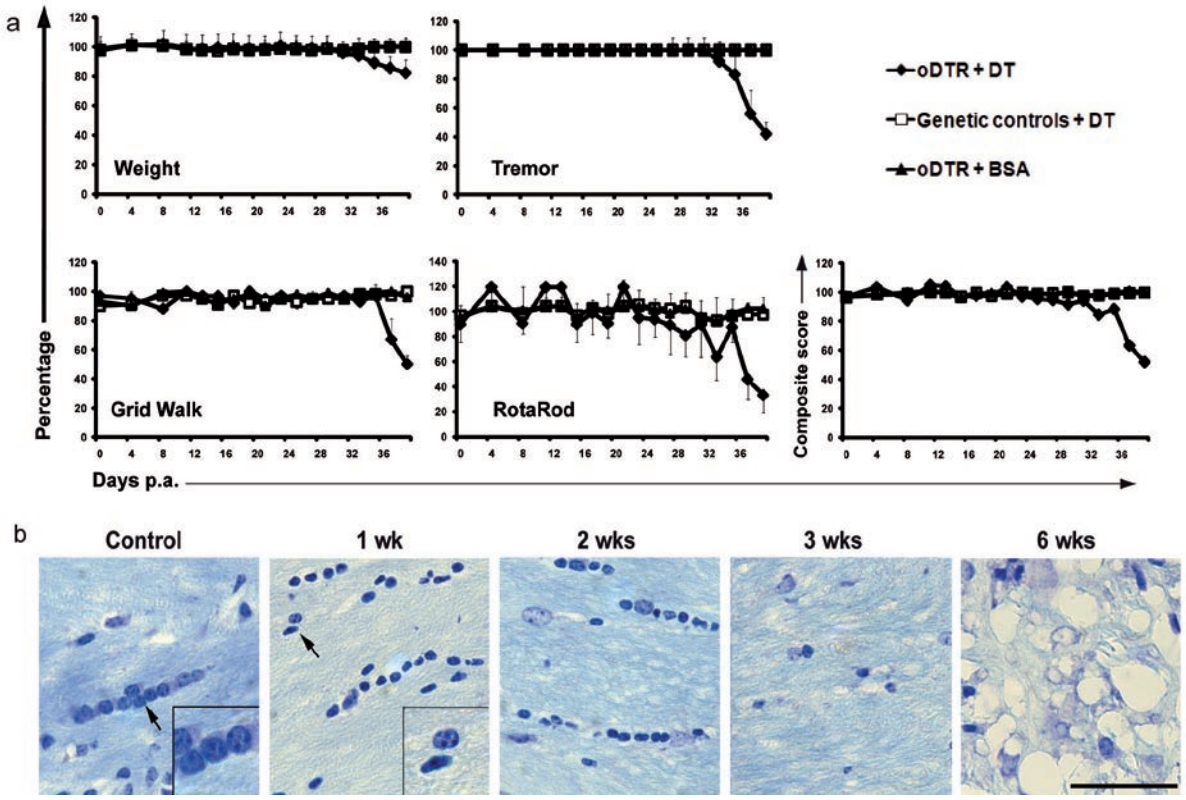

Figure 15

(a) oDTR clinical presentation: oDTR and control mice (MOGi-Cre or iDTR) were injected with 200 ng DT over a course of 7 days. In addition, a control group of oDTR mice received 200 ng of BSA over the same period of time. The animals were scored by a RotaRod and a grid walk motor tests. Weight of animals and tremor observed during the motor tests were recorded. The means of weight, tremor and motor assays measurements were combined in one representative composite score. (b) oDTR animals were treated with DT and sacrificed at the indicated time points. Nissl staining of the pons is shown. Magnifications in control and 1 week (wk) samples show condensed cytoplasm and shrunk nuclei after DT application in oDTR mice. Scale bar, 50 µm.

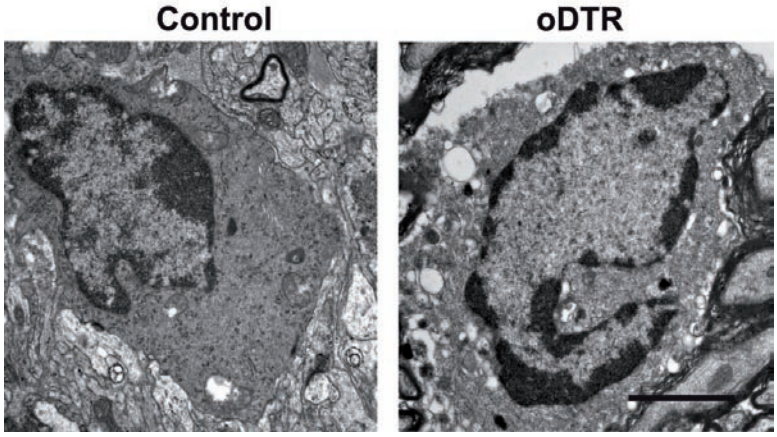

Figure 16

Electron micrographs of brain stem sections show a normal-appearing ODC in the control mouse (left) compared to a moribund, densely-vacuolated ODC in the DT-treated oDTR mouse (right). Samples were collected 14 days p.a.. Scale bar, 2 µm.

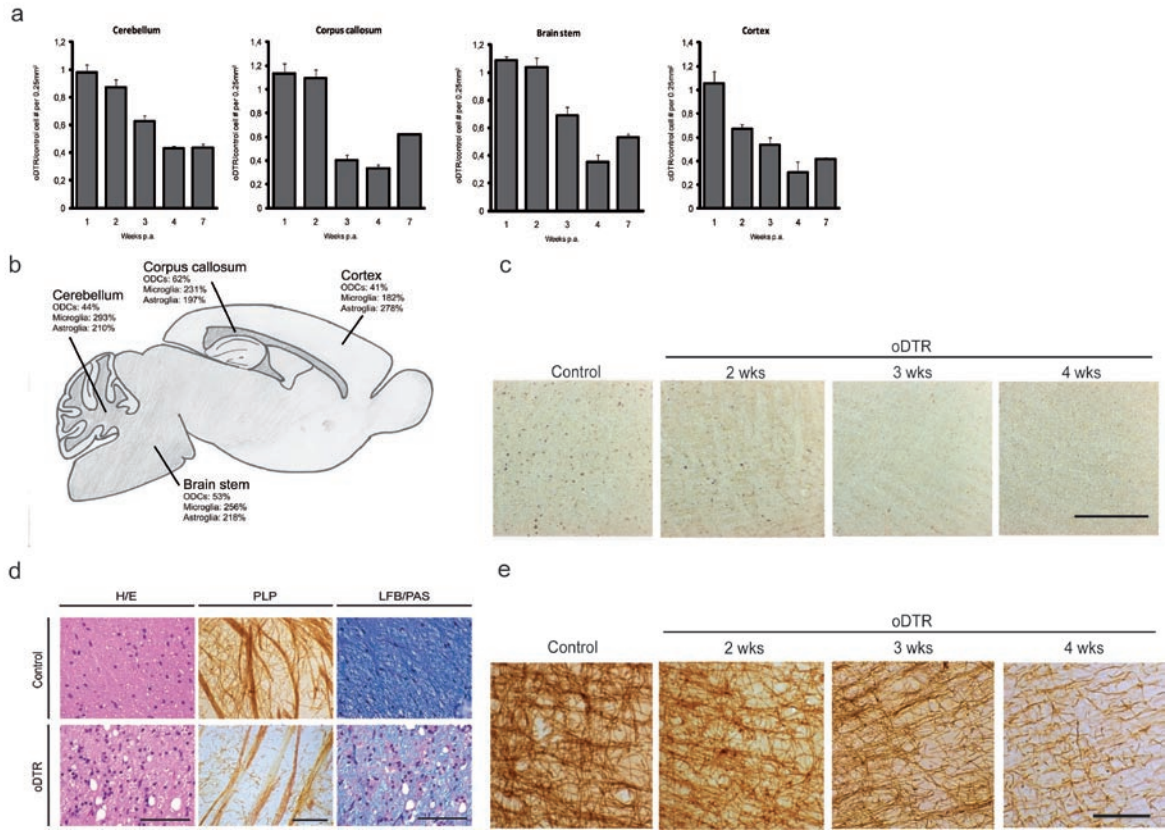

Figure 17

(a) oDTR and control mice were treated with DT and sacrificed at indicated time points. CNS sections were stained with ASPA-specific Ab and positive cells were manually counted. The mean ratio between cell density in oDTR versus control mice is shown, ± s.e.m. (n=3, 4 sections per animal). (b) Sketch diagram illustrating a sagittal section of a murine brain. Areas analyzed and relative endpoint percentages of glial cells (7 weeks p.a. compared to control) are shown (b) oDTR mice were treated with 200 ng daily DT for a week. At reported time points p.a. brain sections were stained for the mature ODC-specific protein ASPA. Here we show the progressive disappearance of ODC nuclei from the striatum of DT-treated oDTR animals. Scale bar, 200 µm. (d) CNS sections were stained for H/E, PLP and LFB/PAS. For H/E and LFB/PAS mice were sacrificed 6 weeks p.a., for PLP staining 4 weeks p.a. Shown are magnifications of spinal cord (H/E and LFB/PAS) and striatum (PLP). Scale bar for H/E and LFB/PAS stainings, 100 µm. Scale bar for PLP staining, 50 µm. (e) oDTR and control mice were treated with DT and brain sections stained at different time points p.a. for the myelin protein PLP. Scale bar, 50 µm.

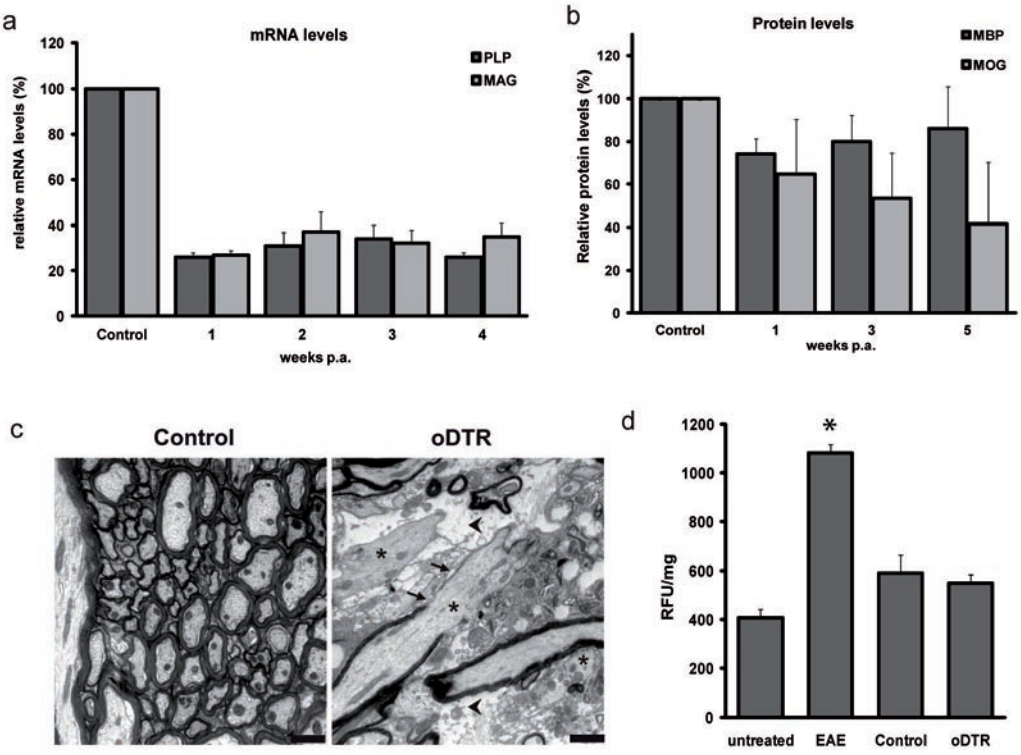

Figure 18

(a) oDTR mice were sacrificed at indicated time points, RNA isolated from the spinal cord and analyzed by RT-PCR for PLP and MAG expression. Bar graphs indicate mean values relative to control ± s.e.m. (n=3). (b) oDTR mice were sacrificed at indicated time points and brain lysates analyzed by immunoblotting against MBP and MOG. Bar graphs indicate mean values ± s.e.m. (n=3). (c) Electron micrographs of cerebellum from DT-treated control and oDTR mice show groups of normal-appearing myelinated axons in control brain (left) compared to demyelinated axons (asterisks), smaller vacuoles (arrows) and larger edematic areas (arrow heads) in material from oDTR mice (right). Samples were collected 7 weeks p.a., scale bar 1 µm. (d) Evans blue analysis shows no difference in BBB integrity between oDTR and control animals 1 week after DT treatment. MOG/CFA immunized animals were used as positive, untreated animals as negative control.

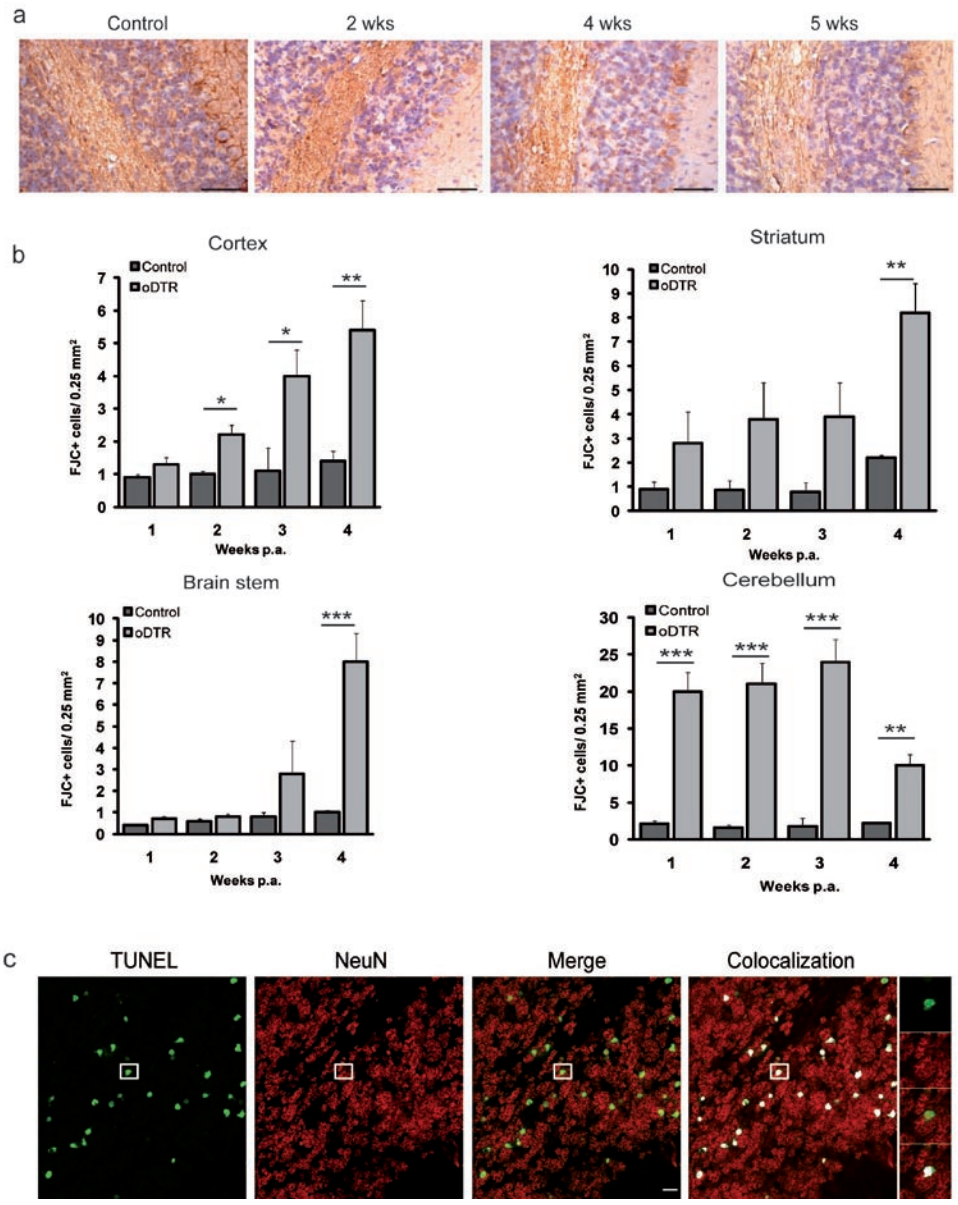

Figure 19

(a) oDTR/control animals were injected with DT and sacrificed at indicated time points. Representative NF-immunostained sections from cerebellum are shown. Scale bar, 50 µm. (b) DT-treated oDTR and control mice were sacrified at indicated time points p.a. and brain sections were stained with Fluoro-Jade C. Positively stained cells were quantified in the indicated areas (n=3). (c) Mice were treated with DT and sacrificed 1 week p.a.. CNS samples were collected and stained for TUNEL (green) and for the neuronal marker NeuN (red). Colocalizations of TUNEL and NeuN staining are shown in white. Shown is cerebellum, scale bar 20 µm. On the right, inlets show 10x magnification of a double-positive neuronal cell.

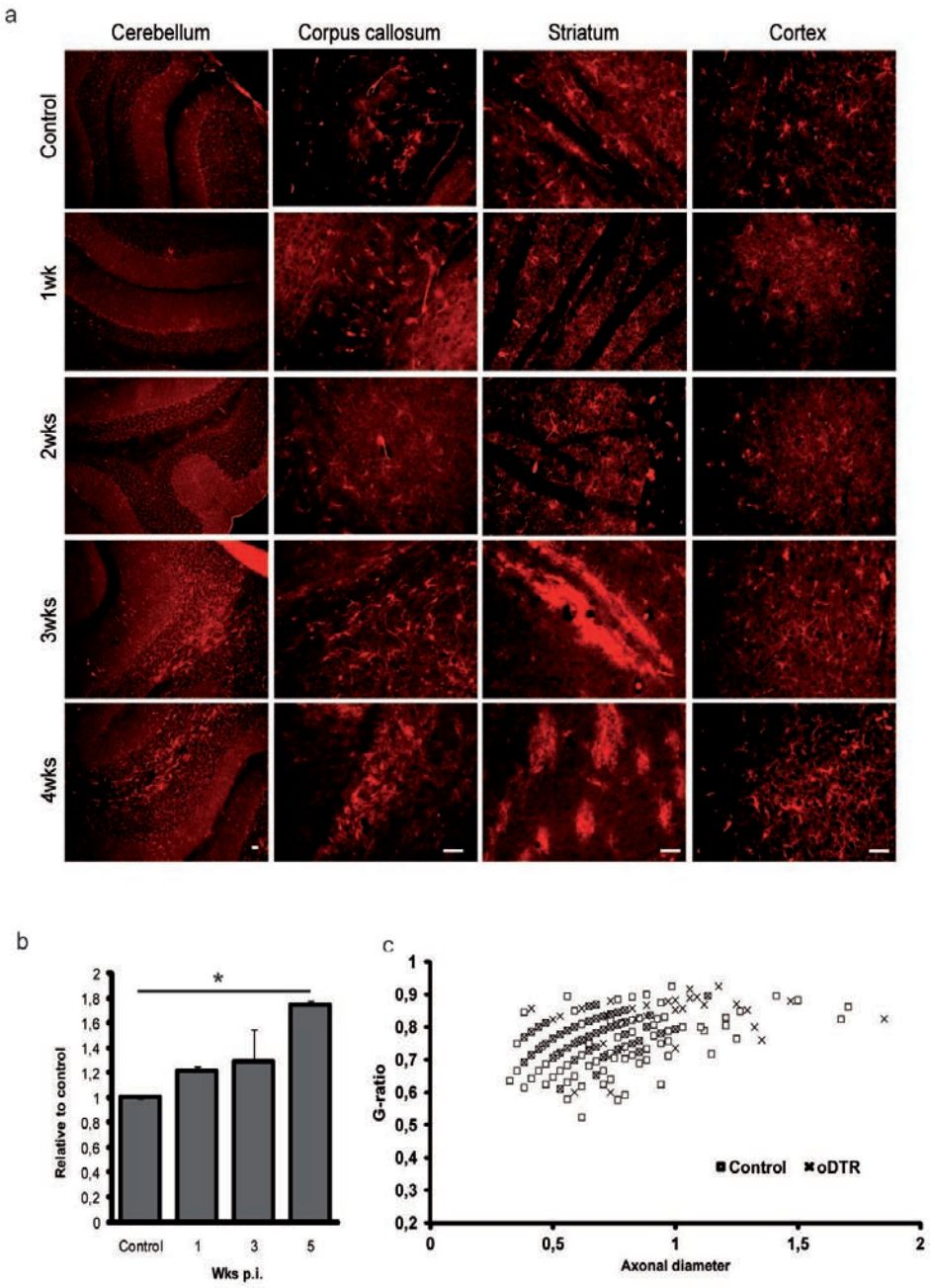

Figure 20

(a) DT-treated oDTR and control mice were sacrificed at indicated time points p.a. and brain sections immunostained for NG2 in the indicated areas. Scale bar, 50µm. (b) oDTR and control mice were sacrificed at indicated time points and brain lysates analyzed by immunoblotting against NG2 and Vinculin. Bar graphs indicate mean values relative to control ± s.e.m. (n=3). (c) DT-treated oDTR and control mice were sacrificed 5 weeks p.a. and corpus callosum samples were investigated by TEM. Shown is a scattergram of g-ratios in relation to axonal diameter. Average g-ratio in oDTR animals was 0.7967 ± 0.0055 compared to 0.7536 ± 0.014 in control animals, $p<0.0001$.

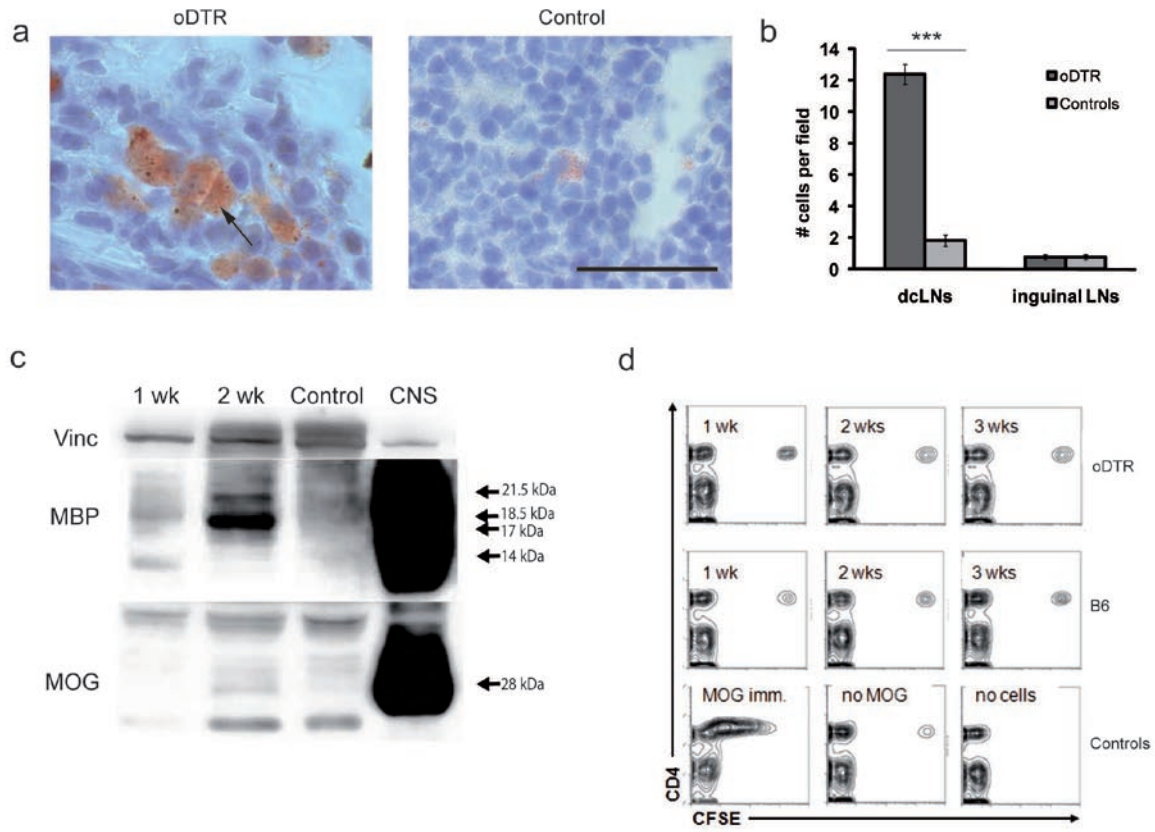

Figure 21

*(a) Sections from dcLNs of DT- and BSA-treated oDTR mice were stained with OilRedO (ORO) 3 weeks p.a. Arrow indicates representative ORO$^+$ cells. Scale bar, 20µm. (b) Quantification of ORO$^+$ cells in dcLNs and inguinal LNs of DT- and BSA- treated oDTR animals, 3 weeks p.a. (data representative of 4 mice per group. Mean values and s.e.m.. ***, P<0.001, two tailed Student's t test). (c) oDTR and control mice were treated with DT and sacrificed 1 and 2 weeks p.a.. Tissue lysates of lumbar LNs were analyzed by immunoblotting using antibodies specific for Vinculin (Vinc, loading control), MBP, and MOG. Total CNS extract was used as a positive control (160 µg of oDTR and control extracts and 80 µg CNS extract were loaded). Arrows indicate expected molecular weights for MOG protein and MBP isoforms. (d) Flow cytometric analysis of antigen leakage as detected by myelin-specific T cells. 10^7 CFSE-labeled 2D2 T cells were injected into oDTR mice 1, 2, and 3 weeks (wks) p.a. and recovered four days later. As controls served C57BL/6 (B6) mice either untreated (bottom, center and right) or immunized with MOG_{35-55} in CFA (bottom, left).*

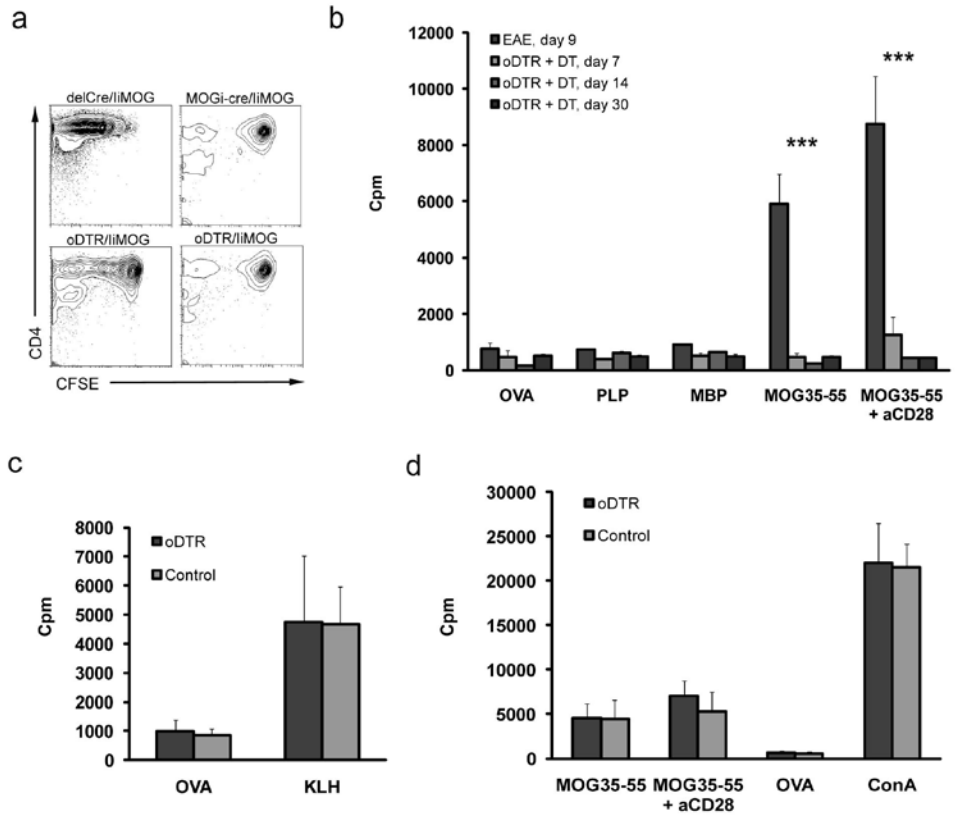

Figure 22

*(a) oDTR/IiMOG mice as well as MOGi-Cre/IiMOG controls were injected with 25ng/g DT per day from d -3 to d 0. At d 0 CFSE-labeled 2D2 cells (CD90.1) were transferred into the CD90.2 oDTR/IiMOG and control mice. PT was applied i.p. at d 0 and 2 followed by an agonistic mAb against CD40 (30 µg at d 5). Five days after transfer cells from axillary and inguinal LNs were analyzed by flow cytometry. As positive control served animals treated the same way and expressing IiMOG in all cells (del-Cre/IiMOG, top left). (b) Cells were isolated from DT-treated oDTR and control animals 7, 14, and 30 days p.a and stimulated in culture with OVA, PLP, MBP, and MOG peptide with or without CD28-specific antibody. For positive control, cells were isolated from LNs of B6 mice 9 days after immunization with MOG_{35-55} in CFA and stimulated in culture with the same proteins (***, $P<0.001$). (c) oDTR and control animals were treated with DT for 1 week and subcutaneously injected with KLH/CFA or MOG_{35-55}/CFA (d) with additional i.p. injection of PT (right). 9 days post immunization animals were sacrificed, cells isolated from lymph nodes, and restimulated in vitro with KLH and MOG_{35-55}, respectively, with or without CD28 co-stimulation. Addition of OVA and ConA served as negative and positive control (mean and s.e. of 3 mice per group).*

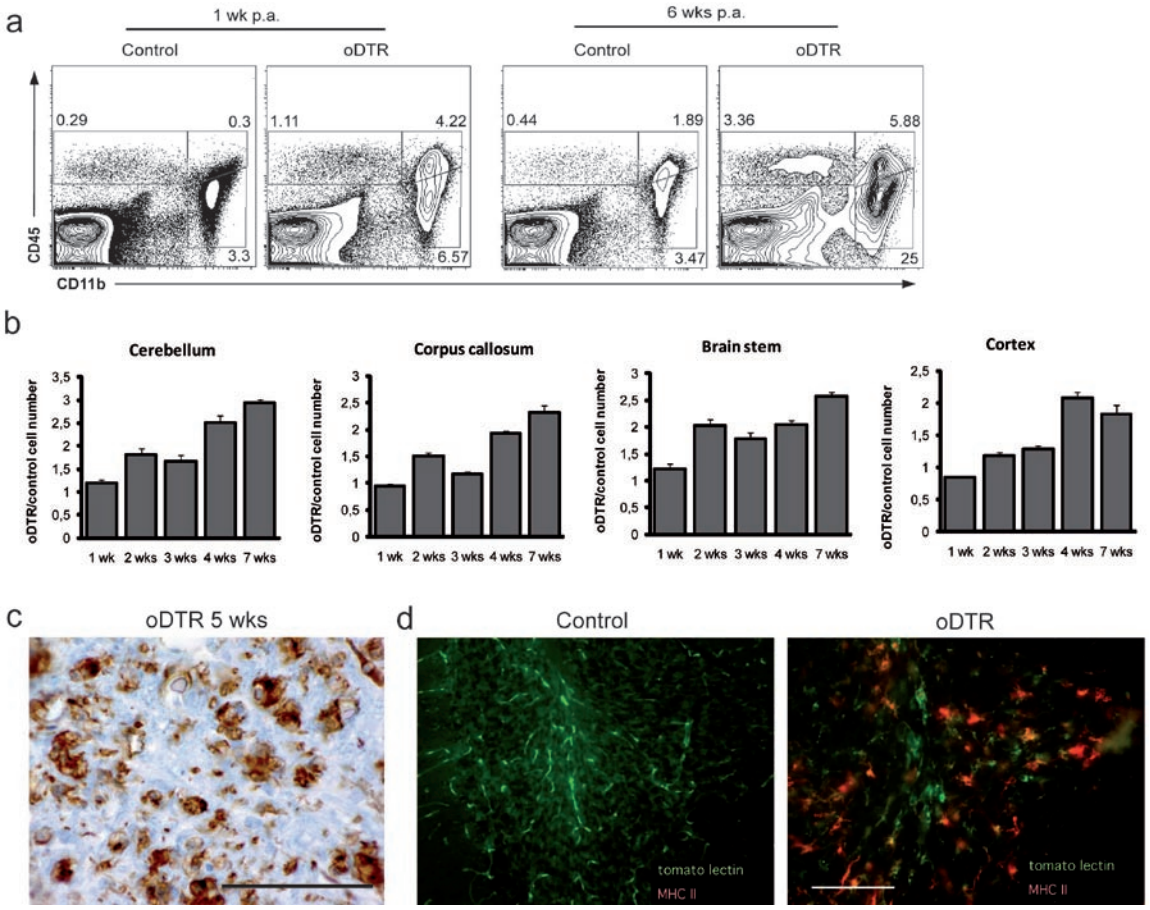

Figure 23

(a) Flow cytometric analysis of cells isolated from the CNS of oDTR and control animals 1 week (left) and 6 weeks (right) p.a.. Indicated are gates and percentages of cells in the respective gate for invading cells (CD45^{hi} CD11b^{-}), macrophages (CD45^{hi} CD11b^{hi}), and microglia (CD45^{int}CD11b^{hi}). Data representative of two independent experiments, n=6. (b) oDTR and control mice were treated with DT and sacrificed at indicated time points. CNS sections were stained with Iba1-specific Ab and positive cells were manually counted. The ratio between cell density in oDTR versus control mice is shown (n=3, 4 sections per animal). (c) Brain sections from oDTR mice 5 weeks p.a. were stained with Iba1 antibody. Scale bar, 100 µm. (d) Brain sections of oDTR and control mice showing activated microglia/macrophages 4 weeks p.a. (microglia: MHCII-specific antibody, red; tomato-lectin: green). Scale bar, 200 µm.

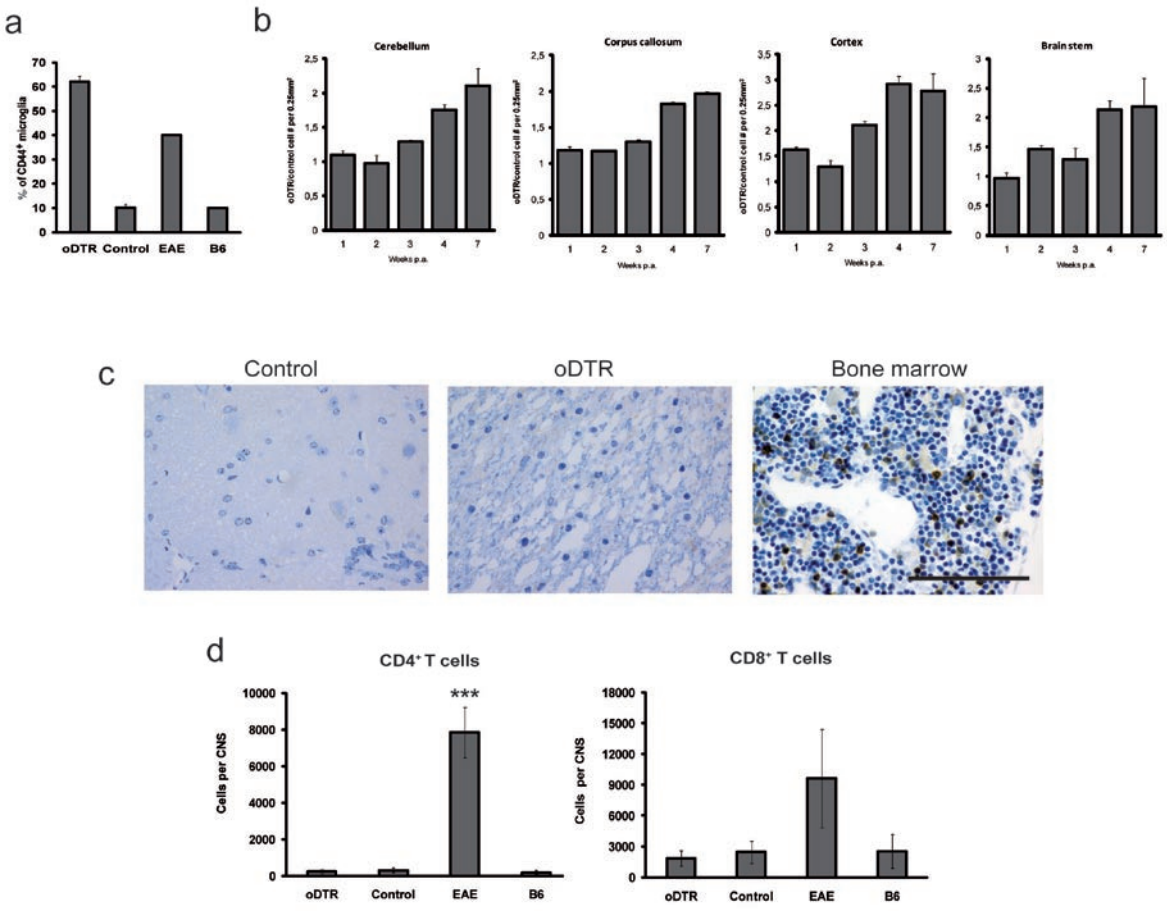

Figure 24

*(a) oDTR and control mice were treated with DT. Cells from the CNS were isolated, stained for CD45, CD11b, CD44 and analyzed by flow cytometry. Bar graph shows the percentages of microglia expressing CD44 (mean and s.e. of 3 mice per group). (b) oDTR and control mice were treated with DT and sacrificed at indicated time points. CNS sections were stained with GFAP-specific Ab and positive cells were manually counted. The ratio between cell density in oDTR versus control mice is shown (n=3, 4 sections per animal). (c) Histological sections from the CNS of indicated animals and bone marrow (positive control) were stained with antibody to CD3. Scale bar, 100 µm. (d) oDTR and control animals were treated with 400 ng DT at d0, 2, 4, and 6. 50 days p.a. cells were isolated from the CNS, stained for CD45, CD11b, CD4, and CD8 and analyzed by flow cytometry. Absolute number of infiltrating $CD4^+$ (left) and $CD8^+$ (right) T cells are shown. Data are representative of two independent experiments (mean and s.e.m. of 5 mice per group). As positive and negative control served cells isolated from the CNS of oDTR animals 20 days post-immunization with CFA and MOG peptide (mean and s.e.m. of 3 mice per group) and of untreated C57/Bl6 (B6) animals (mean and s.e.m. of 2 mice per group), respectively. ***, P<0.001.*

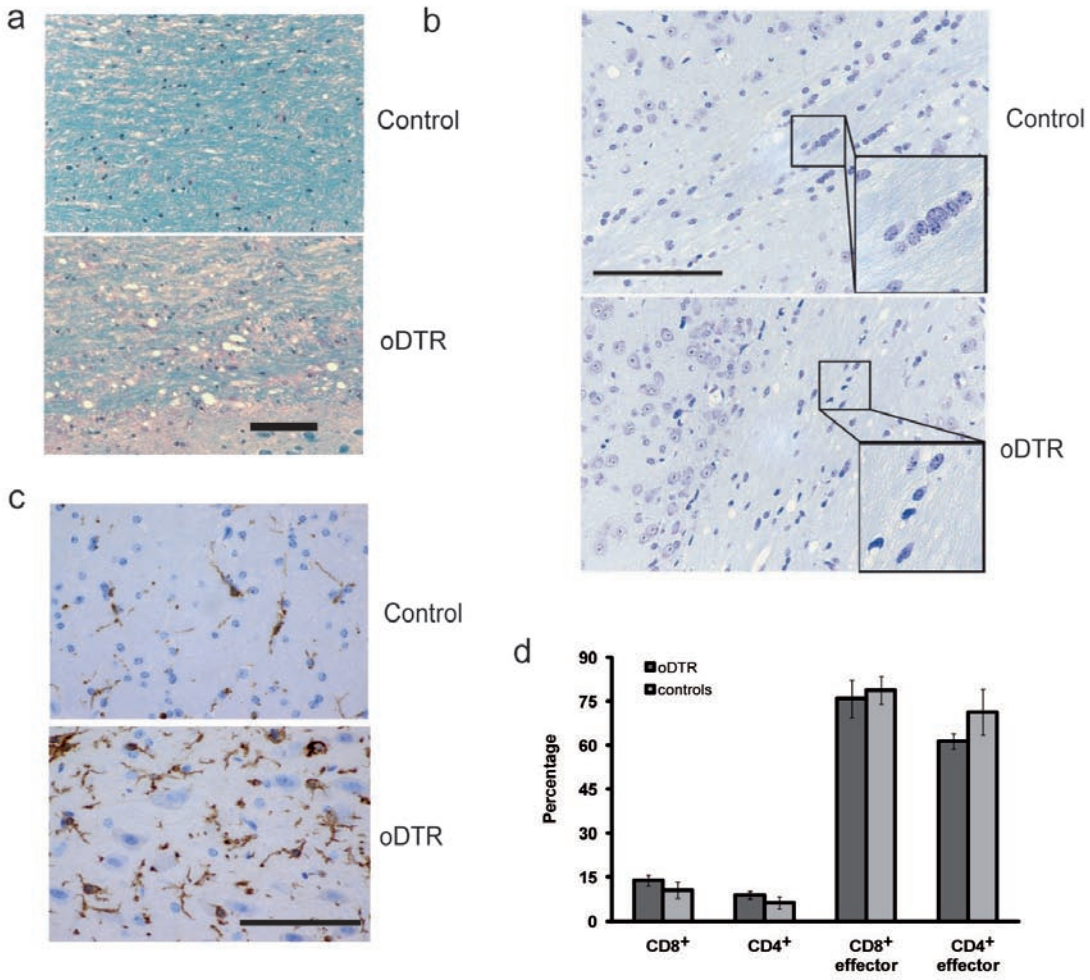

Figure 25

(a) Following a 5 months-treatment with a weekly dose of 50 ng DT, oDTR and control mice were sacrificed and LFB-PAS staining performed on slices. Shown is brain stem, scale bar 200 µm (n=3). (b) Mice were treated with one single dose of 50 ng DT and sacrificed 3 days later. Slices were Nissl-stained, pons is shown. Scale bar 200 µm (n=3). (c) Mice were treated as in (a) and slices were stained with Iba1-specific antibodies. Shown is cerebellum, scale bar, 100 µm (n=3). (d) Flow cytometric analysis of cells isolated from the CNS of oDTR and control animals after 5 months of chronic ODC death. $CD4^+$ and $CD8^+$ T cells are gated from the $CD11b^-$ $CD45^{hi}$ population, $CD4^+$ effector cells gated on $CD44^{hi}$ $CD62L^{low}$ $CD4^+$ total cells, $CD8^+$ effector cells gated on $CD44^{hi}$ $CD62L^{low}$ $CD8^+$ total cells. Bar graphs represent mean percentage of cells in the respective populations and s.e.m., n=6.

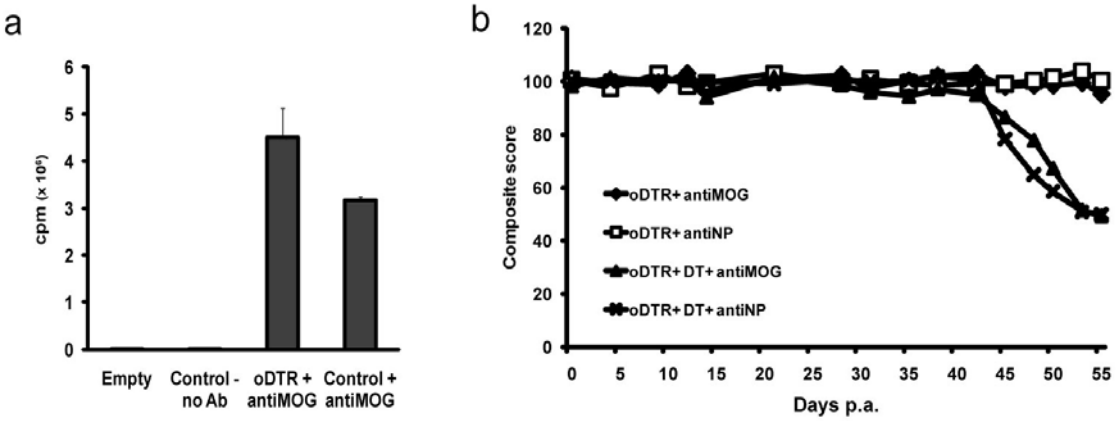

Figure 26

(a) oDTR and control mice were injected with DT and, after 4 weeks, with ^{125}I-labeled MOG-specific antibodies. Mice were sacrificed after 12 hours, perfused, and the CNS were analyzed for radioactive incorporation by use of a gamma-counter (n=2). (b) oDTR and control animals were treated i.p. with 400 ng DT at d0, 2, 4, and 6, and i.v. with 200 µg of either MOG-specific or NP-specific antibody at d14, 21 and 28 and scored as described in ***Fig. 15a****.*

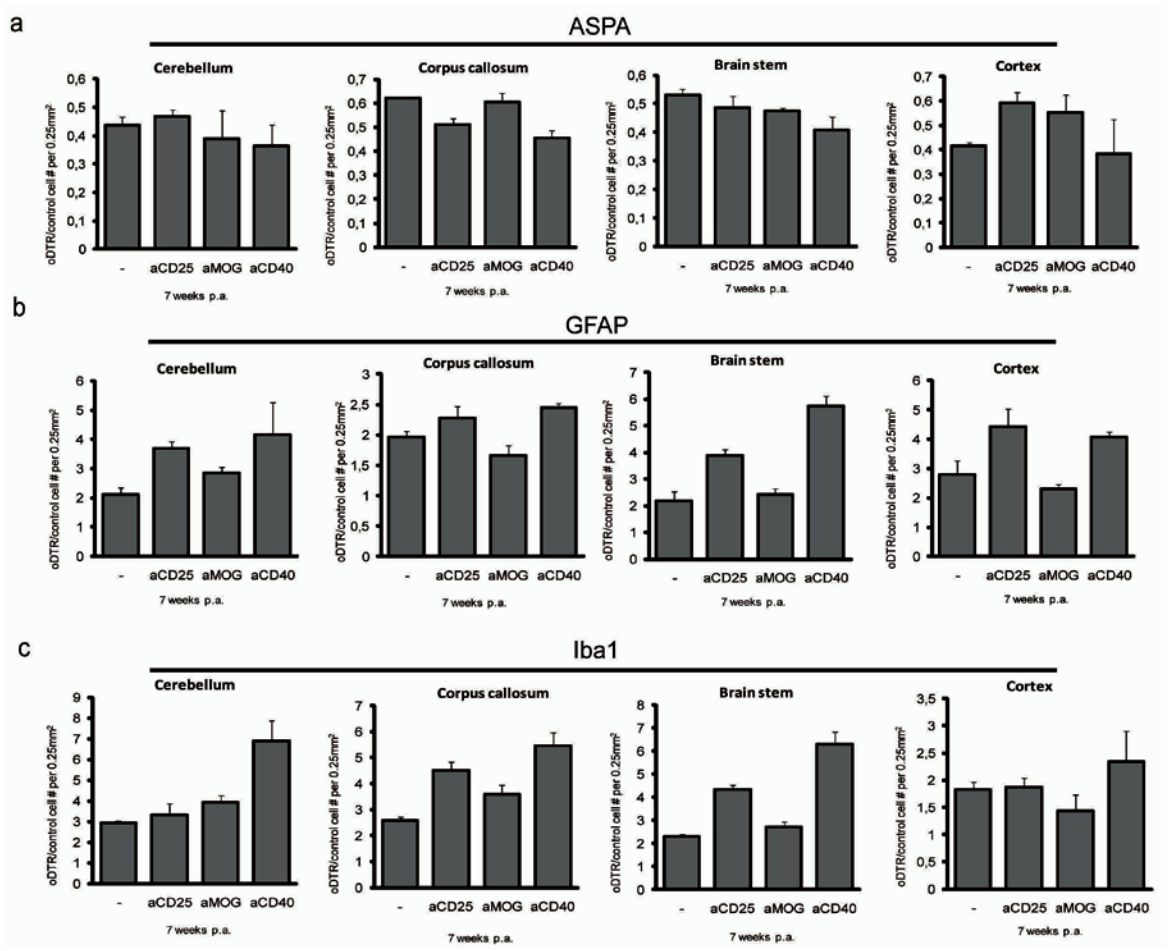

Figure 27

oDTR and control mice were treated with DT only or DT+ CD25-, MOG-, or CD40-specific antibodies and sacrificed 7 weeks p.a.. CNS sections were stained with ASPA-specific (a), GFAP-specific (b) or Iba1-specific (c) Abs and positive cells were manually counted. The mean ratio between cell density in oDTR versus control mice is shown, ± s.e.m. (n=3, 4 sections per animal).

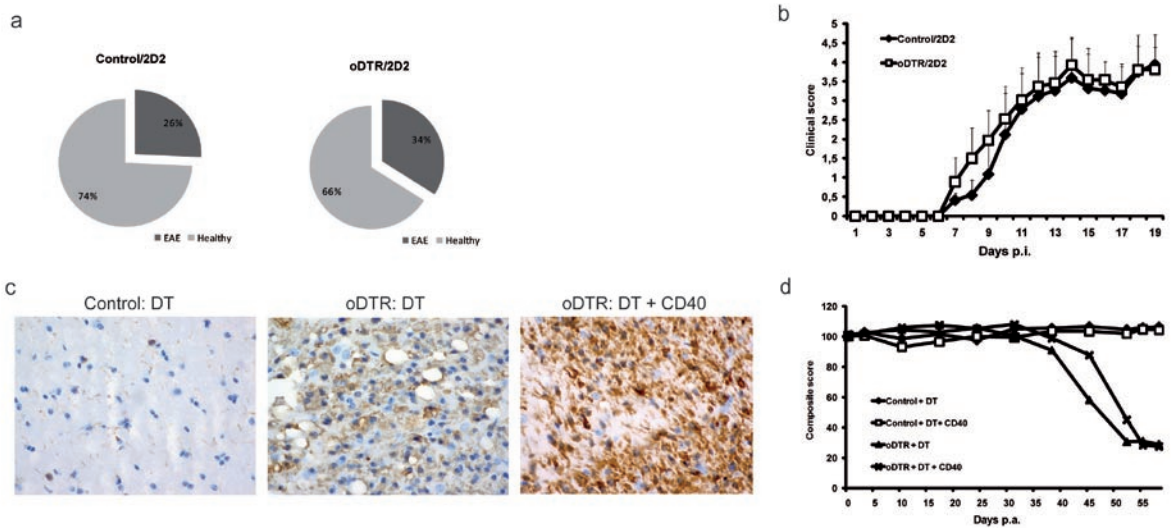

Figure 28

(a) oDTR/2D2 and MOGi-Cre/2D2 mice were injected with DT 3 times (25 ng/g) and 7 d p.a. treated with CFA (d0) and PT (d0 and +2). Graphs show percentages of sick animals in the respective groups. Data were pooled from three independent experiments (n=32). (b) oDTR/2D2 and MOGi-Cre/2D2 mice were treated as in (a), shown is the EAE disease course. Data was pooled from three independent experiments (n=32). (c) oDTR and control animals were treated with 250 ng DT weekly and 2 animals per group received at d30, 37, and 44 p.a. 200 µg of agonistic CD40-specific antibody. Brain sections from these animals were stained with anti-Iba1 55 days p.a.. Shown is corpus callosum, scale bar 100 µm. (d) oDTR and control animals were treated as in (c), scoring as in ***Fig. 15a.***

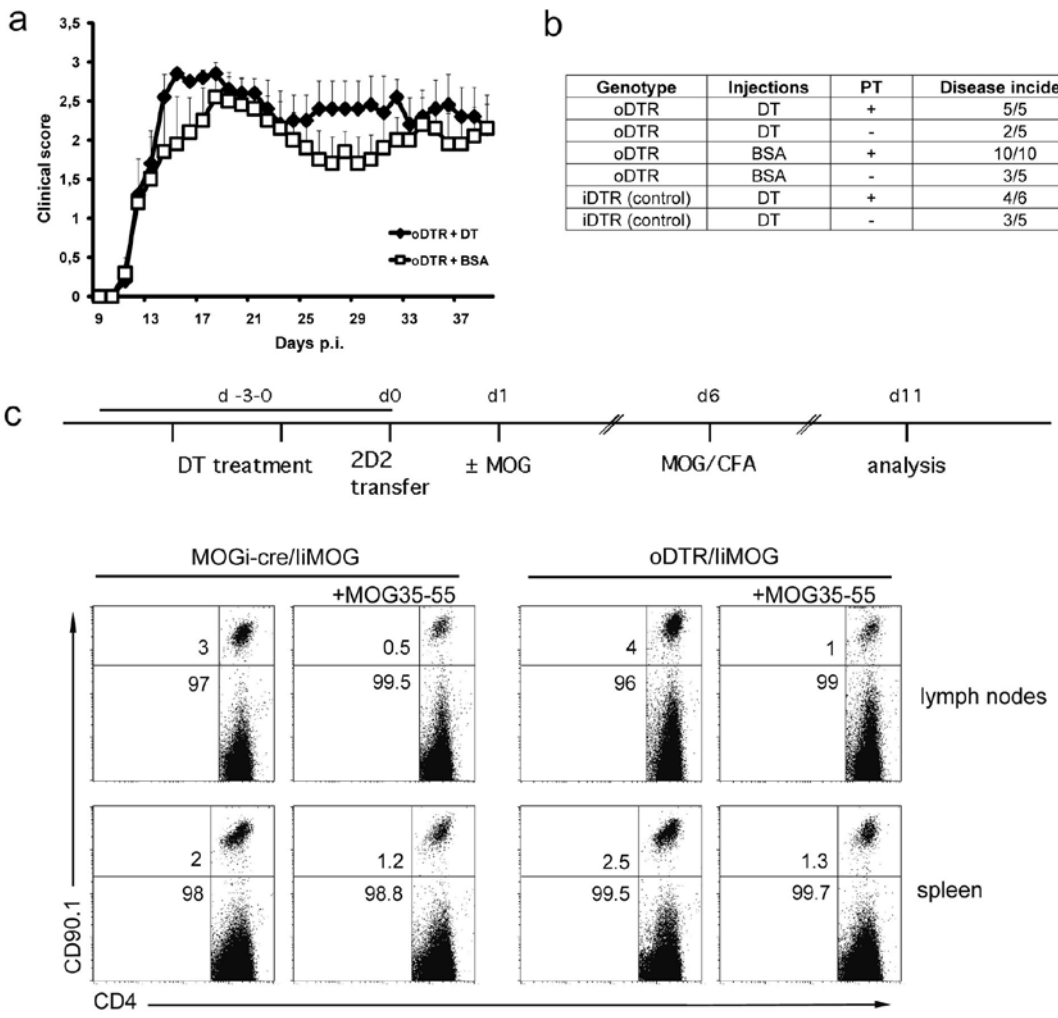

Genotype	Injections	PT	Disease incidence
oDTR	DT	+	5/5
oDTR	DT	-	2/5
oDTR	BSA	+	10/10
oDTR	BSA	-	3/5
iDTR (control)	DT	+	4/6
iDTR (control)	DT	-	3/5

Figure 29

(a) oDTR mice were treated with 200 ng DT or BSA daily for a week and then immunized with MOG_{35-55} in CFA on day 0. PT was injected at d0 and d2. Animals were scored as described in Methods section (Data representative of two independent experiments, 8 mice per group. Shown are mean values and s.e.m.). (b) Disease incidence of CFA/MOG_{35-55}-immunized animals with or without PT or DT application. (c) oDTR/IiMOG mice and MOGi-Cre/IiMOG controls were treated as described for tolerance induction. LN cells were stained for CD90.1 and CD4, and analysed by flow cytometry. Shown are cells gated on $CD4^+$ cells. The percentages of cells lying in the $CD90.1^+$ $CD4^+$ and $CD90.1^-$ $CD4^+$ gates are indicated.

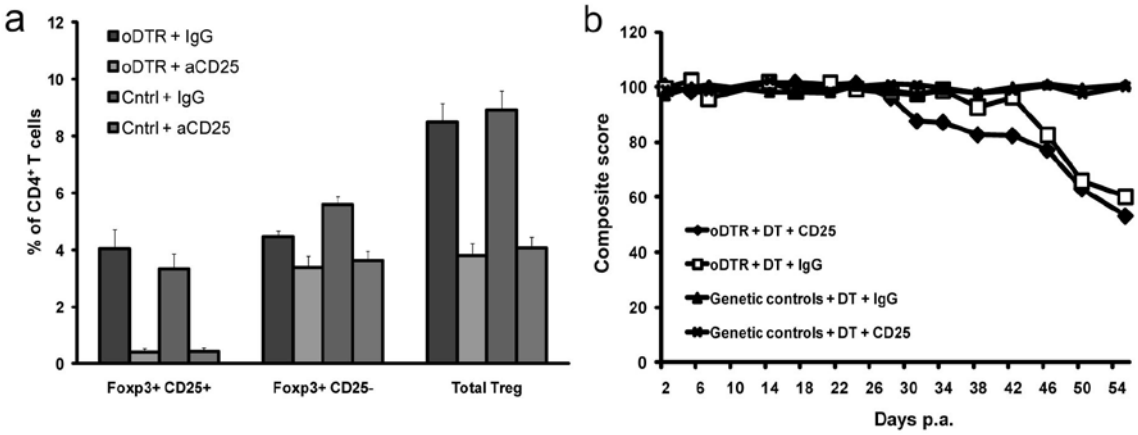

Figure 30

(a) oDTR and control mice were treated with DT and at d1, 3, and 5 injected with 150 µg of CD25-specific antibody or IgG isotype control. At day 8 blood was collected and stained for CD45, CD4, CD25, Foxp3 and analyzed by flow cytometry. Bar graph shows mean percentages and s.e.m. of $Foxp3^{+}CD25^{+}$ cells within the $CD4^{+}$ population, n=9. (b) oDTR and control animals were treated as in (a). Scoring as in ***Fig. 15a****. Data are relative to two independent experiments, n=10.*

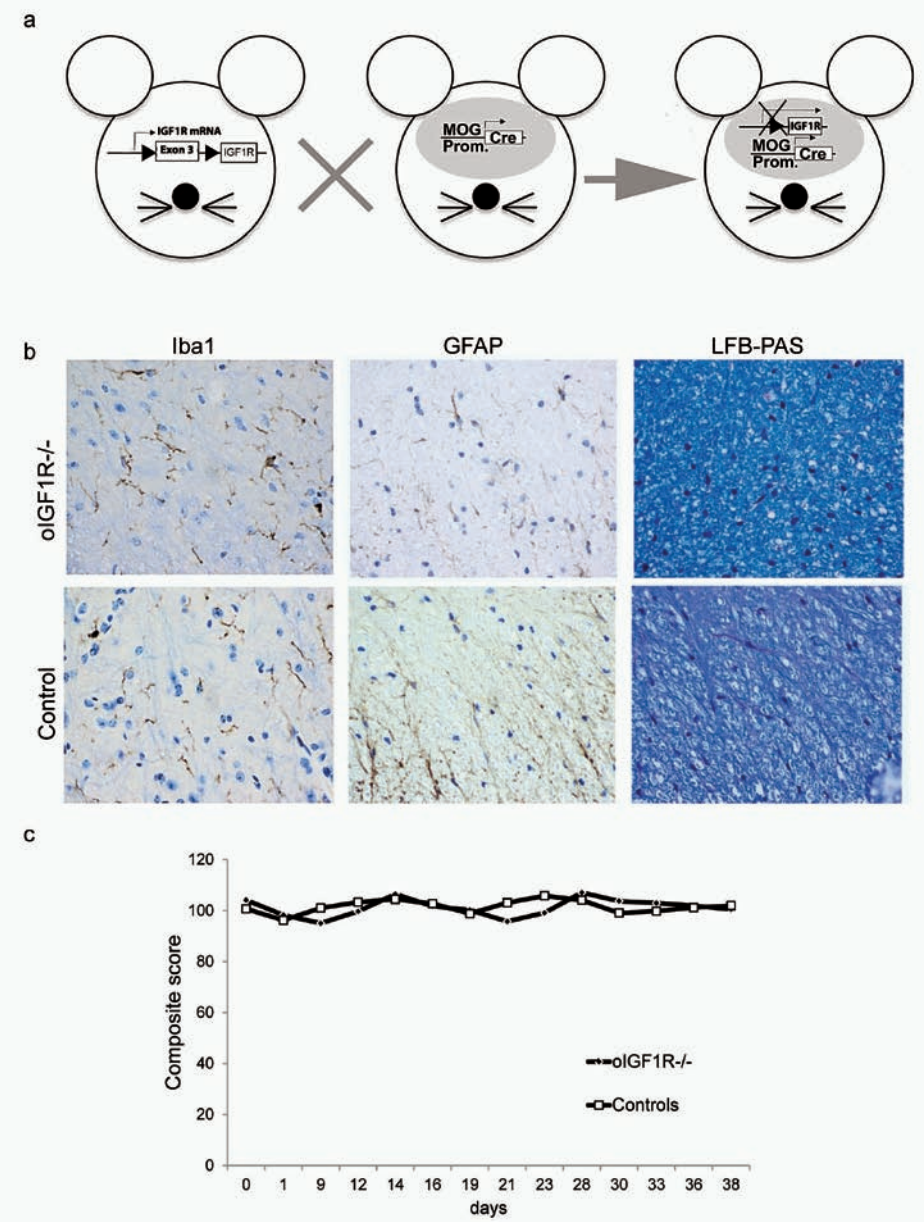

Figure 31

a) Mice carrying an IGF1R gene with the 3rd exon floxed (IGF1Rfl/fl) were crossed to mice expressing the Cre recombinase specifically in ODCs (MOGiCre). In the resulting offspring (oIGF1R-/-), Cre proteins recombine IGF1R locus in ODCs resulting in conditional KO of IGF1R. b) Histological analysis of 4 months old-oIGF1R-/- animals and WT control animals show no major abnormalities in oIGF1R-/- mice. Staining were performed with Luxol Fas Blue-Periodic Acid Schiff (LFB-PAS) and with antibodies specific for Iba1 (microglia) and GFAP (astrocytes). Scale bar, 250 µm. c) 3 months old oIGF1R-/- and control mice were tested as in ***Fig. 15a*** *up to 38 days.*

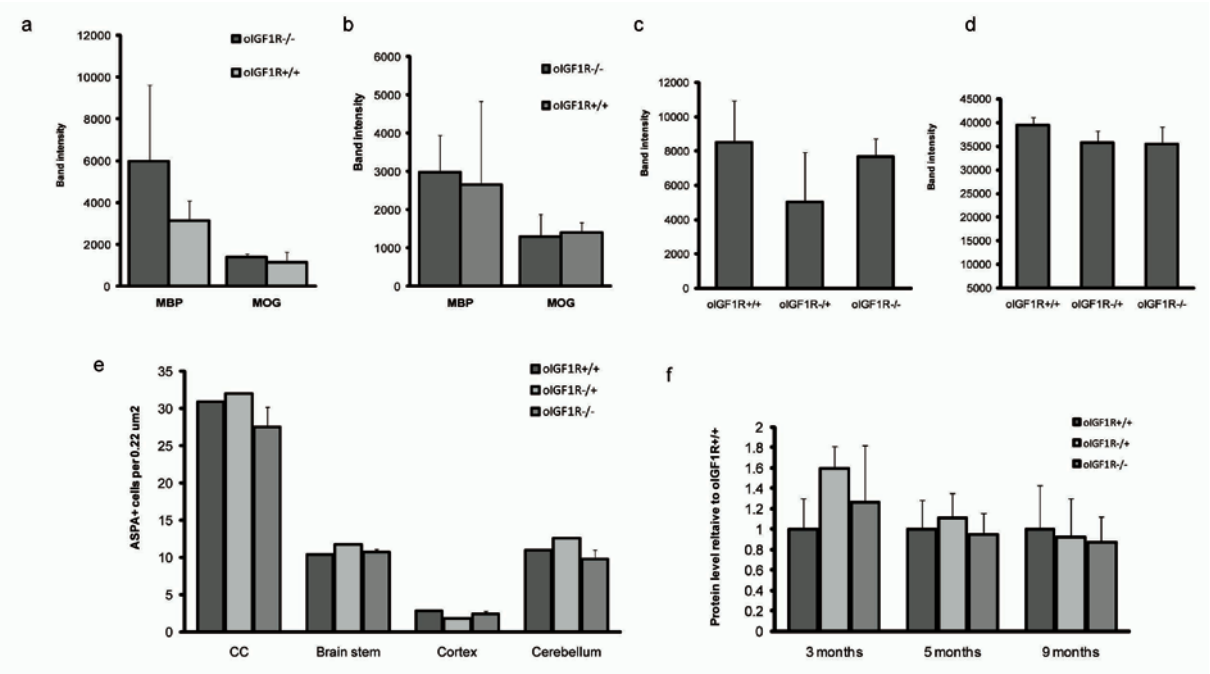

Figure 32

oIGF1R-/- and oIGF1R+/+ control mice were sacrificed at 3 (a) and 5 (b) months of age and CNS lysates analyzed by immunoblotting against MBP and MOG. Band intensity is shown, n=5. (c) oIGF1R-/- and controls were sacrificed at 9 months of age and CNS lysates immunoblotted with MOG- and (d) PLP- specific Abs. (e) oIGF1R-/- and control mice were sacrificed at 3 months of age and CNS sagittal sections stained with ASPA-specific antibodies. ASPA+ cells were manually counted with Image J software. ODC density per brain region is shown (n=4 sections per region, per mouse). (f) CNS lysates from oIGF1R-/- and control mice of indicated ages were immunoblotted with NG2-specific antibodies. Shown are the band intensities relative to the oIGF1R+/+ controls.

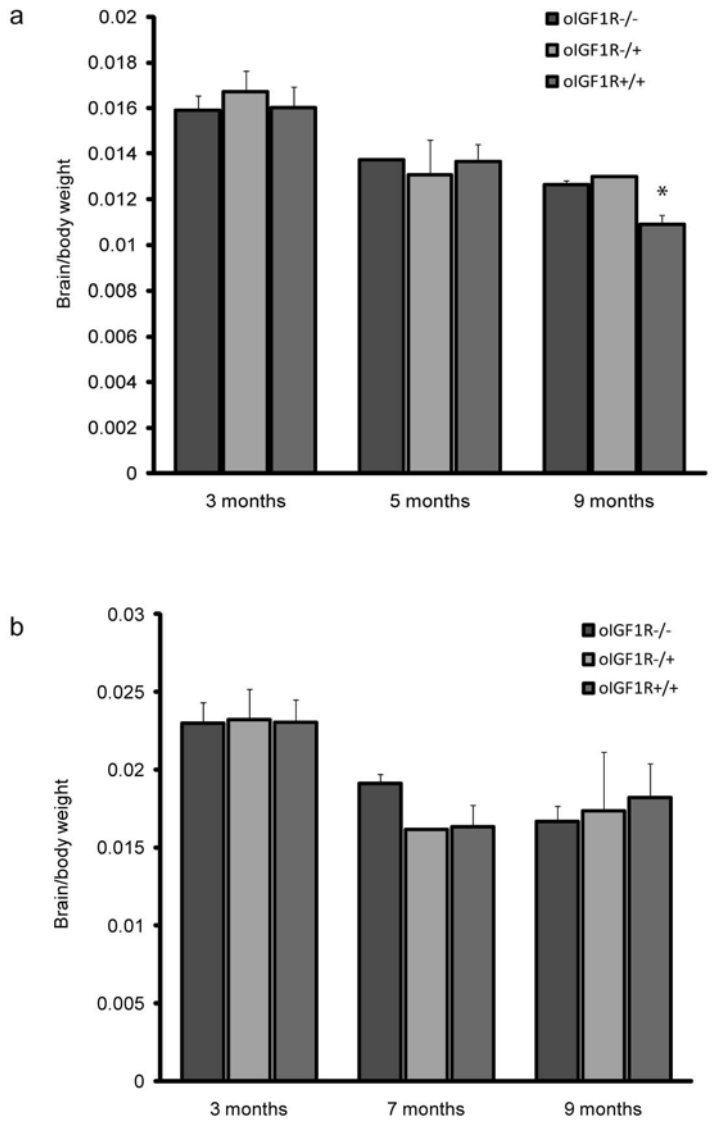

Figure 33

*oIGF1R-/- and control mice were weighted and sacrificed at 3,7, and 9 months of age. Brain weight was measured, shown is brain/body weight ratio, n=7. Male (a) and female (b) average weights ± s.e.m. are displayed. * = p<0.05, Student's T test.*

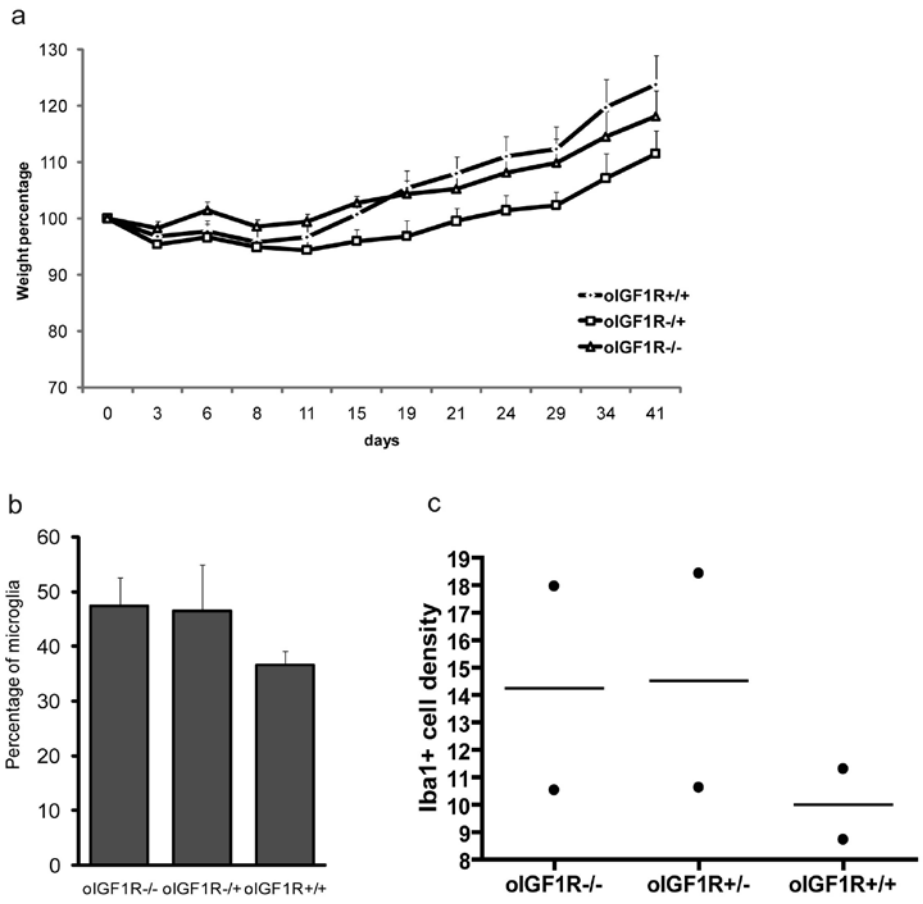

Figure 34

(a) oIGF1R-/-, oIGF1R-/+ and control mice were fed with 0.2% cuprizone for 6 weeks and regularly weighted. Data were pooled from two independent experiments, n=10. (b) FACS analysis of cells isolated from the CNS of cuprizone-fed mice, 3 weeks p.a. (c) CNS sections from oIGF1R-/- and controls fed with cuprizone for 3 weeks were Iba1-stained and positive cells quantified.

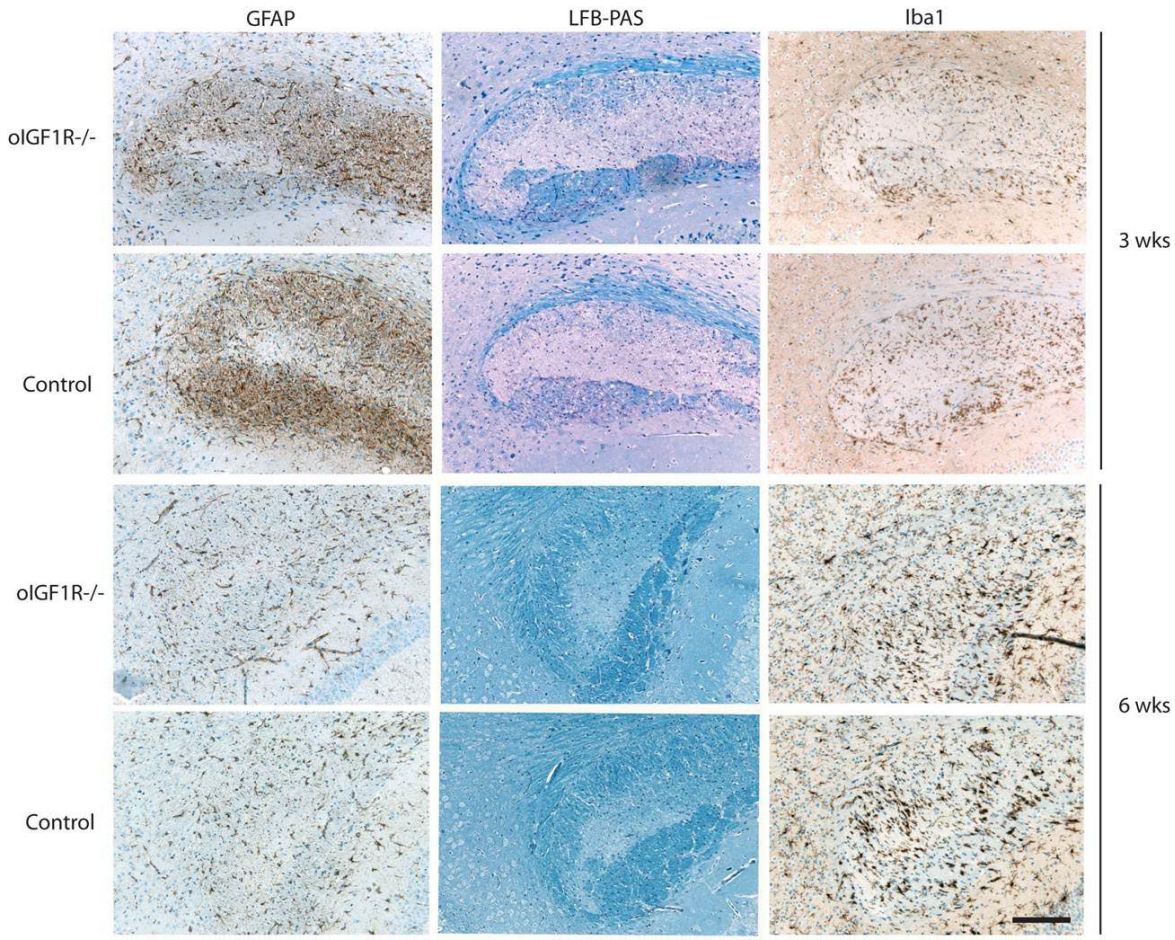

Figure 35

Histological analysis of the splenium of the corpus callosum in cuprizone-fed oIGF1R-/- and control mice. Sagittal sections were stained with Iba1- and GFAP-specific antibodies, or stained with LFB-PAS. Above, samples from 3 weeks-treated animals, below, samples from 6 weeks treated animals. Scale bar, 200 µm.

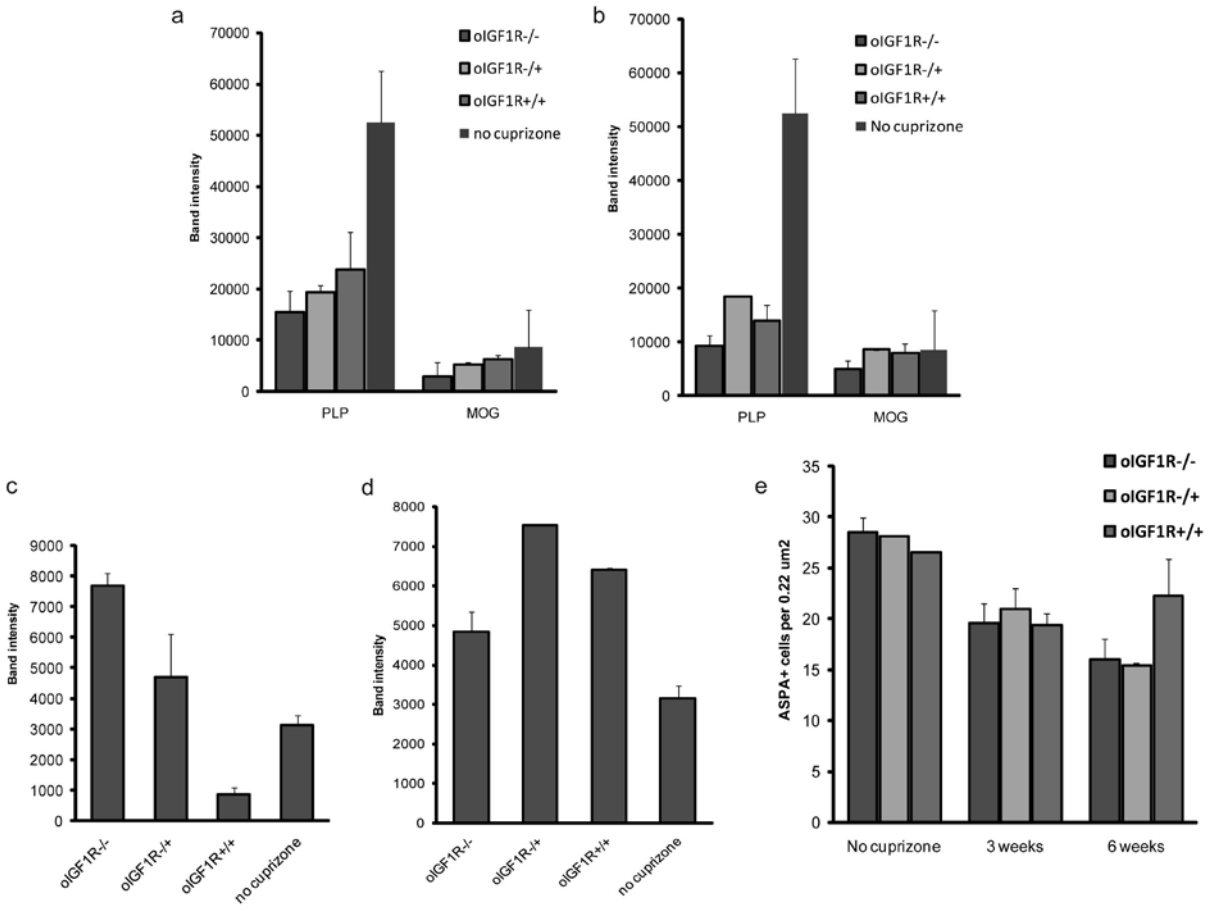

Figure 36

oIGF1R-/- and control mice were fed with 0,2% cuprizone and then sacrificed after 3 (a,c) or 5 weeks (b,d).Brain lysates were immunoblotted using PLP- and MOG-specific antibodies (a,b) or NG2-specific antibodies (c,d). As control served mice which did not receive cuprizone in the diet (no cuprizone). (e) oIGF1R-/- and control mice were sacrificed 3 and 5 weeks after cuprizone feeding and CNS sagittal sections stained with ASPA-specific antibodies. Number of ASPA+ cells was manually estimated with Image J software. ODC density per corpus callosum is shown (n=4 sections per region, per mouse).

a

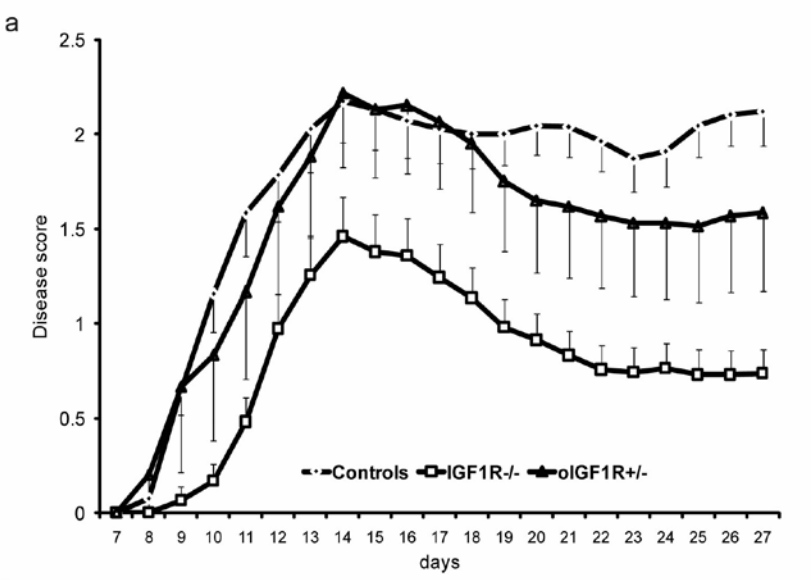

b

Genotype	Incidence	Onset	Av. max score
oIGF1R+/+	42/46 (85.7%)	11.3 ± 0.8	2.45 ± 0.11
oIGF1R-/+	18/21 (91.3%)	12 ± 0.8	2.65 ± 0.31
oIGF1R-/-	36/52 (69%)	11.6 ± 0.3	2.5 ± 0.11

c

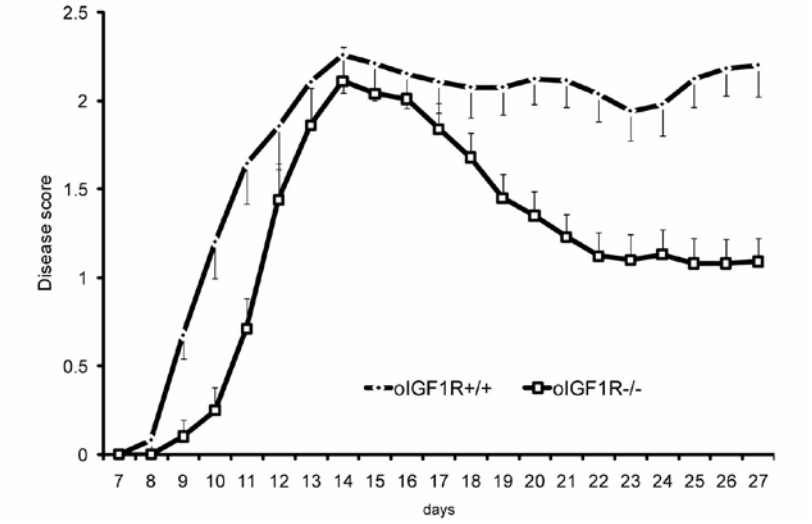

Figure 37

(a) oIGF1R-/-, oIGF1R-/+ and control animals were immunized with MOG_{35-55} in CFA and injected with PT on day 0 and day +2. Animals were scored for clinical signs of disease. Data pooled from 5 independent experiments. (b) Summary table of 5 EAE experiments with clinical parameters of oIGF1R-/-, oIGF1R-/+ and control animals. oIGF1R-/- mice show lower incidence of clinical EAE. (c) The graph represents pooled EAE clinical scores as in (a). Only animals which developed clinical EAE are displayed.

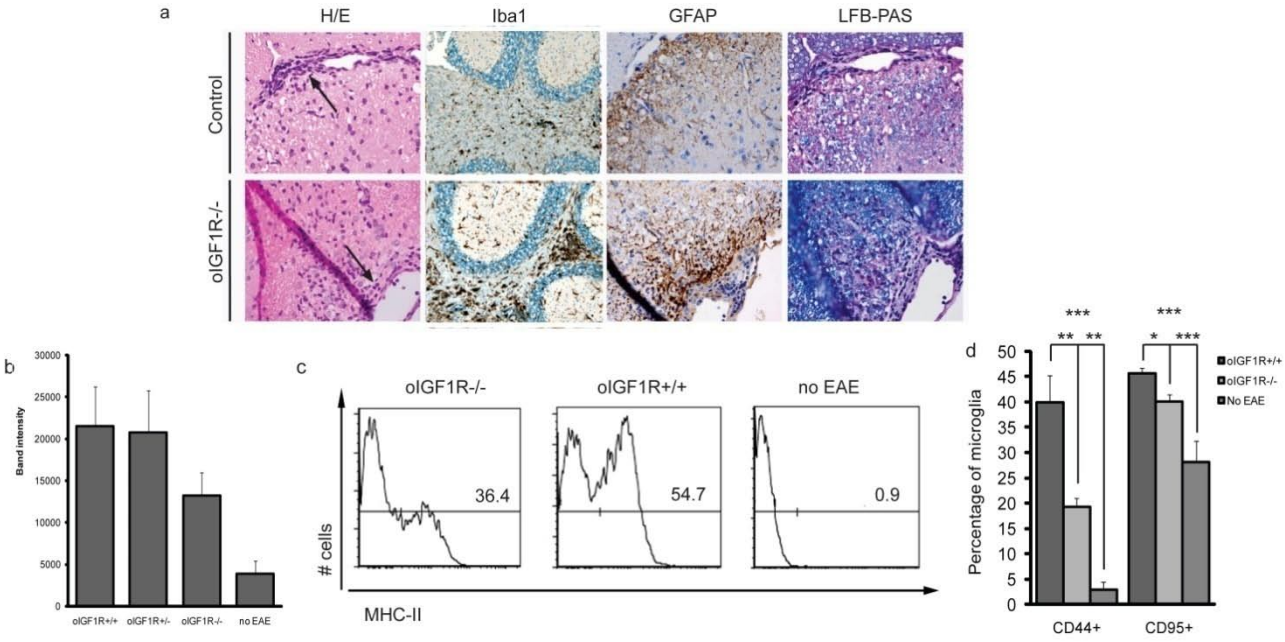

Figure 38

*(a) oIGF1R-/- and control animals were immunized with MOG_{35-55} in CFA, and mice sacrificed 1 month p.i. CNS sagittal sections were analyzed by histology with Hematoxylin/Eosin (H/E), LFB-PAS, and with antibodies specific for Iba1 (microglia) and GFAP (astrocytes). Scale bar, 250 µm. (b) oIGF1R-/- and control animals were immunized with MOG_{35-55} in CFA, and sacrificed 1 month p.i. CNS lysates were immunoblotted using antibodies specific for GFAP. Band intensity is shown, n=5. (c) oIGF1R-/- and control animals were immunized with MOG_{35-55} in CFA, CNS cells were isolated and stained for CD45, CD11b, and MHC-II. Analysis was performed by flow cytometry. Shown are percentages of MHC-II+ microglia/macrophages gated on CD45high-CD11b+ cells. Data are representative of two independent experiments. As negative control served cells isolated from the CNS of steady-state animals. (d) Mice were treated as in (c) and cells analyzed by flow cytometry using CD44- and CD95-positive antibodies (n = 4, ***P < 0.001, **P < 0.001, *P < 0.05, Student's t test.)*

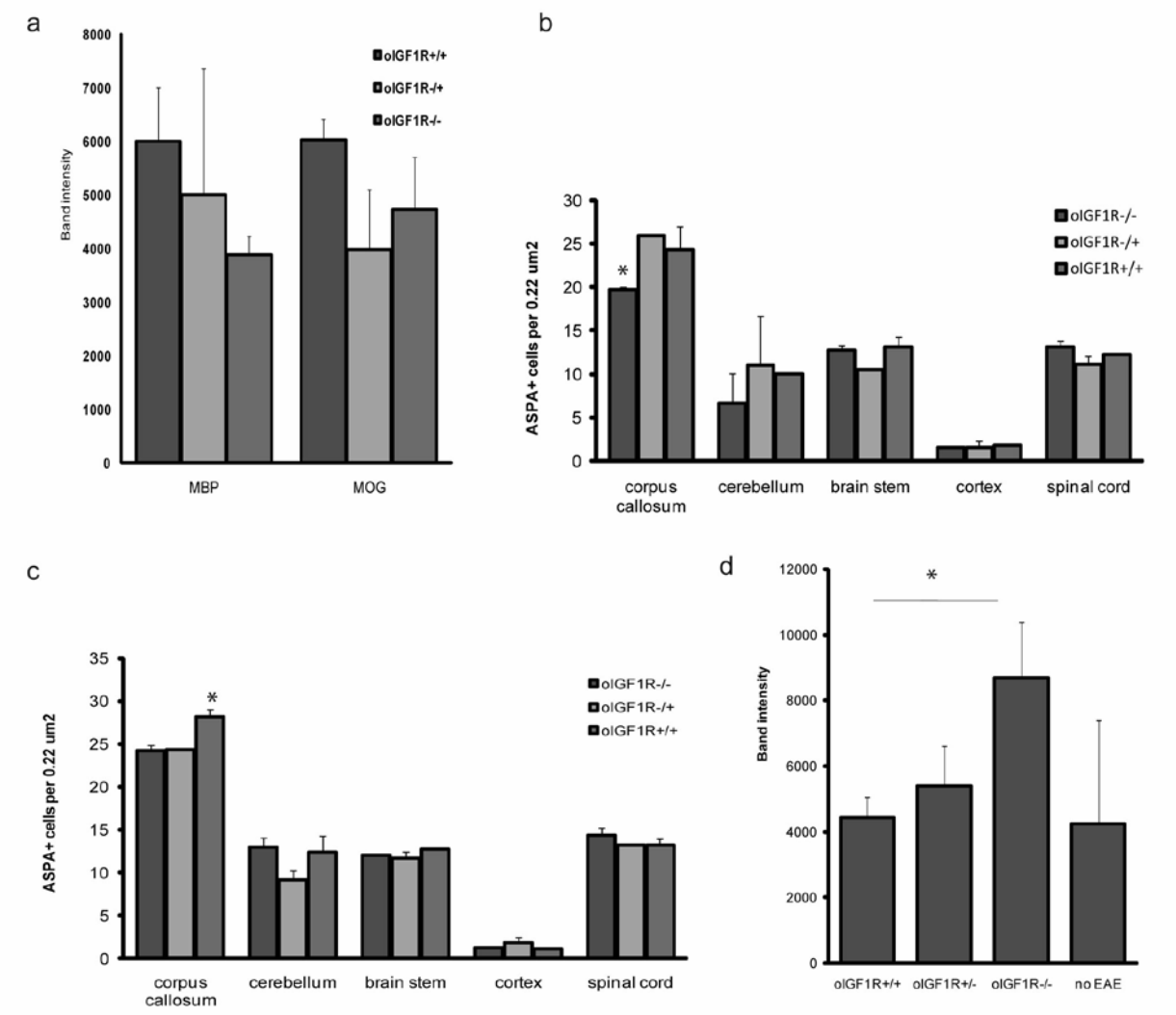

Figure 39

*(a) oIGF1R-/- and control animals were immunized with MOG_{35-55} in CFA, and mice sacrificed 1 month p.i. CNS lysates were immunoblotted using antibodies specific for MBP and MOG. Band intensity is shown, n=5. (b) EAE was induced in oIGF1R-/- and control mice, animals sacrificed 15 days and (c) 1 month p.i.; CNS sagittal sections were stained with ASPA-specific antibodies. ASPA+ cells were manually counted with Image J. ODC density per CNS region is shown (n=4 sections per region, per mouse). *=p<0.05, Student T test. (d) oIGF1R-/- and control animals were immunized with MOG_{35-55} in CFA, and mice sacrificed 1 month p.i. CNS lysates were immunoblotted using antibodies specific for NG2. Band intensity is shown, n=5. *=p<0.05, Student T test.*

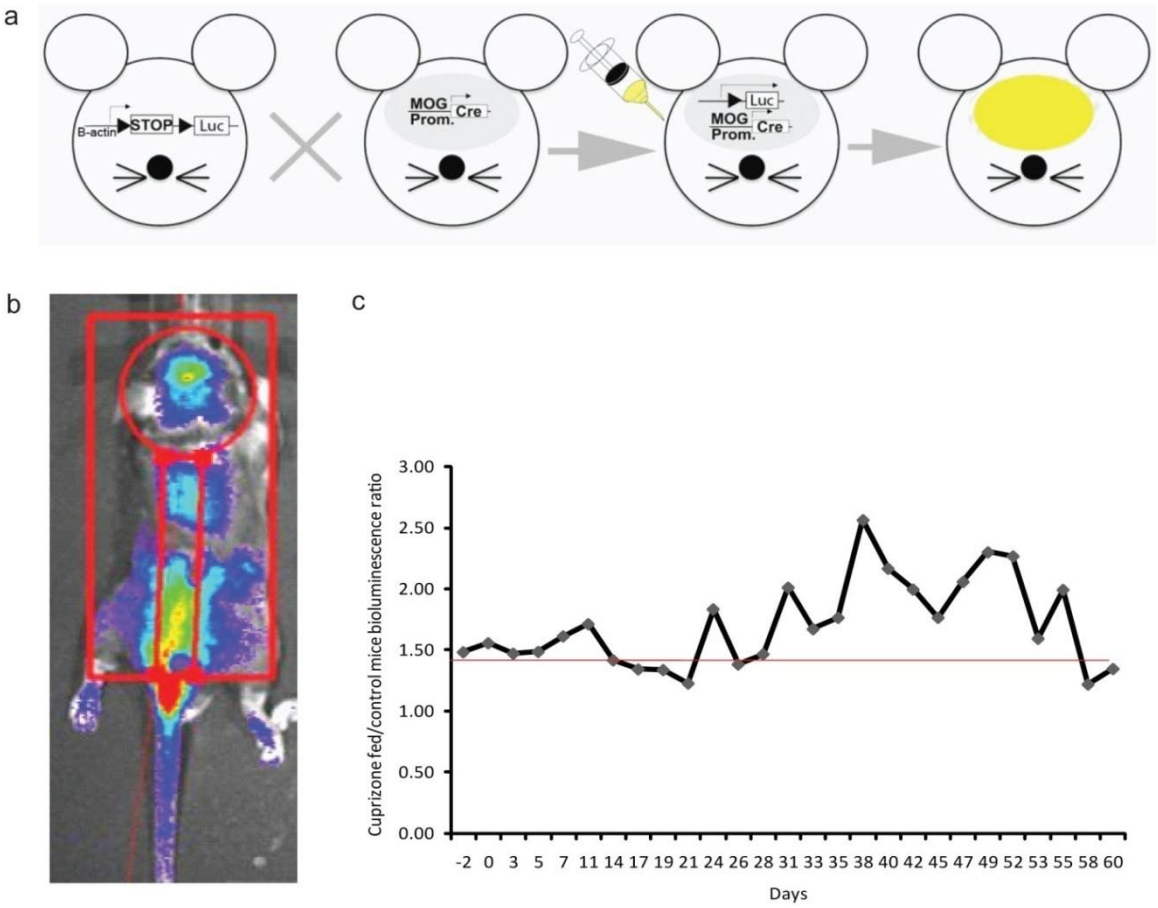

Figure 40

(a) oLucR mice originate from the crossing of MOGi-Cre mice with a strain carrying a Cre-inducible luciferase gene under actin promoter. Injection of luciferin results into bioluminescence production, which can be measured (b) in a ultrasensitive IVIS$_{100}$ camera system after shaving and anesthetizing the animals. The Igor pro software allows the specific measurement of ROIs (region of interests), quantifying photon production from the whole animal (big rectangle) or from specific regions of the CNS (brain, red circle; spinal cord, small rectangle). (c) Cuprizone- and normally-fed oLucR mice were measured for luciferase expression with the IVIS every 3 days along the course of the experiment. Before intoxication, mice were measured for 3 weeks to set the baseline luciferase expression (here depicted in red). Shown is the ratio of bioluminescence between cuprizone-fed and normally-fed (control) oLucR animals (n=5).

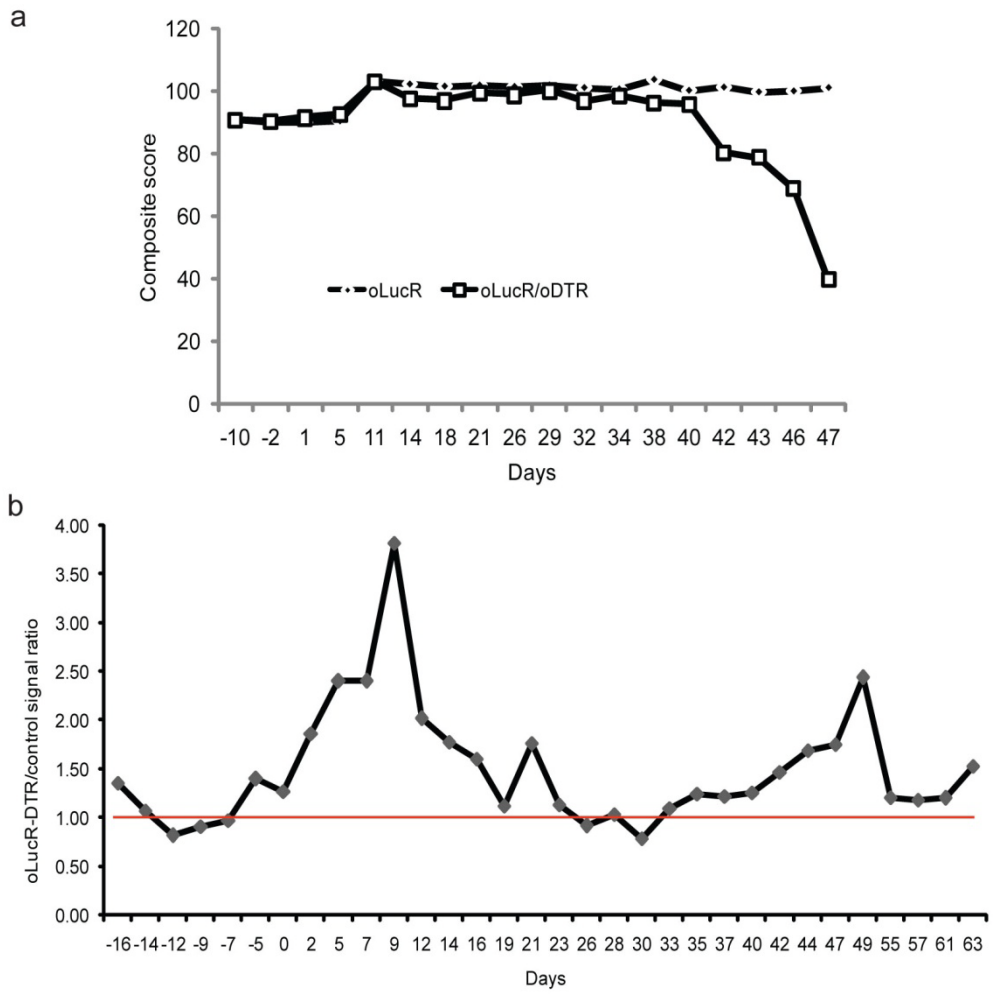

Figure 41

(a) oLucR mice originate from the crossing of MOGi-Cre mice with a strain carrying a Cre-inducible luciferase gene under actin promoter. Injection of luciferin results into bioluminescence production, which can be measured (b) after shaving and anesthetizing the animals in a ultrasensitive $IVIS_{100}$ camera system. The Igor pro software allows the specific measurement of ROIs (region of interests), quantifying photon production from the whole animal (big rectangle) or from regions of the CNS (brain, in the circle; spinal cord, in the small rectangle). (c) Cuprizone- and normally-fed oLucR mice were measured for luciferase expression every 3 days along the course of the experiment. Before intoxication, mice were measured for 3 weeks to set the baseline luciferase expression (here depicted in red). Shown is the ratio of detected bioluminescence between cuprizone-fed and normally-fed (control) oLucR animals.

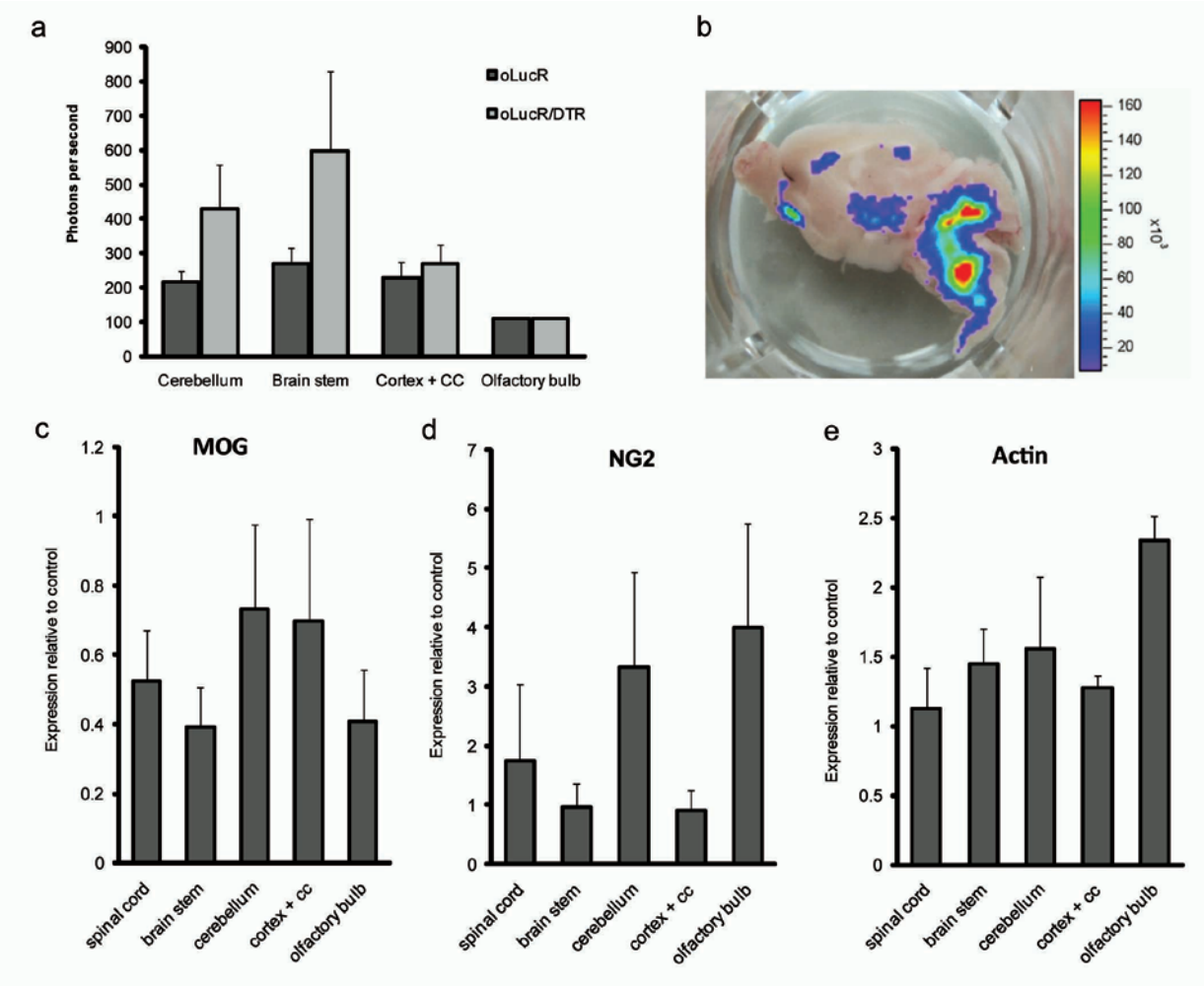

Figure 42

(a) oLucR/DTR and oLucR control mice were treated with DT and sacrificed 7 weeks p.a. Lysates from indicated brain regions were tested in a luminometer assay for luciferase expression. (b) Representative picture of a luciferin-bathed sagittal brain slice from DT-treated oLucR/DTR mice, 30 days p.a.. (c,d,e) oLucR/DTR mice and oLucR mice were treated with DT and sacrificed 9 days p.i. RNA was isolated from the CNS and RT-PCR for MOG, NG2 and Actin performed. Shown are expression values relative to control for the indicated brain regions, n=3.

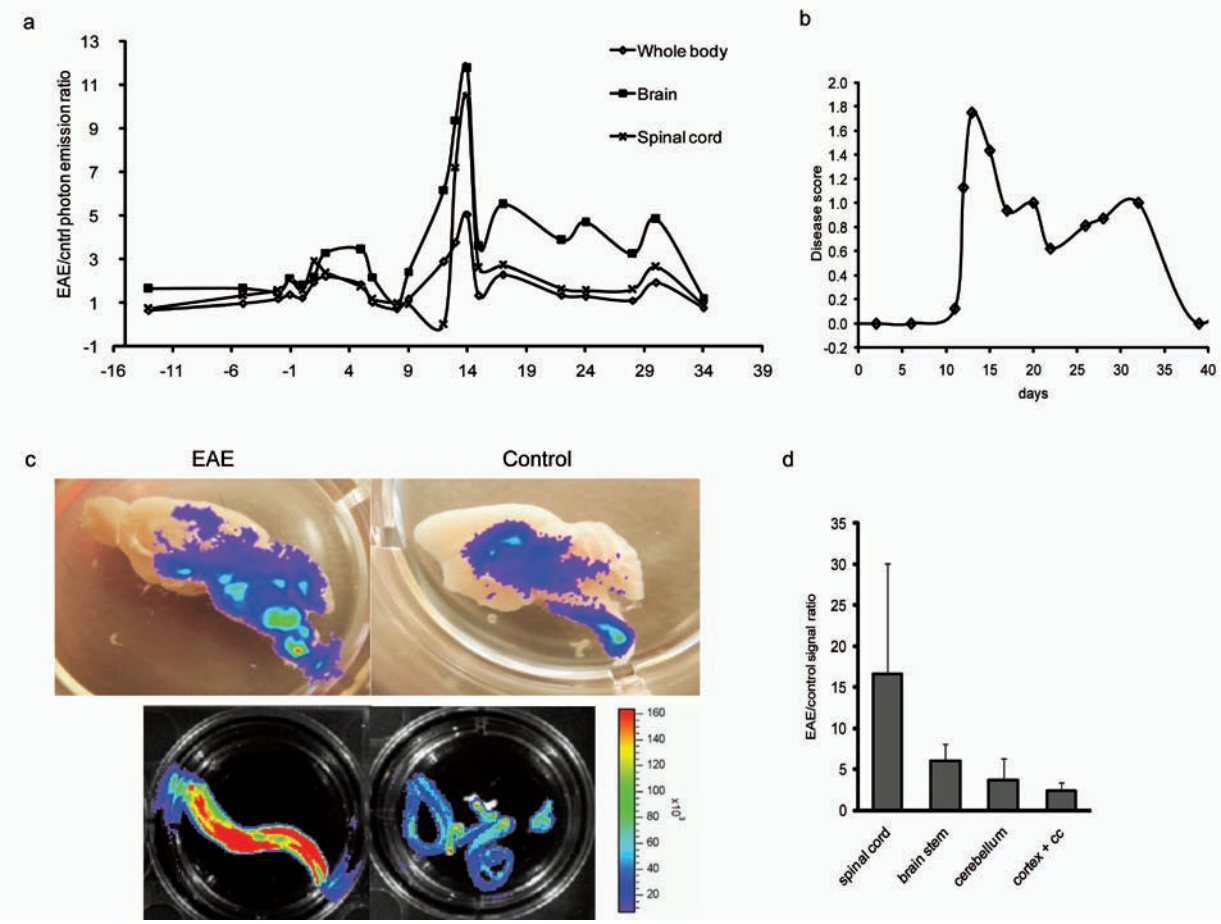

Figure 43

(a) oLucR mice were measured for luciferase expression in a IVIS machine and 12 days later immunized with MOG in CFA. Bioluminescence was monitored until 34 days p.i., shown is photon emission relative to not-immunized oLucR controls. Measurements from the whole animals and specific for brain and spinal cord regions are shown, n=5. Data representative of 2 independent experiments. (b) Clinical score of EAE as in (a). (c) oLucR animals were immunized with MOG in CFA (left) and sacrificed 35 days p.i. Brain slices and spinal cord tissues were bathed in luciferin and imaged in the IVIS machine. On the right, samples from untreated control mice. (d) oLucR mice were immunized with MOG in CFA and sacrificed 35 days p.i. Lysates from indicated brain regions were tested in a luminometer assay for luciferase expression, expression are shown relative to control tissue from not immunized animals.

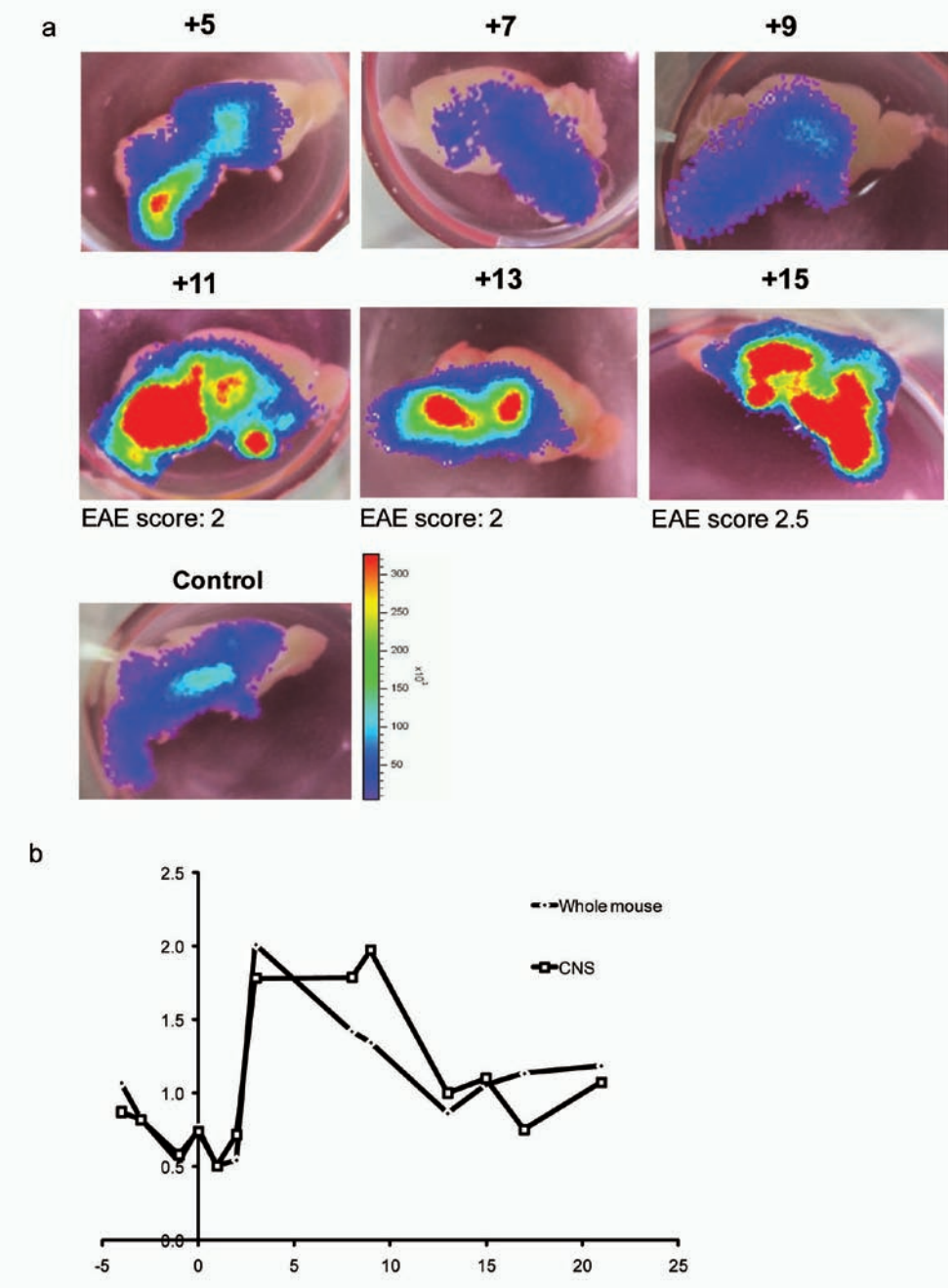

Figure 44

(a) oLucR animals were immunized with MOG in CFA and sacrificed at indicated time points p.i. Brain slices and spinal cord tissues were bathed in 150 µg/ml luciferin and imaged in the IVIS machine for 2'. Clinical score at the time of sacrifice is indicated. On the bottom, control mice remained untreated. Representative slices are shown. (b) oLucR mice were injected with 400 ng PT at day 0 and day 2 and imaged in the IVIS machine. Shown is bioluminescence relative to not-injected controls.

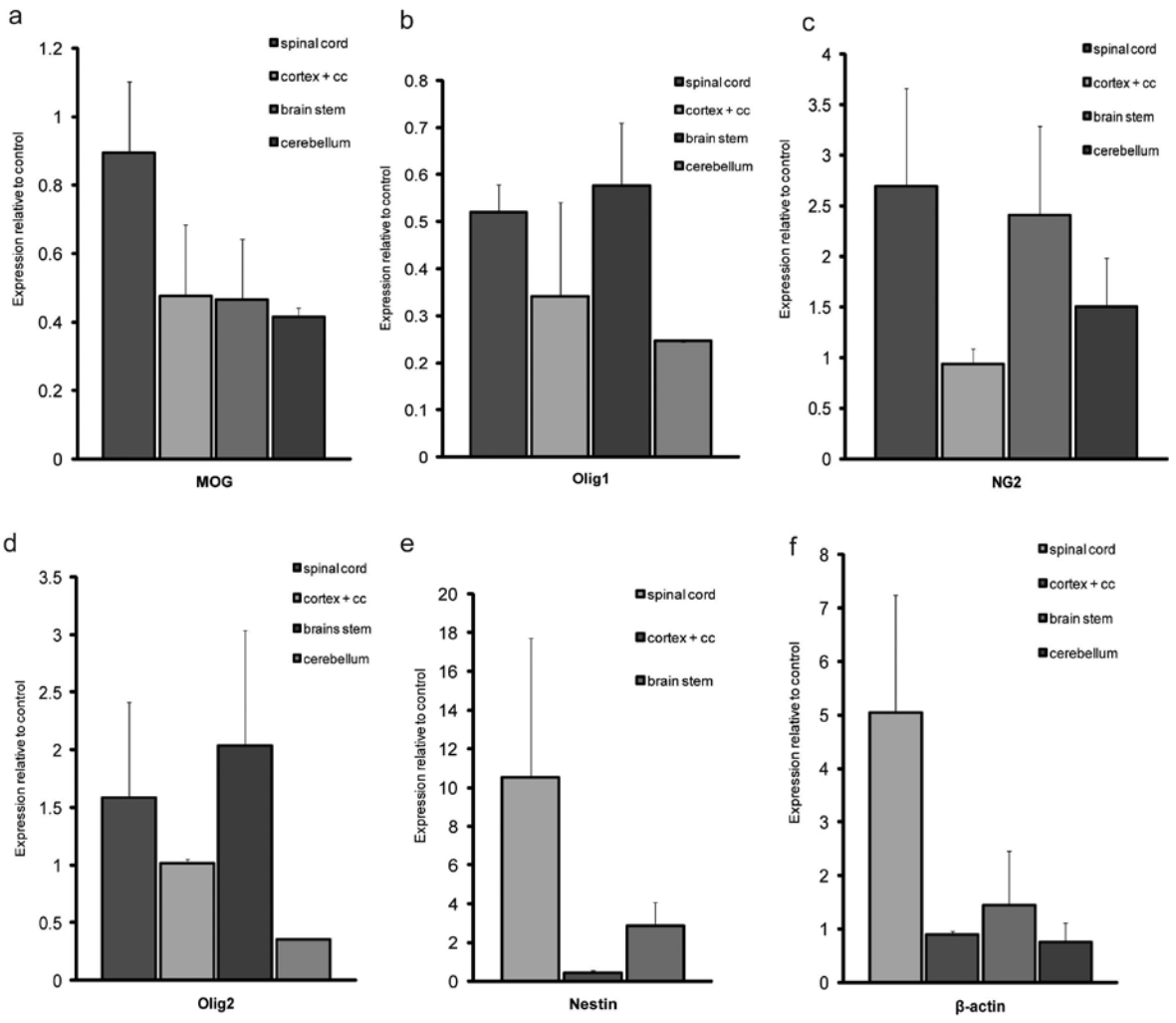

Figure 45

oLucR mice were immunized with MOG in CFA and sacrificed 11 days p.i.. RNA was isolated from the CNS and RT-PCR for (a) MOG, (b) Olig1, (c) NG2, (d) Olig2, (e) Nestin, and (f) Actin performed. Shown are expression values relative to control for the different brain regions, n=3.

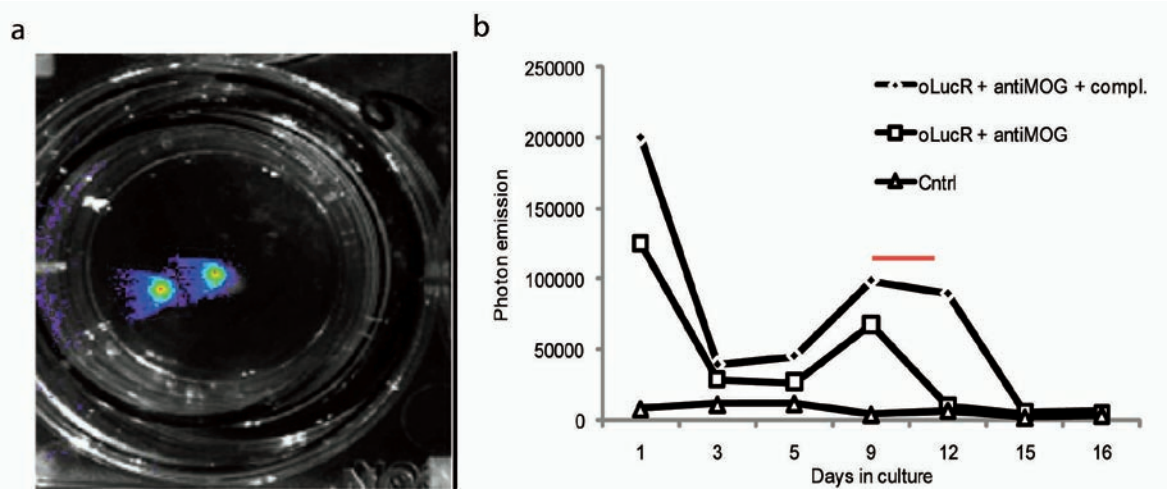

Figure 46

(a) Cerebellar slices from P9 pups were kept in culture with the addition of 150 ug/ml luciferin and imaged in the IVIS machine every other day. (b) AntiMOG and complement or antiMOG alone as a control were added to the culture for 48 hours (red line in the graph) and then washed out with fresh medium. As negative control, wt mice cerebellar slices were used (Cntrl).

DISCUSSION

Is ODC death the initial trigger of Multiple Sclerosis?

MS is generally accepted to be an autoimmune disease with auto-reactive T cells sustaining a multifocal inflammatory demyelination. Recent descriptions of the disease have pointed towards the presence of at least four partially overlapping histological MS subtypes [161]. While Lucchinetti suggest that these subtypes correlate to different disease entities, Barnett and Prineas favor a view in which the types correspond to various stages along the disease course [68] with primary apoptosis of ODCs as common triggering event. To directly and systematically address the question whether ODC death could initiate an MS-like pathology in mice, we needed a system of induced ODC degeneration. One frequently used system is cuprizone-induced demyelination [162]. The latter suffers, however, from severe side-effects [163, 164] and its unknown mode of action makes data interpretation difficult. Investigation of anti-CNS immunity has been aided by the animal model experimental autoimmune encephalomyelitis (EAE). However, since this model uses active immunization against myelin or the transfer of myelin-reactive T cells to trigger the disease, it cannot shed light on the etiology of anti-CNS-immunity. Some attempts to investigate the triggering phase of MS involved the metabolic impairment of ODCs but did not result in pronounced autoimmunity, although scattered infiltrations of lymphocytes were found in the CNS [165-167]. In contrast to the scenario described by Barnett and Prineas, however, substantial ODC death was not observed in these models. To overcome all these limitations, we have developed a mouse model (oDTR, **Fig. 14a**) which allows us to selectively induce ODC death by targeted expression of a diphtheria toxin receptor (DTR) and injection of diphtheria toxin (DT) [129]. By ectopic expression of a DTR murine cells become sensitive to DT, which induces cell death by termination of protein synthesis (**Fig. 14b**). Thus, in contrast to other animal models of demyelination, the mechanism of DT is well-established [168] and genetically restricted to mature MOG-producing ODCs [129]. In this respect, two almost identical mouse models of experimental DT-mediated ODC depletion were published in the literature and showed no lymphocyte infiltrations in the CNS [134, 135]. However, these models are not suitable to investigate the triggering phase of neuroinflammation as the inducer used in these studies –tamoxifen- was shown in the past to suppress autoimmunity including EAE [169].

In our model we observed massive ODC death and progressive disruption of myelin tissue in all CNS white matter areas with progressive clinical signs like cachexia, ataxia, kyphosis, and tremor. Several other animal models described tremor as result of myelin defects within the cerebellar motorfunction control circuitry [165, 170-172] and we confirm this by detecting degenerating neurons in the cerebellum of treated mice. In addition, we found progressive gliosis and activation of microglia/macrophages shown by high MHC class II expression and upregulation of CD44 [173, 174] similar to other models of myelin damage [175-177]. Importantly, this strong activation resembles microglia reactivity in early-stage MS plaques as described [68, 178, 179].

Similar to observations in MS patients [136, 137], ODC death resulted in accumulation of myelin material in lumbar and dcLNs. These CNS-draining LNs are required for development of relapses and epitope spreading in EAE [46] and are thus candidate locations for activation of CNS-reactive lymphocytes. Nonetheless, following both acute and chronic DT-mediated ODC death we did not detect any significant T cell activation through myelin antigens and did not find any significant parenchymal or perivascular lymphocyte infiltrations.

Because bystander activation has been for a long time discussed as mechanism triggering MS, we assessed whether induced ODC death acted in synergy with established activators of adaptive immunity to induce an MS-like disease. We applied CFA and PT, injected MOG-reactive T cells, depleted Treg cells, and treated the animals with anti-CD40 antibodies. Despite these strong biases towards eliciting an adaptive T cell-driven immune response, we did not find any sign of anti-CNS autoimmunity or any significant change in the course of the disease. Also the presence of demyelinating antibodies as found in MS did not facilitate lymphocytic infiltrates or altered disease development. Because none of our experiments showed autoimmune inflammation, we tested whether induced ODC death led to tolerance as described by one research group for cuprizone-treated animals [180]. Yet we could not find any evidence for tolerance induction in our model.

However, myelin-specific 2D2 T cells showed weak proliferation in some DT/PT/anti-CD40-treated oDTR/IiMOG animals and the incidence of EAE in DT/CFA/PT-treated 2D2/oDTR was slightly (albeit insignificantly) higher compared to treated 2D2/control. Thus, although our data might support the notion of rare stochastic activation of the adaptive immunity following ODC death, our overall endeavour clearly failed to detect

a presence of T and B cells during ODC death remotely comparable to EAE or MS. Hence, even in our most biased experimental designs, activation of myelin-specific T cells following ODC death seems to be a minor stochastic event. However, we are aware of the limitations imposed by the use of a single mouse strain on a fixed genetic background (C57/Bl6). In order to confirm and extend our observations, we are thus currently backcrossing the oDTR system to a different genetic background, the SJL, and will repeat the same experiments of induced ODC death associated to different immune manipulations.

As already mentioned, others have also tried to link pathologically modified ODCs with CNS inflammation. While some myelin alterations result in severe neural degeneration without development of inflammation [131-133] other lead to an inflammatory environment also involving invading lymphocytes. For instance, ODC-restricted deletion of *Pex5* [165] results in diffuse neuronal death and CNS infiltrations by B and $CD8^+$ T lymphocytes. Similar to these observations, mice over-expressing proteolipid protein (PLP) in ODCs show late-onset neuronal degeneration followed by an influx of $CD8^+$ T cells into the brain parenchyma [166, 167]. In contrast to our system in which ODCs are killed rapidly through protein translation blockade [168], in both, the *Pex5* and *PLP* systems genetic alterations result in late-onset demyelination and neuronal death without pronounced effects on ODC survival. These compromised ODCs may signal their distress to the immune system and such a chronic trigger may lead to the described recruitment of cytotoxic T lymphocytes. Our data, on the other hand, clearly support the notion that ODC death *per se* does not represent a powerful activator of adaptive immunity.

Along this line, these observations can be of interest regarding other disease entities presenting with ODC death, demyelination, and inflammation. In one such disease X-linked adrenoleukodystrophy (X-ALD), mutations in the *ABCD1* gene, a peroxisomal transporter, result in accumulation of saturated very long chain-fatty acid which leads to inflammatory CNS lesions comprising of macrophages, reactive astroglia, and T cells [181]. It is still unknown whether inflammation in X-ALD patients is cause or result of the characteristic demyelinating processes. Interestingly, for unknown reasons *Abcd1* mutations in mice [182-184] do not result in sustained inflammation of the CNS, while *Pex5*-mutant mice, also showing alteration of peroxisome metabolism, can be used as a model for the neuroinflammatory component of X-ALD. Also infectious agents were

suggested to play a role in the etiology of MS and investigated in animal models. Infection of mouse CNS with either mouse hepatitis virus (MHV) and Theiler's murine encephalomyelitis virus (TMEV) results in activation of virus-specific T cells and killing of infected ODCs with subsequent demyelination [185, 186]. While MHV infection progresses into a chronic disease associated with inflammation, TMEV infection results in epitope spreading and consequent activation of myelin-reactive T cells [187]. Conversely, in the human during progressive multifocal leukoencephalopathy, reactivation of the JC virus in the CNS results in focal demyelinated lesions classically devoid of lymphocyte infiltrates [188], although some inflammatory forms have also been described [189].

Taken together, we have addressed a hypothesis that has been postulated repeatedly, and we have excluded a large number of possibilities leading up to MS-like pathologies. Even though DT administration in oDTR animals resulted in histopathological changes resembling the early stage-MS lesions as described by Barnett and Prineas, our insult to the CNS does not lead up to the severe inflammation commonly described in late stage-MS plaques [161] and other neuroinflammatory diseases. Thus, assuming that a multifactorial and heterogenous human disease as MS can really be modeled in animal experiments, our work shows that mere ODC death is not sufficient to trigger adaptive immune response.

What is the role of IGF1R in mature ODCs?

The IGF-1/IGF1R axis has been shown to influence OPC differentiation, myelination and repair [100, 106-108], and generally to act as a neuroprotective and pro-survival factor in the ODC lineage and in surrounding parenchymal cells [115] [117-119]. Even though ODC death *per se* does not represent an immunogenic event, ODC apoptosis remains a fundamental factor in the context of induced neuroinflammation and contributes substantially to disability development and progression [89]. Also, some genetic impairments which lead to chronic ODC stress eventually result in the activation of adaptive immune response [165-167], thus indicating a possible role of mature ODCs in influencing the immune system under physiological conditions and signaling their distress under pathological conditions [67]. Unfortunately, only one

study has so far addressed IGF1R function in late developmental ODC stages [101], and the literature still lacks a characterization of the role of IGF1R specifically for mature ODCs. Also, the IGF-1/IGF1R impact on ODC apoptosis and survival within inflammatory CNS lesions is utterly unclear. Published EAE studies are highly controversial and show contrasting treatment outcomes [107, 109, 112, 121, 123]. In these works, broad deletion of IGF1R from different cells or systemic administration of IGF-1 –with pleiotropic effects on several cell types- make data interpretation virtually impossible. To overcome these limitations we have developed the oIGF1R-/- model (**Fig. 31a**) in which IGF1R deletion is restricted to MOG-producing mature ODCs. Interestingly, while deletion of IGF1R on pre-mature ODCs was shown to affect myelin content and brain weight already in young animals [101], oIGF1R-/- mice appeared identical to their littermate counterparts in terms of myelination and ODC number until 9 months of age (**Fig. 31b, 32, 33b**). Counterintuitively, in male oIGF1R-/- mice the brain/body weight ratio was significantly higher than in male control mice at 9 months of age (**Fig. 33a**).

When immunized with MOG in CFA, oIGF1R-/- mice were surprisingly protected from the development of EAE (69% of sick animals among oIGF1R-/- mice, 85.7% in control animals, **Fig. 37a,b**). Also, among the animals displaying clinical paralysis, oIGF1R-/- mice showed an intrinsically ameliorated disease compared to littermate controls (**Fig. 37c**). Histological and western blot analyses did not reveal gross myelin differences among different genotypes; also, ODC density in the classically inflamed areas in EAE, spinal cord and brain stem, appeared the same in all experimental mice. Rather, we were able to detect a significant decrease in ODC density in the corpus callosum of oIGF1R-/- animals, both during the acute and the chronic phase of disease (**Fig. 39b,c**). This data is unexpected, as neuroinflammation in EAE is not prominent in the corpus callosum. Furthermore, NG2 protein levels, indicative of number and activation state of OPCs, were drastically increased in oIGF1R-/- (**Fig. 39d**) animals. Since OPC recruitment is a consequence of ODC death and demyelination [43], these data might indicate a higher susceptibility to damage of IGF1R-/- ODCs. Analogous indications come from experiments in other demyelinating paradigms. Cuprizone-fed oIGF1R-/- mice display a lower ODC density in the corpus callosum 5 weeks p.a., with NG2 level again strongly higher than in littermate control animals (**Fig. 36d,e**). Similar to what we observed following EAE induction, histological analysis of cuprizone-intoxicated mice did not reveal gross differences among genotypes. Nonetheless, a

slight reduction in myelin content could be observed specifically in oIGF1R-/- mice, and microglia numbers were increased compared to oIGF1R+/+ controls (**Fig. 36a,b and Fig. 35b,c**).

Thus, in accordance to the proposed anti-apoptotic and myelogenic function of IGF1R on cells of the ODC lineage [106, 113, 119, 190], we found indications of a higher mortality of ODCs in oIGF1R-/- compared to control animals. In order to confirm these indications, future analysis will directly address the rate of ODC death in oIGF1R-/- animals within lesions in EAE and cuprizone intoxication and quantify longitudinally OPC recruitment during demyelinating insults.

Different hypotheses could be put forward to explain the surprising protection from EAE in oIGF1R-/- mice. In the first place, a higher number of dying IGF1R-/- ODCs might lead to protection from neuroinflammation by release of immunosuppressive apoptotic bodies [72] [191]. Interestingly, this hypothesis is consistent with the reduction in inflammatory markers such as CD95, CD44 and MHC-II in microglia/macrophages and with the decreased levels of GFAP displayed in EAE-induced oIGF1R-/- mice (**Fig. 38b,c,d**). A detailed phenotypical analysis of microglia/macrophages would thus shed light on their possible anti-inflammatory role and explain the conundrum of the higher Iba-1 reactivity observed 1 month p.i. (**Fig. 38a**). At the same time, EAE amelioration in oIGF1R-/- mice might result from indirect effects on the IGF-1/IGF1R axis within the CNS. For instance, absence of the receptor from ODCs may lead to increased IGF-1 uptake in surrounding cells -i.e. neurons-, thus protecting the latter from bystander death and impacting in turn the clinical score through a reduced motor impairment [115]. A quantitative analysis of neuronal death and functionality might shed light on this point. Also, IGF-1 has also multiple effects on endothelial cells, glia and CNS-invading inflammatory lymphocytes [125], but the plethora of biological effects derived from this hypothetical higher bioavailability of IGF-1 remain difficult to address.

All together, we have described for the first time a deletion of IGF1R specifically in late myelinating ODCs, without involvement of OPCs [106, 113, 114, 121, 123]. Interestingly, IGF1R does not seem to exert important functions in ODCs in the steady-state, not-inflamed CNS: both myelin content and ODC number were not reduced through this specific deletion. Most likely, the relevance of IGF-1 signaling decreases at the end of ODC differentiation, while it seems necessary for myelination and OPC

survival at earlier stages [190]. Nonetheless, non-physiological situations as cuprizone intoxication show impaired recovery in oIGF1R-/-. Thus, the importance of IGF1R in remyelination and ODC survival is highlighted by demyelinating experimental conditions and leads to lower ODC density and higher OPC recruitment. Also during EAE, slightly higher myelin loss, increased progenitor recruitment and lower ODC density in corpus callosum point toward a pro-survival function of IGF1R in ODCs. However, as oIGF1R-/- display a counterintuitive protection from EAE, data interpretation becomes complex. The absence of the receptor seems to be clinically beneficial only in the peculiar context of EAE, in which ODCs experience prolonged stress in a hostile inflammatory environment. Direct and indirect effects of the absence of IGF1R might account for the observed clinical amelioration and have been discussed above.

Taken together, the function of IGF1R in mature ODCs during neuroinflammation remain controversial, both in EAE [107, 109, 112, 121, 123] and MS. In the latter, different studies showed an upregulation of different components of the IGF-1/IGF1R axis within and surrounding sclerotic lesions, again suggesting a role in inflammation and demyelination [120, 192]. Also, one clinical study has addressed the possible therapeutic effect of recombinant IGF-1 in MS, but showed no efficacy in ameliorating the disease [193]. Understanding the mechanism(s) protecting mice from inflammation following IGF1R deletion on ODCs (**Fig. 37a-c**) could thus potentially shed light on the controversial role of ODCs in neuroinflammation both in EAE and MS.

What is the behavior of ODCs during demyelination?

The use of visible and fluorescent light in engineered biological systems has brought great advantages to researchers since its first applications, as expression of reporter proteins allows *in vivo* noninvasive visualization of specific tissues and cells [194]. Working with ODCs under different demyelinating paradigms, we thus wanted to create a novel system allowing the *in vivo* quantification of myelin amount and ODC number. For this purpose, we have developed the oLucR mouse model in which β-actin-driven expression of a luciferase gene is restricted by Cre-lox recombination to MOG^+ cells, thus mature ODCs (**Fig. 40a**). After being shaved and anesthetized, oLucR mice were

injected with luciferin leading to production of light within ODCs; photon detection was performed through an ultrasensitive CCD camera in a IVIS system. As luciferase is expressed by ODCs under an housekeeping promoter, we thought that the number of ODCs and the amount of myelin in oLucR mice would be proportional to the recorded bioluminescence. However, IVIS recordings of oLucR animals under different demyelinating paradigms produced unexpected results. During cuprizone-feeding, oLucR mice showed progressive increase in photon emission from the CNS, and a decrease in signal during the subsequent remyelination phase (**Fig. 40c**). DT-induced ODC death in oLucR/DTR mice also resulted in two periods of increased bioluminescence: the first, during the DT administration period, and the second, in the late phase of the disease, after development of clinical disabilities (**Fig. 41b**). Thus, even 60% of ODC depletion in all white matter areas (**Fig. 17a,b**) would not lead to a decreased CNS-specific bioluminescence in our *in vivo* system. Finally, when immunized with MOG in CFA, oLucR mice showed a transient signal increase after disease induction and a strong, sharp emission peak close to the beginning of clinical EAE (**Fig. 43a**). PT treatment alone, known to increase BBB permeability, resulted in a transient increase in photon signal, thus suggesting that variations in luciferin access to the CNS might partially contribute to the observed fluctuations (**Fig. 44b**). However, we cannot exclude a direct effect of PT on ODCs [195]. *Ex vivo* and *in vitro* analysis of freshly-cut brain slices and CNS protein extracts could confirm the bioluminescence changes observed *in vivo* in the EAE and DT paradigms, and increased photon emission could be observed in demyelinating cerebellar slice cultures, a system completely devoid of a classic neurovascular junction (**Fig. 46b**). Thus, bioluminescence variations in oLucR tissues appeared intrinsic to luciferase-expressing ODCs and could not be explained by a mere *in vivo* artifact. Interestingly, luciferase signal appeared stronger in highly-damaged CNS regions: bioluminescence increase was more prominent in the spinal cord and brain stem in EAE-induced animals, and in the brain stem and cerebellum of DT-treated oLucR/DTR animals (**Fig. 42a,b, 43c,d**). Counterintuitively, it appears that demyelinating insults would increase luciferase signal in the ODCs of oLucR mice.

In the oLucR system, Cre-mediated recombination allows the expression of luciferase in MOG-expressing ODCs under the control of a β-actin promoter. Thus, an increased activity of this promoter would result in a higher number of luciferase molecules and in an increase in light emission. Even though β-actin has been traditionally considered as

an housekeeping gene, it has been recently shown that its expression can be substantially upregulated during cell proliferation, activation, and differentiation [196, 197]. As already described, actin filaments in ODCs are mostly associated to CNP-1 proteins, and are the main constituents of thinner membrane domains of the myelin sheath [19]. Actin molecules are among the major players in the plasticity of cell body/myelin structures; consequently, the β-actin gene and its product must be subjected to strong expression changes during development, cell reorganization and myelination. It seems likely that concomitantly to immune attack, intoxication or demyelination, ODCs surrounding experimental lesions may experience stress-related dynamics which result in a drastic increase in β-actin production and, as a consequence, increased luciferase expression. Accordingly, β-actin expression in EAE-induced oLucR and DT-treated oLucR/DTR mice was higher than in control mice (**Fig. 42e, 45f**). However, transgenic luciferase expression in oLucR animals is restricted to mature MOG-expressing cells. Little is known about the *in vivo* plasticity of fully-mature, post mitotic ODCs regarding myelin organization and mobility. Different studies indicated that ODCs lack the ability to repair demyelinating lesions [91, 99-101]. Nonetheless, other observations seemed to prove that mature ODCs maintain some structural plasticity and are capable of extending their processes in an attempt to remyelinate naked axons [93, 97, 98]. Accordingly, we put forward an hypothesis in which ODCs within demyelinating lesions increase their plasticity and activation state starting to produce new myelin and/or reorganizing pre-existing sub-structures of the myelin sheath. These processes might account for the initial signal increase recorded in DT-treated oDTR/oLucR animals, in which the sudden massive death of ODCs may lead to an increased activity in surviving cells, and for the sharp peak detected at the clinical beginning of EAE, in which ODCs experience a direct immune attack.
Even so, it remains difficult to explain the absence of any decreased bioluminescence following massive demyelination. Most likely, the disappearance of luciferase molecules following ODC death is masked and compensated by increased gene transcription in surrounding, activated ODCs. Unfortunately, it is not easy to address this experimentally.

Altogether, we failed to establish an *in vivo* animal model allowing quantification of myelin amount during demyelinating paradigms. However, some evidences exist that oLucR mice can provide an *in vivo* readout of diffuse remyelination. 6 weeks after DT-treatment, a progressive increase in photon signal could be consistently observed in

oLucR/DTR (**Fig. 41b**). Since OPCs are massively recruited to demyelinated white matter areas of DT-treated oDTR mice until 4 weeks p.a. (**Fig. 20a**), this late peak could possibly represent a *de novo* transcription of luciferase from newly formed mature ODCs, which started expressing MOG around 2 weeks after initial recruitment [198].

Taken together, the counterintuitive increases in the bioluminescence of ODCs within demyelinating regions raises fundamental issues regarding mature ODC biology. The observed trends in photon signal clearly support an hypothesis in which mature ODCs would play an active role and increase their plasticity in response to different kinds of parenchymal stress. Thus, these observations might be an additional contribution to our renewed concept of biology and function of ODCs, not anymore a mere “holding glue” of the CNS.

REFERENCES

1. Sherwood, C.C., et al., *Evolution of increased glia-neuron ratios in the human frontal cortex.* Proc Natl Acad Sci U S A, 2006. **103**(37): p. 13606-11.
2. Schummers, J., H. Yu, and M. Sur, *Tuned responses of astrocytes and their influence on hemodynamic signals in the visual cortex.* Science, 2008. **320**(5883): p. 1638-43.
3. Agulhon, C., et al., *What is the role of astrocyte calcium in neurophysiology?* Neuron, 2008. **59**(6): p. 932-46.
4. Liedtke, W., et al., *GFAP is necessary for the integrity of CNS white matter architecture and long-term maintenance of myelination.* Neuron, 1996. **17**(4): p. 607-15.
5. Mignot, C., et al., *Alexander disease: putative mechanisms of an astrocytic encephalopathy.* Cell Mol Life Sci, 2004. **61**(3): p. 369-85.
6. Du, Y. and C.F. Dreyfus, *Oligodendrocytes as providers of growth factors.* J Neurosci Res, 2002. **68**(6): p. 647-54.
7. Ginhoux, F., et al., *Fate mapping analysis reveals that adult microglia derive from primitive macrophages.* Science, 2010. **330**(6005): p. 841-5.
8. Stevens, B., et al., *The classical complement cascade mediates CNS synapse elimination.* Cell, 2007. **131**(6): p. 1164-78.
9. Nimmerjahn, A., F. Kirchhoff, and F. Helmchen, *Resting microglial cells are highly dynamic surveillants of brain parenchyma in vivo.* Science, 2005. **308**(5726): p. 1314-8.
10. Aloisi, F., *Immune function of microglia.* Glia, 2001. **36**(2): p. 165-79.
11. Mori, S. and C.P. Leblond, *Electron microscopic identification of three classes of oligodendrocytes and a preliminary study of their proliferative activity in the corpus callosum of young rats.* J Comp Neurol, 1970. **139**(1): p. 1-28.
12. Butt, A.M., et al., *Biochemical subtypes of oligodendrocyte in the anterior medullary velum of the rat as revealed by the monoclonal antibody Rip.* Glia, 1995. **14**(3): p. 185-97.
13. Bunge, M.B., R.P. Bunge, and H. Ris, *Ultrastructural study of remyelination in an experimental lesion in adult cat spinal cord.* J Biophys Biochem Cytol, 1961. **10**: p. 67-94.
14. Bakiri, Y., et al., *Morphological and electrical properties of oligodendrocytes in the white matter of the corpus callosum and cerebellum.* J Physiol, 2011. **589**(Pt 3): p. 559-73.
15. Hartline, D.K. and D.R. Colman, *Rapid conduction and the evolution of giant axons and myelinated fibers.* Curr Biol, 2007. **17**(1): p. R29-35.
16. Watkins, T.A., et al., *Distinct stages of myelination regulated by gamma-secretase and astrocytes in a rapidly myelinating CNS coculture system.* Neuron, 2008. **60**(4): p. 555-69.
17. Simons, M. and K. Trajkovic, *Neuron-glia communication in the control of oligodendrocyte function and myelin biogenesis.* J Cell Sci, 2006. **119**(Pt 21): p. 4381-9.
18. Sanchez, I., et al., *Local control of neurofilament accumulation during radial growth of myelinating axons in vivo. Selective role of site-specific phosphorylation.* J Cell Biol, 2000. **151**(5): p. 1013-24.
19. Richter-Landsberg, C., *The oligodendroglia cytoskeleton in health and disease.* J Neurosci Res, 2000. **59**(1): p. 11-8.

20. van Heyningen, P., A.R. Calver, and W.D. Richardson, *Control of progenitor cell number by mitogen supply and demand.* Curr Biol, 2001. **11**(4): p. 232-41.
21. Bradl, M. and H. Lassmann, *Oligodendrocytes: biology and pathology.* Acta Neuropathol, 2010. **119**(1): p. 37-53.
22. Pringle, N.P. and W.D. Richardson, *A singularity of PDGF alpha-receptor expression in the dorsoventral axis of the neural tube may define the origin of the oligodendrocyte lineage.* Development, 1993. **117**(2): p. 525-33.
23. Trapp, B.D., et al., *Differentiation and death of premyelinating oligodendrocytes in developing rodent brain.* J Cell Biol, 1997. **137**(2): p. 459-68.
24. Solly, S.K., et al., *Myelin/oligodendrocyte glycoprotein (MOG) expression is associated with myelin deposition.* Glia, 1996. **18**(1): p. 39-48.
25. Brinkmann, B.G., et al., *Neuregulin-1/ErbB signaling serves distinct functions in myelination of the peripheral and central nervous system.* Neuron, 2008. **59**(4): p. 581-95.
26. Jessen, K.R. and R. Mirsky, *The origin and development of glial cells in peripheral nerves.* Nat Rev Neurosci, 2005. **6**(9): p. 671-82.
27. Stevens, B., et al., *Adenosine: a neuron-glial transmitter promoting myelination in the CNS in response to action potentials.* Neuron, 2002. **36**(5): p. 855-68.
28. Trajkovic, K., et al., *Neuron to glia signaling triggers myelin membrane exocytosis from endosomal storage sites.* J Cell Biol, 2006. **172**(6): p. 937-48.
29. Ishibashi, T., et al., *Astrocytes promote myelination in response to electrical impulses.* Neuron, 2006. **49**(6): p. 823-32.
30. McTigue, D.M. and R.B. Tripathi, *The life, death, and replacement of oligodendrocytes in the adult CNS.* J Neurochem, 2008. **107**(1): p. 1-19.
31. Bauer, J., et al., *Endoplasmic reticulum stress in PLP-overexpressing transgenic rats: gray matter oligodendrocytes are more vulnerable than white matter oligodendrocytes.* J Neuropathol Exp Neurol, 2002. **61**(1): p. 12-22.
32. Benarroch, E.E., *Oligodendrocytes: Susceptibility to injury and involvement in neurologic disease.* Neurology, 2009. **72**(20): p. 1779-85.
33. Todorich, B., et al., *Oligodendrocytes and myelination: the role of iron.* Glia, 2009. **57**(5): p. 467-78.
34. Juurlink, B.H., *Response of glial cells to ischemia: roles of reactive oxygen species and glutathione.* Neurosci Biobehav Rev, 1997. **21**(2): p. 151-66.
35. Schenck, M., et al., *Ceramide: physiological and pathophysiological aspects.* Arch Biochem Biophys, 2007. **462**(2): p. 171-5.
36. Salter, M.G. and R. Fern, *NMDA receptors are expressed in developing oligodendrocyte processes and mediate injury.* Nature, 2005. **438**(7071): p. 1167-71.
37. Tanaka, J., et al., *Nitric oxide-mediated cGMP synthesis in oligodendrocytes in the developing rat brain.* Glia, 1997. **19**(4): p. 286-97.
38. Matute, C., et al., *P2X(7) receptor blockade prevents ATP excitotoxicity in oligodendrocytes and ameliorates experimental autoimmune encephalomyelitis.* J Neurosci, 2007. **27**(35): p. 9525-33.
39. Bakiri, Y., D. Attwell, and R. Karadottir, *Electrical signalling properties of oligodendrocyte precursor cells.* Neuron Glia Biol, 2009. **5**(1-2): p. 3-11.
40. Jurewicz, A., et al., *Tumour necrosis factor-induced death of adult human oligodendrocytes is mediated by apoptosis inducing factor.* Brain, 2005. **128**(Pt 11): p. 2675-88.
41. Horiuchi, M., et al., *MEK-ERK signaling is involved in interferon-gamma-induced death of oligodendroglial progenitor cells.* J Biol Chem, 2006. **281**(29): p. 20095-106.

42. Nave, K.A., *Myelination and support of axonal integrity by glia.* Nature, 2010. **468**(7321): p. 244-52.
43. Franklin, R.J. and C. Ffrench-Constant, *Remyelination in the CNS: from biology to therapy.* Nat Rev Neurosci, 2008. **9**(11): p. 839-55.
44. Dyakin, V.V., et al., *The contributions of myelin and axonal caliber to transverse relaxation time in shiverer and neurofilament-deficient mouse models.* Neuroimage, 2010. **51**(3): p. 1098-105.
45. Galea, I., I. Bechmann, and V.H. Perry, *What is immune privilege (not)?* Trends Immunol, 2007. **28**(1): p. 12-8.
46. van Zwam, M., et al., *Surgical excision of CNS-draining lymph nodes reduces relapse severity in chronic-relapsing experimental autoimmune encephalomyelitis.* J Pathol, 2009. **217**(4): p. 543-51.
47. Liu, Y., et al., *Neuron-mediated generation of regulatory T cells from encephalitogenic T cells suppresses EAE.* Nat Med, 2006. **12**(5): p. 518-25.
48. Compston, A. and A. Coles, *Multiple sclerosis.* Lancet, 2008. **372**(9648): p. 1502-17.
49. Noseworthy, J.H., et al., *Multiple sclerosis.* N Engl J Med, 2000. **343**(13): p. 938-52.
50. Lassmann, H., W. Bruck, and C.F. Lucchinetti, *The immunopathology of multiple sclerosis: an overview.* Brain Pathol, 2007. **17**(2): p. 210-8.
51. Lucchinetti, C., et al., *A quantitative analysis of oligodendrocytes in multiple sclerosis lesions. A study of 113 cases.* Brain, 1999. **122 (Pt 12)**: p. 2279-95.
52. Kutzelnigg, A., et al., *Cortical demyelination and diffuse white matter injury in multiple sclerosis.* Brain, 2005. **128**(Pt 11): p. 2705-12.
53. Tanaka, R., Y. Iwasaki, and H. Koprowski, *Ultrastructural studies of perivascular cuffing cells in multiple sclerosis brain.* Am J Pathol, 1975. **81**(3): p. 467-78.
54. von Budingen, H.C., et al., *Clonally expanded plasma cells in the cerebrospinal fluid of MS patients produce myelin-specific antibodies.* Eur J Immunol, 2008. **38**(7): p. 2014-23.
55. Hafler, D.A., et al., *Risk alleles for multiple sclerosis identified by a genomewide study.* N Engl J Med, 2007. **357**(9): p. 851-62.
56. Gregory, S.G., et al., *Interleukin 7 receptor alpha chain (IL7R) shows allelic and functional association with multiple sclerosis.* Nat Genet, 2007. **39**(9): p. 1083-91.
57. Lundmark, F., K. Duvefelt, and J. Hillert, *Genetic association analysis of the interleukin 7 gene (IL7) in multiple sclerosis.* J Neuroimmunol, 2007. **192**(1-2): p. 171-3.
58. Sawcer, S., et al., *Genetic risk and a primary role for cell-mediated immune mechanisms in multiple sclerosis.* Nature, 2011. **476**(7359): p. 214-9.
59. Munz, C., et al., *Antiviral immune responses: triggers of or triggered by autoimmunity?* Nat Rev Immunol, 2009. **9**(4): p. 246-58.
60. Sospedra, M. and R. Martin, *Immunology of multiple sclerosis.* Annu Rev Immunol, 2005. **23**: p. 683-747.
61. Dhib-Jalbut, S., *Pathogenesis of myelin/oligodendrocyte damage in multiple sclerosis.* Neurology, 2007. **68**(22 Suppl 3): p. S13-21; discussion S43-54.
62. Raine, C.S., *The Norton Lecture: a review of the oligodendrocyte in the multiple sclerosis lesion.* J Neuroimmunol, 1997. **77**(2): p. 135-52.
63. Wolswijk, G., *Oligodendrocyte survival, loss and birth in lesions of chronic-stage multiple sclerosis.* Brain, 2000. **123 (Pt 1)**: p. 105-15.

64. Appel, S.H. and M.B. Bornstein, *The Application of Tissue Culture to the Study of Experimental Allergic Encephalomyelitis. Ii. Serum Factors Responsible for Demyelination.* J Exp Med, 1964. **119**: p. 303-12.
65. Breij, E.C., et al., *Homogeneity of active demyelinating lesions in established multiple sclerosis.* Ann Neurol, 2008. **63**(1): p. 16-25.
66. Bergsteindottir, K., et al., *In the presence of dexamethasone, gamma interferon induces rat oligodendrocytes to express major histocompatibility complex class II molecules.* Proc Natl Acad Sci U S A, 1992. **89**(19): p. 9054-8.
67. Zeis, T. and N. Schaeren-Wiemers, *Lame ducks or fierce creatures? The role of oligodendrocytes in multiple sclerosis.* J Mol Neurosci, 2008. **35**(1): p. 91-100.
68. Barnett, M.H. and J.W. Prineas, *Relapsing and remitting multiple sclerosis: pathology of the newly forming lesion.* Ann Neurol, 2004. **55**(4): p. 458-68.
69. Barnett, M.H. and I. Sutton, *The pathology of multiple sclerosis: a paradigm shift.* Curr Opin Neurol, 2006. **19**(3): p. 242-7.
70. Filippi, M., et al., *Magnetization transfer changes in the normal appearing white matter precede the appearance of enhancing lesions in patients with multiple sclerosis.* Ann Neurol, 1998. **43**(6): p. 809-14.
71. Narayana, P.A., et al., *Serial proton magnetic resonance spectroscopic imaging, contrast-enhanced magnetic resonance imaging, and quantitative lesion volumetry in multiple sclerosis.* Ann Neurol, 1998. **43**(1): p. 56-71.
72. Savill, J. and V. Fadok, *Corpse clearance defines the meaning of cell death.* Nature, 2000. **407**(6805): p. 784-8.
73. Matute, C. and F. Perez-Cerda, *Multiple sclerosis: novel perspectives on newly forming lesions.* Trends Neurosci, 2005. **28**(4): p. 173-5.
74. Pittoni, V. and G. Valesini, *The clearance of apoptotic cells: implications for autoimmunity.* Autoimmun Rev, 2002. **1**(3): p. 154-61.
75. Lleo, A., et al., *The consequences of apoptosis in autoimmunity.* J Autoimmun, 2008. **31**(3): p. 257-62.
76. Artemiadis, A.K. and M.C. Anagnostouli, *Apoptosis of oligodendrocytes and post-translational modifications of myelin basic protein in multiple sclerosis: possible role for the early stages of multiple sclerosis.* Eur Neurol, 2010. **63**(2): p. 65-72.
77. Matsushima, G.K. and P. Morell, *The neurotoxicant, cuprizone, as a model to study demyelination and remyelination in the central nervous system.* Brain Pathol, 2001. **11**(1): p. 107-16.
78. Hiremath, M.M., et al., *Microglial/macrophage accumulation during cuprizone-induced demyelination in C57BL/6 mice.* J Neuroimmunol, 1998. **92**(1-2): p. 38-49.
79. Jeffery, N.D. and W.F. Blakemore, *Remyelination of mouse spinal cord axons demyelinated by local injection of lysolecithin.* J Neurocytol, 1995. **24**(10): p. 775-81.
80. Kotter, M.R., et al., *Macrophage depletion impairs oligodendrocyte remyelination following lysolecithin-induced demyelination.* Glia, 2001. **35**(3): p. 204-12.
81. Woodruff, R.H. and R.J. Franklin, *Demyelination and remyelination of the caudal cerebellar peduncle of adult rats following stereotaxic injections of lysolecithin, ethidium bromide, and complement/anti-galactocerebroside: a comparative study.* Glia, 1999. **25**(3): p. 216-28.
82. Laatsch, R.H., et al., *The encephalomyelitic activity of myelin isolated by ultracentrifugation.* J Exp Med, 1962. **115**: p. 777-88.

83. Lebar, R., et al., *The M2 autoantigen of central nervous system myelin, a glycoprotein present in oligodendrocyte membrane.* Clin Exp Immunol, 1986. **66**(2): p. 423-34.
84. Tuohy, V.K., et al., *A synthetic peptide from myelin proteolipid protein induces experimental allergic encephalomyelitis.* Journal of immunology, 1988. **141**(4): p. 1126-30.
85. Munoz, J.J., C.C. Bernard, and I.R. Mackay, *Elicitation of experimental allergic encephalomyelitis (EAE) in mice with the aid of pertussigen.* Cell Immunol, 1984. **83**(1): p. 92-100.
86. Baxter, A.G., *The origin and application of experimental autoimmune encephalomyelitis.* Nat Rev Immunol, 2007. **7**(11): p. 904-12.
87. Pender, M.P., et al., *Apoptosis in the nervous system in experimental allergic encephalomyelitis.* J Neurol Sci, 1991. **104**(1): p. 81-7.
88. Bonetti, B., et al., *Cell death during autoimmune demyelination: effector but not target cells are eliminated by apoptosis.* Journal of immunology, 1997. **159**(11): p. 5733-41.
89. Hovelmeyer, N., et al., *Apoptosis of oligodendrocytes via Fas and TNF-R1 is a key event in the induction of experimental autoimmune encephalomyelitis.* Journal of immunology, 2005. **175**(9): p. 5875-84.
90. Lees, J.R. and A.H. Cross, *A little stress is good: IFN-gamma, demyelination, and multiple sclerosis.* J Clin Invest, 2007. **117**(2): p. 297-9.
91. Keirstead, H.S. and W.F. Blakemore, *Identification of post-mitotic oligodendrocytes incapable of remyelination within the demyelinated adult spinal cord.* Journal of neuropathology and experimental neurology, 1997. **56**(11): p. 1191-201.
92. Fancy, S.P., C. Zhao, and R.J. Franklin, *Increased expression of Nkx2.2 and Olig2 identifies reactive oligodendrocyte progenitor cells responding to demyelination in the adult CNS.* Mol Cell Neurosci, 2004. **27**(3): p. 247-54.
93. Gensert, J.M. and J.E. Goldman, *Endogenous progenitors remyelinate demyelinated axons in the adult CNS.* Neuron, 1997. **19**(1): p. 197-203.
94. Nunes, M.C., et al., *Identification and isolation of multipotential neural progenitor cells from the subcortical white matter of the adult human brain.* Nat Med, 2003. **9**(4): p. 439-47.
95. Levine, J.M. and R. Reynolds, *Activation and proliferation of endogenous oligodendrocyte precursor cells during ethidium bromide-induced demyelination.* Exp Neurol, 1999. **160**(2): p. 333-47.
96. Guazzo, E.P., *A technique for producing demyelination of the rat optic nerves.* J Clin Neurosci, 2005. **12**(1): p. 54-8.
97. Knapp, P.E., *Injury stimulates outgrowth and motility of oligodendrocytes grown in vitro.* Exp Cell Res, 1997. **234**(1): p. 7-17.
98. Chang, A., et al., *Premyelinating oligodendrocytes in chronic lesions of multiple sclerosis.* N Engl J Med, 2002. **346**(3): p. 165-73.
99. Sim, F.J., et al., *The age-related decrease in CNS remyelination efficiency is attributable to an impairment of both oligodendrocyte progenitor recruitment and differentiation.* The Journal of neuroscience : the official journal of the Society for Neuroscience, 2002. **22**(7): p. 2451-9.
100. Ye, P., J. Carson, and A.J. D'Ercole, *In vivo actions of insulin-like growth factor-I (IGF-I) on brain myelination: studies of IGF-I and IGF binding protein-1 (IGFBP-1) transgenic mice.* The Journal of neuroscience : the official journal of the Society for Neuroscience, 1995. **15**(11): p. 7344-56.

101. Zeger, M., et al., *Insulin-like growth factor type 1 receptor signaling in the cells of oligodendrocyte lineage is required for normal in vivo oligodendrocyte development and myelination.* Glia, 2007. **55**(4): p. 400-11.
102. Adams, T.E., et al., *Structure and function of the type 1 insulin-like growth factor receptor.* Cell Mol Life Sci, 2000. **57**(7): p. 1050-93.
103. Baserga, R., *The contradictions of the insulin-like growth factor 1 receptor.* Oncogene, 2000. **19**(49): p. 5574-81.
104. Bondy, C.A. and C.M. Cheng, *Signaling by insulin-like growth factor 1 in brain.* European journal of pharmacology, 2004. **490**(1-3): p. 25-31.
105. Anlar, B., K.A. Sullivan, and E.L. Feldman, *Insulin-like growth factor-I and central nervous system development.* Hormone and metabolic research = Hormon- und Stoffwechselforschung = Hormones et metabolisme, 1999. **31**(2-3): p. 120-5.
106. Mason, J.L., et al., *Insulin-like growth factor-1 inhibits mature oligodendrocyte apoptosis during primary demyelination.* The Journal of neuroscience : the official journal of the Society for Neuroscience, 2000. **20**(15): p. 5703-8.
107. Luzi, P., et al., *Generation of transgenic mice expressing insulin-like growth factor-1 under the control of the myelin basic protein promoter: increased myelination and potential for studies on the effects of increased IGF-1 on experimentally and genetically induced demyelination.* Neurochemical research, 2004. **29**(5): p. 881-9.
108. Carson, M.J., et al., *Insulin-like growth factor I increases brain growth and central nervous system myelination in transgenic mice.* Neuron, 1993. **10**(4): p. 729-40.
109. Guan, J., et al., *Insulin-like growth factor-1 and post-ischemic brain injury.* Progress in neurobiology, 2003. **70**(6): p. 443-62.
110. Cao, Y., et al., *Insulin-like growth factor (IGF)-1 suppresses oligodendrocyte caspase-3 activation and increases glial proliferation after ischemia in near-term fetal sheep.* Journal of cerebral blood flow and metabolism : official journal of the International Society of Cerebral Blood Flow and Metabolism, 2003. **23**(6): p. 739-47.
111. Lin, S., et al., *IGF-1 protects oligodendrocyte progenitor cells and improves neurological functions following cerebral hypoxia-ischemia in the neonatal rat.* Brain research, 2005. **1063**(1): p. 15-26.
112. Liu, X., D.L. Yao, and H. Webster, *Insulin-like growth factor I treatment reduces clinical deficits and lesion severity in acute demyelinating experimental autoimmune encephalomyelitis.* Multiple sclerosis, 1995. **1**(1): p. 2-9.
113. Li, W., et al., *Chronic relapsing experimental autoimmune encephalomyelitis: effects of insulin-like growth factor-I treatment on clinical deficits, lesion severity, glial responses, and blood brain barrier defects.* Journal of neuropathology and experimental neurology, 1998. **57**(5): p. 426-38.
114. Cannella, B., et al., *Insulin-like growth factor-1 fails to enhance central nervous system myelin repair during autoimmune demyelination.* The American journal of pathology, 2000. **157**(3): p. 933-43.
115. Vincent, A.M., et al., *IGF-I prevents glutamate-induced motor neuron programmed cell death.* Neurobiology of disease, 2004. **16**(2): p. 407-16.
116. Barres, B.A., et al., *Multiple extracellular signals are required for long-term oligodendrocyte survival.* Development, 1993. **118**(1): p. 283-95.
117. McMahon, E.J., K. Suzuki, and G.K. Matsushima, *Peripheral macrophage recruitment in cuprizone-induced CNS demyelination despite an intact blood-brain barrier.* Journal of neuroimmunology, 2002. **130**(1-2): p. 32-45.

118. Mason, J.L., et al., *Insulin-like growth factor (IGF) signaling through type 1 IGF receptor plays an important role in remyelination.* The Journal of neuroscience : the official journal of the Society for Neuroscience, 2003. **23**(20): p. 7710-8.
119. Komoly, S., et al., *Insulin-like growth factor I gene expression is induced in astrocytes during experimental demyelination.* Proceedings of the National Academy of Sciences of the United States of America, 1992. **89**(5): p. 1894-8.
120. Wilczak, N., et al., *IGF binding protein alterations on periplaque oligodendrocytes in multiple sclerosis: implications for remyelination.* Neurochemistry international, 2008. **52**(8): p. 1431-5.
121. Genoud, S., et al., *Targeted expression of IGF-1 in the central nervous system fails to protect mice from experimental autoimmune encephalomyelitis.* Journal of neuroimmunology, 2005. **168**(1-2): p. 40-5.
122. Liu, Z., et al., *Control of insulin-like growth factor-II/mannose 6-phosphate receptor gene transcription by proximal promoter elements.* Molecular endocrinology, 1995. **9**(11): p. 1477-87.
123. Lovett-Racke, A.E., et al., *Regulation of experimental autoimmune encephalomyelitis with insulin-like growth factor (IGF-1) and IGF-1/IGF-binding protein-3 complex (IGF-1/IGFBP3).* The Journal of clinical investigation, 1998. **101**(8): p. 1797-804.
124. Yao, D.L., et al., *Insulin-like growth factor I treatment reduces demyelination and up-regulates gene expression of myelin-related proteins in experimental autoimmune encephalomyelitis.* Proceedings of the National Academy of Sciences of the United States of America, 1995. **92**(13): p. 6190-4.
125. O'Donnell, S.L., et al., *IGF-I and microglia/macrophage proliferation in the ischemic mouse brain.* Glia, 2002. **39**(1): p. 85-97.
126. Forster, I. and K. Rajewsky, *Expansion and functional activity of Ly-1+ B cells upon transfer of peritoneal cells into allotype-congenic, newborn mice.* Eur J Immunol, 1987. **17**(4): p. 521-8.
127. Reynolds, E.S., *The use of lead citrate at high pH as an electron-opaque stain in electron microscopy.* J Cell Biol, 1963. **17**: p. 208-12.
128. Buch, T., et al., *A Cre-inducible diphtheria toxin receptor mediates cell lineage ablation after toxin administration.* Nature methods, 2005. **2**(6): p. 419-26.
129. Buch, T., et al., *A Cre-inducible diphtheria toxin receptor mediates cell lineage ablation after toxin administration.* Nat Methods, 2005. **2**(6): p. 419-26.
130. Hershfield, J.R., et al., *Aspartoacylase is a regulated nuclear-cytoplasmic enzyme.* FASEB J, 2006. **20**(12): p. 2139-41.
131. Griffiths, I., et al., *Axonal swellings and degeneration in mice lacking the major proteolipid of myelin.* Science, 1998. **280**(5369): p. 1610-3.
132. Yin, X., et al., *Evolution of a neuroprotective function of central nervous system myelin.* J Cell Biol, 2006. **172**(3): p. 469-78.
133. Lappe-Siefke, C., et al., *Disruption of Cnp1 uncouples oligodendroglial functions in axonal support and myelination.* Nat Genet, 2003. **33**(3): p. 366-74.
134. Traka, M., et al., *A genetic mouse model of adult-onset, pervasive central nervous system demyelination with robust remyelination.* Brain, 2010. **133**(10): p. 3017-29.
135. Pohl, H.B., et al., *Genetically induced adult oligodendrocyte cell death is associated with poor myelin clearance, reduced remyelination, and axonal damage.* J Neurosci, 2011. **31**(3): p. 1069-80.

136. de Vos, A.F., et al., *Transfer of central nervous system autoantigens and presentation in secondary lymphoid organs.* Journal of Immunology, 2002. **169**(10): p. 5415-5423.
137. Fabriek, B.O., et al., *In vivo detection of myelin proteins in cervical lymph nodes of MS patients using ultrasound-guided fine-needle aspiration cytology.* J Neuroimmunol, 2005. **161**(1-2): p. 190-4.
138. Bettelli, E., et al., *Myelin oligodendrocyte glycoprotein-specific T cell receptor transgenic mice develop spontaneous autoimmune optic neuritis.* Journal of Experimental Medicine, 2003. **197**(9): p. 1073-1081.
139. Frommer, F., et al., *Tolerance without clonal expansion: self-antigen-expressing B cells program self-reactive T cells for future deletion.* J Immunol, 2008. **181**(8): p. 5748-59.
140. Elgueta, R., et al., *Molecular mechanism and function of CD40/CD40L engagement in the immune system.* Immunol Rev, 2009. **229**(1): p. 152-72.
141. Krishnamoorthy, G., et al., *Myelin-specific T cells also recognize neuronal autoantigen in a transgenic mouse model of multiple sclerosis.* Nat Med, 2009. **15**(6): p. 626-32.
142. Gallucci, S. and P. Matzinger, *Danger signals: SOS to the immune system.* Curr Opin Immunol, 2001. **13**(1): p. 114-9.
143. Carson, M.J., *Microglia as liaisons between the immune and central nervous systems: functional implications for multiple sclerosis.* Glia, 2002. **40**(2): p. 218-31.
144. Becher, B. and J.P. Antel, *Comparison of phenotypic and functional properties of immediately ex vivo and cultured human adult microglia.* Glia, 1996. **18**: p. 1-10.
145. Link, H. and R. Muller, *Immunoglobulins in multiple sclerosis and infections of the nervous system.* Arch Neurol, 1971. **25**(4): p. 326-44.
146. Herndon, R.M. and J. Kasckow, *Electron microscopic studies of cerebrospinal fluid sediment in demyelinating disease.* Ann Neurol, 1978. **4**(6): p. 515-23.
147. Prineas, J.W. and R.G. Wright, *Macrophages, lymphocytes, and plasma cells in the perivascular compartment in chronic multiple sclerosis.* Lab Invest, 1978. **38**(4): p. 409-21.
148. Urich, E., et al., *Autoantibody-mediated demyelination depends on complement activation but not activatory Fc-receptors.* Proc Natl Acad Sci U S A, 2006. **103**(49): p. 18697-702.
149. Linington, C., et al., *Augmentation of demyelination in rat acute allergic encephalomyelitis by circulating mouse monoclonal antibodies directed against a myelin/oligodendrocyte glycoprotein.* Am J Pathol, 1988. **130**(3): p. 443-54.
150. Kabat, E.A., A. Wolf, and A.E. Bezer, *The Rapid Production of Acute Disseminated Encephalomyelitis in Rhesus Monkeys by Injection of Heterologous and Homologous Brain Tissue with Adjuvants.* J Exp Med, 1947. **85**(1): p. 117-130.
151. O'Sullivan, B. and R. Thomas, *CD40 and dendritic cell function.* Crit Rev Immunol, 2003. **23**(1-2): p. 83-107.
152. Taraban, V.Y., T.F. Rowley, and A. Al-Shamkhani, *Cutting edge: a critical role for CD70 in CD8 T cell priming by CD40-licensed APCs.* J Immunol, 2004. **173**(11): p. 6542-6.
153. Mueller, D.L., *Mechanisms maintaining peripheral tolerance.* Nat Immunol, 2010. **11**(1): p. 21-7.

154. Sakaguchi, S., et al., *Foxp3+ CD25+ CD4+ natural regulatory T cells in dominant self-tolerance and autoimmune disease.* Immunol Rev, 2006. **212**: p. 8-27.
155. Zozulya, A.L. and H. Wiendl, *The role of CD8 suppressors versus destructors in autoimmune central nervous system inflammation.* Hum Immunol, 2008. **69**(11): p. 797-804.
156. Costantino, C.M., C. Baecher-Allan, and D.A. Hafler, *Multiple sclerosis and regulatory T cells.* J Clin Immunol, 2008. **28**(6): p. 697-706.
157. Frank, M., et al., *Developmental expression pattern of the myelin proteolipid MAL indicates different functions of MAL for immature Schwann cells and in a late step of CNS myelinogenesis.* Journal of neurochemistry, 1999. **73**(2): p. 587-97.
158. Lyons, S.K., et al., *The generation of a conditional reporter that enables bioluminescence imaging of Cre/loxP-dependent tumorigenesis in mice.* Cancer Res, 2003. **63**(21): p. 7042-6.
159. Bruckener, K.E., et al., *Permeabilization in a cerebral endothelial barrier model by pertussis toxin involves the PKC effector pathway and is abolished by elevated levels of cAMP.* Journal of cell science, 2003. **116**(Pt 9): p. 1837-46.
160. Hofstetter, H.H., C.L. Shive, and T.G. Forsthuber, *Pertussis toxin modulates the immune response to neuroantigens injected in incomplete Freund's adjuvant: induction of Th1 cells and experimental autoimmune encephalomyelitis in the presence of high frequencies of Th2 cells.* Journal of immunology, 2002. **169**(1): p. 117-25.
161. Lucchinetti, C.F., W. Bruck, and H. Lassmann, *Evidence for pathogenic heterogeneity in multiple sclerosis.* Ann Neurol, 2004. **56**(2): p. 308.
162. Hiremath, M.M., et al., *Microglial/macrophage accumulation during cuprizone-induced demyelination in C57BL/6 mice.* Journal of Neuroimmunology, 1998. **92**: p. 38-49.
163. Mitchell, R.E., S. Biswas, and S.M. Le Vine, *Cuprizone and piperonyl butoxide, proposed inhibitors of T-cell function, attenuate experimental allergic encephalomyelitis in SJL mice.* Journal of Neuroimmunology, 2001. **119**: p. 205-213.
164. Zatta, P., et al., *Copper and zinc dismetabolism in the mouse brain upon chronic cuprizone treatment.* Cell Mol.Life Sci., 2005. **62**: p. 1502-1513.
165. Kassmann, C.M., et al., *Axonal loss and neuroinflammation caused by peroxisome-deficient oligodendrocytes.* Nat Genet, 2007. **39**(8): p. 969-76.
166. Ip, C.W., et al., *Immune cells contribute to myelin degeneration and axonopathic changes in mice overexpressing proteolipid protein in oligodendrocytes.* J Neurosci, 2006. **26**(31): p. 8206-16.
167. Kroner, A., et al., *Ectopic T-cell specificity and absence of perforin and granzyme B alleviate neural damage in oligodendrocyte mutant mice.* Am J Pathol, 2010. **176**(2): p. 549-55.
168. Honjo, T., et al., *Adenosine diphosphate ribosylation of aminoacyl transferase II and inhibition of protein synthesis by diphtheria toxin.* J Biol Chem, 1971. **246**(13): p. 4251-60.
169. Elloso, M.M., et al., *Suppression of experimental autoimmune encephalomyelitis using estrogen receptor-selective ligands.* J Endocrinol, 2005. **185**(2): p. 243-52.
170. Chernoff, G.F., *Shiverer: an autosomal recessive mutant mouse with myelin deficiency.* J Hered, 1981. **72**(2): p. 128.

171. Sidman, R.L., M.M. Dickie, and S.H. Appel, *Mutant Mice (Quaking and Jimpy) with Deficient Myelination in the Central Nervous System.* Science, 1964. **144**: p. 309-11.
172. Duncan, I.D., J.P. Hammang, and B.D. Trapp, *Abnormal compact myelin in the myelin-deficient rat: absence of proteolipid protein correlates with a defect in the intraperiod line.* Proc Natl Acad Sci U S A, 1987. **84**(17): p. 6287-91.
173. Wang, H., et al., *Use of suppression subtractive hybridization for differential gene expression in stroke: discovery of CD44 gene expression and localization in permanent focal stroke in rats.* Stroke, 2001. **32**(4): p. 1020-7.
174. Kim, M.D., H.J. Cho, and T. Shin, *Expression of osteopontin and its ligand, CD44, in the spinal cords of Lewis rats with experimental autoimmune encephalomyelitis.* J Neuroimmunol, 2004. **151**(1-2): p. 78-84.
175. Bedard, A., et al., *Identification of genes preferentially expressed by microglia and upregulated during cuprizone-induced inflammation.* Glia, 2007. **55**(8): p. 777-89.
176. Remington, L.T., et al., *Microglial recruitment, activation, and proliferation in response to primary demyelination.* Am J Pathol, 2007. **170**(5): p. 1713-24.
177. Hiremath, M.M., et al., *MHC class II exacerbates demyelination in vivo independently of T cells.* J Neuroimmunol, 2008. **203**(1): p. 23-32.
178. Adams, C.W., R.N. Poston, and S.J. Buk, *Pathology, histochemistry and immunocytochemistry of lesions in acute multiple sclerosis.* J Neurol Sci, 1989. **92**(2-3): p. 291-306.
179. Gay, F.W., et al., *The application of multifactorial cluster analysis in the staging of plaques in early multiple sclerosis. Identification and characterization of the primary demyelinating lesion.* Brain, 1997. **120 (Pt 8)**: p. 1461-83.
180. Mana, P., et al., *Demyelination caused by the copper chelator cuprizone halts T cell mediated autoimmune neuroinflammation.* J Neuroimmunol, 2009. **210**(1-2): p. 13-21.
181. Berger, J. and J. Gartner, *X-linked adrenoleukodystrophy: clinical, biochemical and pathogenetic aspects.* Biochim Biophys Acta, 2006. **1763**(12): p. 1721-32.
182. Lu, J.F., et al., *A mouse model for X-linked adrenoleukodystrophy.* Proc Natl Acad Sci U S A, 1997. **94**(17): p. 9366-71.
183. Forss-Petter, S., et al., *Targeted inactivation of the X-linked adrenoleukodystrophy gene in mice.* J Neurosci Res, 1997. **50**(5): p. 829-43.
184. Kobayashi, T., et al., *Adrenoleukodystrophy protein-deficient mice represent abnormality of very long chain fatty acid metabolism.* Biochem Biophys Res Commun, 1997. **232**(3): p. 631-6.
185. Bergmann, C.C., T.E. Lane, and S.A. Stohlman, *Coronavirus infection of the central nervous system: host-virus stand-off.* Nat Rev Microbiol, 2006. **4**(2): p. 121-32.
186. Oleszak, E.L., et al., *Theiler's virus infection: a model for multiple sclerosis.* Clin Microbiol Rev, 2004. **17**(1): p. 174-207.
187. McMahon, E.J., et al., *Epitope spreading initiates in the CNS in two mouse models of multiple sclerosis.* Nat.Med., 2005. **11**(3): p. 335-339.
188. Koralnik, I.J., *New insights into progressive multifocal leukoencephalopathy.* Curr Opin Neurol, 2004. **17**(3): p. 365-70.
189. Hoffmann, C., et al., *Progressive multifocal leucoencephalopathy with unusual inflammatory response during antiretroviral treatment.* J Neurol Neurosurg Psychiatry, 2003. **74**(8): p. 1142-4.

190. Chesik, D., J. De Keyser, and N. Wilczak, *Insulin-like growth factor system regulates oligodendroglial cell behavior: therapeutic potential in CNS.* Journal of molecular neuroscience : MN, 2008. **35**(1): p. 81-90.
191. De Simone, R., M.A. Ajmone-Cat, and L. Minghetti, *Atypical antiinflammatory activation of microglia induced by apoptotic neurons: possible role of phosphatidylserine-phosphatidylserine receptor interaction.* Molecular neurobiology, 2004. **29**(2): p. 197-212.
192. Gveric, D., M.L. Cuzner, and J. Newcombe, *Insulin-like growth factors and binding proteins in multiple sclerosis plaques.* Neuropathol Appl Neurobiol, 1999. **25**(3): p. 215-25.
193. Frank, J.A., et al., *A pilot study of recombinant insulin-like growth factor-1 in seven multiple sderosis patients.* Multiple sclerosis, 2002. **8**(1): p. 24-9.
194. Contag, C.H. and M.H. Bachmann, *Advances in in vivo bioluminescence imaging of gene expression.* Annu Rev Biomed Eng, 2002. **4**: p. 235-60.
195. Moorman, S.J., *The inhibition of motility that results from contact between two oligodendrocytes in vitro can be blocked by pertussis toxin.* Glia, 1996. **16**(3): p. 257-65.
196. Ruan, W. and M. Lai, *Actin, a reliable marker of internal control?* Clin Chim Acta, 2007. **385**(1-2): p. 1-5.
197. Rubie, C., et al., *Housekeeping gene variability in normal and cancerous colorectal, pancreatic, esophageal, gastric and hepatic tissues.* Mol Cell Probes, 2005. **19**(2): p. 101-9.
198. Lindner, M., et al., *Sequential myelin protein expression during remyelination reveals fast and efficient repair after central nervous system demyelination.* Neuropathol Appl Neurobiol, 2008. **34**(1): p. 105-14.

ABBREVIATIONS

ODC – oligodendrocyte

CNS – central nervous system

MS – multiple sclerosis

EAE – experimental autoimmune encephalomyelitis

BBB – blood brain barrier

APC – antigen presenting cell

LPS – lipopolysaccharide

OPC – ODC precursor cell

PNS – peripheral nervous system

MMPs – matrix metalloproteinases

NO – nitric oxide

TCR – T cell receptor

LN – lymph node

dc – deep cervical

CSF – cerebrospinal fluid

Treg – regulatory T cell

RR – relapsing remitting

MRI – magnetic resonance imaging

CFA – complete Freund's adjuvant

SVZ – subventricular zone

DT – diphtheria toxin

PBS – phosphate buffer saline

HBSS – Hank's balanced salt solution

MEM – minimum essential medium Eagle

dNTP – deoxyribonucleotide

DTT – dithiothreitol

TEM – trasmission electron microscopy

LFB-PAS – luxol fast blue-periodic acid Schiff

H/E – hematoxylin and eosin

CFSE – carboxyfluorescin succinimidyl ester

NP – nitrophenyl-hapten

PT – pertussis toxin

BSA – bovine serum albumin

mAb – monoclonal antibody

p.a. – post administration

p.i. – post immunization

DTR – diphtheria toxin receptor

X-ALD – X-linked adrenoleukodystrophy

ACKNOLEDGEMENTS

For their support, their inputs, for scientific discussions and continuous supervision, my biggest thanks clearly go to Prof. Thorsten Buch and Prof. Burkhard Becher. While the first is the actual reason of my presence in Zuerich, and the thinking mind behind most aspects of my projects, the second has been my sheltering chef and my straight guidance through these PhD years. My gratitude goes naturally also to Prof. Esther Stoeckli and Prof. Peter Sonderegger, who have followed my projects and corrected my way during the last 4 years. It goes without saying that many hugs and love has to go to my beloved colleagues (or at least to most of them): they always provided a great environment to work, network and laugh in good and bad times. Some left, some came: my gratitude applies to many scientists now spread all over the globe.

Personally, the biggest thanks goes to my stunning wife, which kept me sane so far drawing heavily on her own energies. And to all the new great friends and music partners that I've found in Zuerich, and made me forget about science-related stress in many vital good laughing evenings.

Finally, it would be impossible to celebrate this period without honoring the people and the things that mostly made me who I am: my dear family, my silly old friends, my bittersweet old country, my caring dogs.

CURRICULUM VITAE

Date of birth: 18/06/1982

Nationality: Italian

Home address: Bucheggstrasse 162, 8057 Zuerich (CH);

Via Olmo n.1, 24030 Villa d'Adda (Bg), Italy.

Mobile Natel: +41762576606

E-mail: hetloc@inwind.it; giuseppe.locatelli@neuroimm.uzh.ch

EDUCATION:

2007 – present **University Zuerich Irchel, Switzerland**

International Ph.D. Program in Neuroscience.

2004 – 2007 **Milano Bicocca University, Italy**

Master's degree in Industrial Biotechnology.
Graduated on July 2007, with full marks and honor (summa cum laude).

Including courses in combinatorial chemistry, pharmacology, purification and analysis laboratories, immunogenomics, computational chemistry, history of medicine, neuropsychopharmacology, molecular genetics II, cellular biochemistry II, economy and business organization II, applied molecular biology, patents, pharmacological organic compounds.

Degree Thesis: "The role of adaptor protein Rai (ShcC) in human tumor neuronal stem cells isolated from glioblastoma multiforme". Supervisor: Ferdinando Chiaradonna, Ph.D.

2001 – 2003 **Milano Bicocca University, Italy**

Bachelor's degree in Biotechnology, with a grade of 109 (out of 110).

Included courses in science sociology, inorganic and organic chemistry, informatics, english language, physics, biology, mathematics, general and molecular genetics, physiology, oncology, biochemistry, immunology, statistics, microbiology, diagnostics, histology and anatomy, general pathology, psychology, molecular biology, molecular pharmacology, bioethics, several laboratory activities.

Thesis: "Genotypic characterization and expression of AID transgene in a genetically modified murine model ". Supervisor: Prof. Marco Parenti.

1996 – 2000 **Secondary school M.G.Agnesi, Merate (Lc), Italy**

Attended the secondary school with an emphasis on science, obtaining full marks and honor (magna cum laude) at the national exams. Thesis: "History of antisemitism".

LANGUAGES:

Italian – mother-tongue; English – good; German – poor.

PROFESSIONAL EXPERIENCEs:

November 2007 – present **University Irchel Zuerich**

I am working as a PhD student in the group of Dr. Thorsten Buch, under the direct supervision of Dr. Prof. Rer. Nat. Burkhard Becher. The aim of my PhD is to combine and integrate knowledge from neuroscience and immunology in order to understand the dynamics of the immune-neural interactions during health and disease. All the projects are based on an *in vivo* approach using different strains of transgenic mice. We are currently investigating the possible link between induced oligodendrocyte death and (auto) immune responses, the role of IGF1R in mature oligodendrocytes during disease, survival and behavior of oligodendrocytes in different conditions. Also, we are assessing a new mouse model which allow us to follow and quantify demyelination *in vivo* through the direct imaging of oligodendrocytes. I'm learning everything about murine *in vivo* experiments and *in vitro* and ex vivo isolation and manipulation of tissues and cells; FACS, ELISA, proteomics and genetics. High frequency of presentations, international collaborations and frequent attendance to national/international neuroscience or immunology meetings are giving me insights on

both the research field and increasing my communication skills and my understanding of the scientific world.

Jan 2006 – October 2007 **IFOM Foundation (Campus IFOM-EIO), Milan, Italy**

During this fundamental period I gained experience in independent research and team work as part of a group characterizing the role of adaptor protein ShcC (also known as N-Shc or Rai) in murine neural stem cells and human tumor neural stem cells. I learnt how to work in tissue culture (especially stem cells culture) with transfection and infection of cell lines; manipulation of expression vectors, mutagenesis and cloning; DNA and protein extraction; PCRs, IPs and western blot analysis. Regularity in presentations of my work at group and lab meetings have given me the opportunity to develop my presentation skills. Departmental Campus seminars have given me an interesting insight into new experimental techniques and oncological research.

Jan 2004 – Apr 2004 **National Research Centre ITB, Segrate (MI), Italy**

Gained experience in laboratory research whilst being involved in a project on the DNA modifying enzyme AID (Activation Induced cytidine Deaminase). I learnt techniques and principles of molecular biology, as well as self-management and team work.

Aug-Oct 2002, 2003, 2006 **Spazio Terzo Mondo bookshop, Seriate (Bg), Italy**

Worked three different years in a bookshop as deliveryman in Milano and Bergamo and at the same time as shop assistant. Good oral communication and good driving (and parking) skills were required.

Sep 1999 – present **Cultural society LUNANUOVA Onlus, Solza (Bg), Italy**

In these 11 years we are pursuing through our non-lucrative cultural society the aim of racial integration, culture diffusion and young interests enhancement. We are also

running the municipal public library and a linked literary coffee bar, organizing concerts, public lectures and art exhibitions. Great organization, communication and practical skills were required in all activities realized so far. I personally acted as main organizer/speaker during three public exhibitions: *The holocaust and Charlie Chaplin's The Great Dictator*, Jan 2007; *Pier Paolo Pasolini, the man and the poet,* Dec 2005-Jan 2006; *Insight on embryogenesis and artificial insemination,* Apr 2005.

Conferences:

Neuroscience 2011, November 2011, Washington D.C. (USA), poster presentation

Swiss MS researchers meeting, September 2010, Zuerich (Swizterland), poster presentation

Cost Neuroinfnet meeting, May 11 2010, Odense (Denmark), speaker

Young MS researcher meeting, June 2009 Charmey (Switzerland), speaker

Cost Neuroinfnet meeting, November 18 2008, Southampton (U.K.), poster presentation

Cost Neuroinfnet meeting, November 20 2007, Zurich (Switzerland), poster presentation

Braga Neuroimmunology summer school, 21 June 2009, Braga (Portugal): poster presentation

Teaching:

May 2011, **TOPEA online tutorial on autoimmune inflammation**

June 2010 – March 2011, **Supervisor of master student**

September 2009, September 2010, **Immunology practical FACS course, University Zuerich**

February-April 2009, **Supervisor of bachelor student**

Publications

Primary oligodendrocyte death does not elicit anti-CNS immunity (Locatelli et al., *Nature Neuroscience 2012*)

The role of IGF1-R in oligodendrocyte damage and CNS inflammation (Locatelli et al., *in preparation*)

A new mouse model for *in vivo* quantification of demyelination and remyelination (Locatelli et al., *in preparation*)

Prizes

Swiss MS researchers meeting 2010, September 3 2010, Zuerich: best poster

Hobbies and Interests:

Music and playing: been a classic guitar and electric bass guitar player in various metal, rock and folk italian bands in the 1999-2008 period. Since 2010, bass player for the Suisse band “Muddy roots”. I played basketball for 8 years until 2002. I am really interested in literature, cinema, theatre and poetry. I also love to cook and experiment in the kitchen.

Contacts:

Prof. rer. Nat. Burkhard Becher, University Irchel (Zuerich), +41 433660676, Burkhard.becher@neuroimm.uzh.ch

Prof. rer. Nat. Thorsten Buch, Technical University Muenich (Muenich), +49 8941404134, Thorsten.Buch@mikrobio.med.tum.de

Giuliana Pelicci, **PhD** Campus IFOM-EIO (Milan), +39 335430107, Giuliana.Pelicci@ifom-ieo-campus.it